1-1-2020

Monitoring Corrosion Of A One Inch Ball Valve In A Hydraulic Loop Using Ultrasonic Technology

Osei Prempeh

UNIVERSITY OF NORTH DAKOTA

MONITORING CORROSION OF A ONE INCH BALL VALVE IN A HYDRAULIC LOOP USING ULTRASONIC TECHNOLOGY

By

OSEI PREMPEH
B.S., Electrical Engineering, University of Texas-Tyler, 2011
M.S., Electrical Engineering, Kansas State University, 2013
MBA., Business Administration, University of Texas-Tyler, 2016

A DISSERTATION

SUBMITTED TO THE GRADUATE SCHOOL

IN PARTIAL FULFILLMENT OF THE REQUIREMENTS

for the degree

DOCTOR OF PHILOSOPHY

Energy Engineering

Grand Forks, North Dakota

May 2020

This dissertation submitted by Osei Prempeh in partial fulfillment of the requirements for the Degree of Doctor of Philosophy from the University of North Dakota, has been read by the faculty advisory committee, under whom the work was done and is hereby approved.

_____
Dr Michael Mann

_____
Dr. Edward Kolodka (Chair)

_____
Dr. Yun Ji

_____
Dr. Xiaodong Hou

_____
Dr. Ali Alshami,

This dissertation is being submitted by the appointed advisory committee as having met all the requirements of the School of Graduate Studies at the University of North Dakota is hereby approved.

_____
Name of Dean
Dean of the School of Graduate Studies

_____
Date

PERMISSION

Title Monitoring Corrosion of a One Inch Ball Valve in A Hydraulic Loop Using Ultrasonic Technology

Department Energy Engineering

Degree Doctor of Philosophy

In presenting this dissertation in partial fulfillment of the requirements for a graduate degree from the University of North Dakota, I agree that the library of this University shall make it freely available for inspection. I further agree that permission for extensive copying for scholarly purposes may be granted by the professor who supervised my dissertation work or, in his absence, by the Chairperson of the department or the dean of the School of Graduate Studies. It is understood that, any copying or publication or other use of this dissertation or part thereof for financial gain shall not be allowed without my written permission. It is also understood that due recognition shall be given to me and to the University of North Dakota in any scholarly use which may be made of any material in my dissertation.

Osei Prempeh
05/06/2020

TABLE OF CONTENT

LIST OF FIGURES

LIST OF TABLES

ACKNOWLEDGEMENTS

I would like to thank the following people for supporting the construction of the hydraulic flow loop for the experiments that I conducted: Todd Harrison of Metso Flow Control Company for supplying a control valve that I used for the construction of the hydraulic flow loop, Vernon Therence and Sandy Skeeters for helping me with the construction of the hydraulic flow loop. Many thanks to Dr. Michael Mann for his advice throughout my research journey, Dr. Edward Kolodka, whose teachings in Metallic Corrosion and Polymer Degradation drove my interest into corrosion engineering research and I also would like to thank Dr. Yun Ji, Dr. Xiaodong Hou, Dr. Ali Alshami for their advising.

Last but not the least, to my dear wife Nancy Prempeh, for her support and encouragement throughout my research journey.

ABSTRACT

Ball valves with carbon steel bodies that help modulate flow rates are valuable parts in the process chemical industry. While corrosion monitoring is widely studied, there is not much information available regarding corrosion monitoring of control valves, as referenced in the literature review for this dissertation. This research investigated some foundational blocks for how corrosion can be monitored for a carbon steel body ball valve using ultrasonic technology. Topics that were addressed during this research include:

- Monitoring corrosion in a carbon steel 1inch ball valve in a constant flow rate environment, in the presence of sodium chloride solution, mixtures of sodium chloride and acetic acid with pH ranging from 4 to 8.
- Monitoring and analysis of the corrosion impact for the inlet and outlet of carbon steel ball valve using handheld ultrasonic thickness meter in constant flow conditions.
- Embedded ultrasonic transducers on carbon steel control valve body for online corrosion monitoring.

Three experiments were conducted under various corrosive environment namely NaCl, acetic acid and NaCl mixtures for a total of 1,872 hours. Flow rates for these experiments were kept constant while process variables such as pressure, temperature, flow rates, total dissolved solids and power of hydrogen were measured. Microscopic images of the inlet and outlet of the valve were reviewed to validate corrosion characteristics of the valve body. Ultrasonic transducers were used to collect thickness data on the valve body in one experiment and

embedded permanently for 648 hours while thickness measurements were monitored during the second and third experiments.

Statistical tools were used to analyze data from thickness measurements. The tools used are normal distribution, probability and regression. The inlet and outlet thickness measurements for the three experiments were not normally distributed as expected. The thickness loss for both inlet and outlet locations where thickness readings were taken on the valve for all three experiment, showed that the thickness losses were nonlinear in nature as expected, although for the 240 hours of run with the ultrasonic transducer embedded on the valve, the outlet readings were very close to linear.

Thickness measurements were tested against ambient conditions and valve positions which include, temperature, air pressure, noise, vibration and varying valve position. Apart from a high temperature at 300°F, which had an impact on the ultrasonic thickness readings, air pressure, noise exposure, vibration and changing valve position did not have adverse impacts on the measured thickness. These investigations have proven that, ultrasonic transducers can be embedded on ball valves with carbon steel bodies, to monitor both corrosion rates and total corrosion. These experiments will build the foundation for the next generation of carbon steel ball valves which have ultrasonic technology embedded to monitor corrosion online and in real time.

CHAPTER I
INTRODUCTION

1.1 Goals of Research

Corrosion in general is a multibillion dollar opportunity that is explored every day in the scientific world [1]. Much of the equipment in the chemical industry can be affected by a variety of corrosion mechanisms depending on the medium present. The equipment that may corrode include valves, which control flow rates in a process. Carbon steel, a material commonly used for the construction of valve bodies, is usually the largest component of a valve body because of its combination of performance and low cost. While corrosion monitoring is widely studied, there is not much information on corrosion monitoring of a valve body.

The objective of this research was to investigate the possibility of online monitoring of the corrosion of ball valves. This research will investigate the following subtopics:

Monitoring corrosion in a carbon steel 1-inch ball valve in a constant flow rate environment, in the presence of sodium chloride solution with the pH maintained at about 8.

1. Monitor corrosion in a carbon steel 1-inch ball valve in a constant flow rate

environment in the presence of sodium chloride solution with pH maintained at about 8.

2. Determine impact of the mixture of NaCl and acetic acid solution on 1-inch carbon steel ball valve

under constant flow conditions maintaining pH of less than 4.

3. Monitor and analyze of the corrosion impact on the inlet and outlet of carbon steel

ball valve using handheld ultrasonic thickness meter in constant flow conditions in the presence of sodium chloride mixed with acetic acid.

4. Access the possibility of embedding ultrasonic technology on carbon steel valve for online corrosion monitoring.

These investigations will build the foundation where the next generation of carbon steel ball valves could have ultrasonic technology embedded to monitor corrosion online and in real time.

1.2 Outline of Dissertation

Chapter two of the dissertation gives an overview of the literature that was reviewed. This outlines the different methods that the corrosion of a material can be monitored either directly online or by other means. The techniques that were reviewed are Radio Frequency (RF), Acoustic Emissions (AE), Electrochemical Noise Measurements (ENM), and Electrochemical Frequency Modulation (EFM). Other methods that were reviewed are the self-diagnostic method, the constant load method, Scanning Electron Microscopy (SEM) and ultrasonic technique. Gaps in the Literature are also identified in chapter two.

Chapter three will discuss corrosion fundamentals, various forms of corrosion, and corrosion thermodynamics. In addition, fundamental of ultrasonic technology are discussed including signal attenuation, wavelength and ultrasonic measuring systems.

Chapter four discusses the methods used for this research and the three methods utilized are discussed. The first method used a hydraulic loop with a one-inch valve installed within the loop with a recirculating sodium chloride solution. The second method used the same test apparatus but with a mixture of sodium chloride and acetic acid as the process fluid. The first method ran for 1,152 hours while the second method ran for 408 hours. In both cases ultrasonic thickness

measurements were taken on the valve body during the duration of run. The third method had the ultrasonic thickness measurements taken with the ultrasonic transducers embedded on the valve body for 240 hours and with acetic acid and sodium chloride as the recirculating fluid.

The results of the research are discussed and analyzed in chapter five . Statistical analyses were conducted for all three experiments and the statistical distribution, probabilities and regression analyses of the ultrasonic thickness measurements are considered in the results and discussion. Ambient conditions and their impact on the ultrasonic thickness measurements were also considered in this chapter. Safety, quality assurance, quality control measures and reliability of thickness measurements were also discussed in chapter five. In chapter six, the conclusions of research findings were summarized along with recommendation for future work.

.

CHAPTER II

LITERATURE REVIEW

2.1 Literature Overview

This review is a survey of current and past methods for monitoring corrosion online and will also look at seawater or sodium chloride and how steel is affected by it in terms of corrosion mechanisms. Different methods for characterizing and monitoring corrosion are also reviewed. The methods reviewed include intrusive and non-intrusive techniques. This review also looked at how these methods of monitoring corrosion has evolved over the years since 2008.

Corrosion monitoring method reviewed include sonotrode, approaches based on Radio Frequency Identification (RFID), Acoustic Emission (AE), Ultrasonic methods and the Electrochemical Noise (EN) technique are discussed [2]–[6]. Other methods also reviewed include the Electrochemical Frequency Modulation (EFM) technique for detecting Stress Corrosion Cracking (SCC) [7], the self-diagnostic method for detecting corrosion in an Air Operated Valve system (AOV), the Constant Load Method for detecting corrosion of steel samples and Scanning Electron Microscopy (SEM) [7]–[10].

2.1.1 Radio Frequency Identification

There are numerous applications for RFID which include but are not limited to, utilities, manufacturing, and government. These entities need methods to identify corrosion that may exist within their systems [11]. Because of the interest in this application, the RFID methods for

detecting corrosion is gaining ground [11]. There are few types of RFID, but the scope of this review considered only Low Frequency and High Frequency RFID as used to detect the corrosion of steel samples. The RFID system is made up of a tag, a transponder and a reader arrangement. The reader has a microcontroller with a RF signal circuit and filters needed to transmit and receive signals. Energy is transferred from the RFID reader to the RFID tag activating the RFID tag [11].

The principle of RFID is based on the measuring of digital communication, via the tag, with the complex impedance measurement of the RFID tag antenna coupled magnetically together with the RFID reader antenna [11]. The total impedance across the reader antenna is expressed as:

$$Z_m = Z_R + W^2 \frac{M^2}{Z_T}$$

Where Z_R is the reader impedance, Z_T is the intrinsic impedance of the RFID tag, M is the mutual coupling between the reader and the RFID tag, Z_m is the total measured impedance across the reader antenna, and W is the frequency carrier in radians. To obtain the corrosion measurements with good accuracy, the real and the imaginary parts of the complex impedance is evaluated [2]. The magnitude of Z_P, the real part of $Z_{re}(f)$ has the largest variance of corrosion between when there is no corrosion and a month later. The magnitude Z_p decreases between the months of one and ten [2].

Zhang et al., investigated corrosion using RFID methods and considered High Frequency RFID where the RFID sensors were installed directly on the surface of the material under investigation. These RFID sensors are affordable when compared to other types such as wireless sensing or electromagnetic Nondestructive Testing methods [2].

Figure 1. shows operation principle of developed passive RFID tag, (a) system schematic of writing and reading digital information into the tag IC memory chip and measuring complex impedance of the reader antenna; (b) tag equivalent circuit; (c) measured impedance spectrum (real part and imaginary part of impedance) and examples of parameters for multivariate analysis [2].

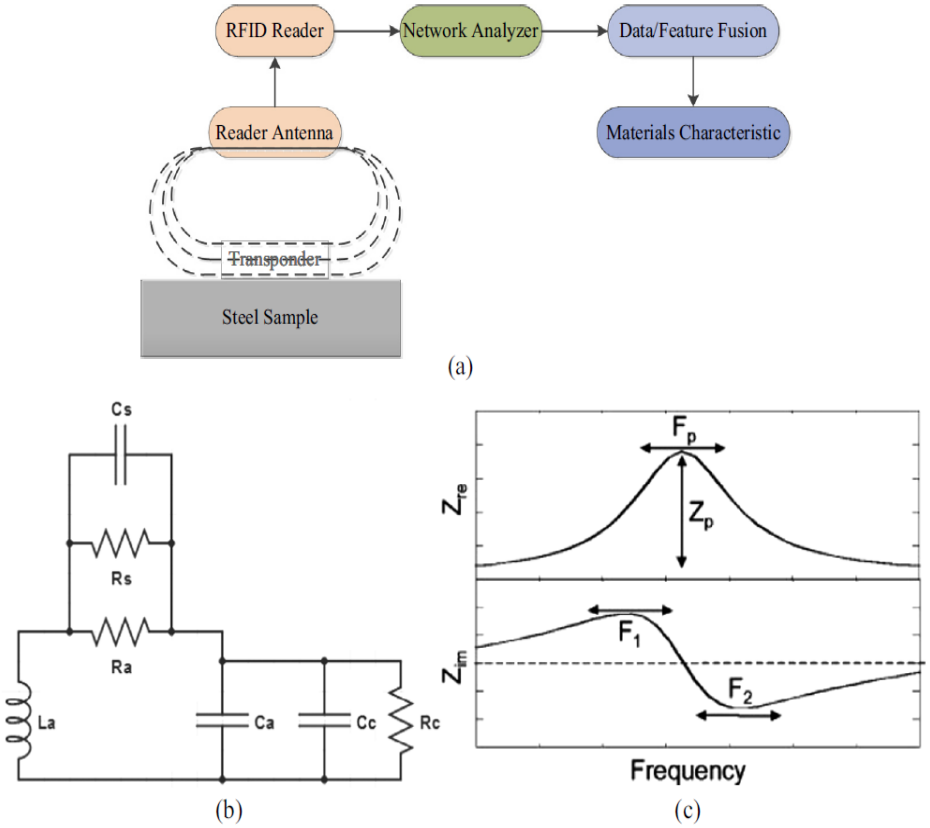

Figure 1. Operating principle of developed passive RFID tags.

Some of the limitations were the distance between the RFID sensor and the sensor reader. When distance was changed both the amplitude and resonant frequency position changed. This makes it a challenge to evaluate the stages of corrosion. The analysis of corrosion was done by considering real and imaginary parts of a complex impedance. During this investigation, the

corrosion of mild steel was investigated using an RFID sensor. [2]. The experiment modeled an RFID as a coil that created excitation which in turn generated an electromagnetic field as shown in *Figure 2* The set up for the experiment is shown in figure 2 [2].

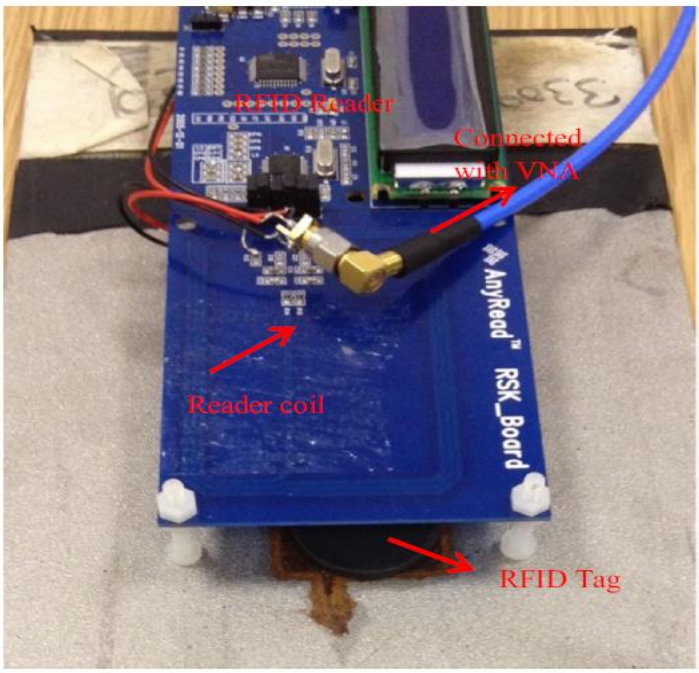

Figure 2. Photograph of sample under testing with Agilent E5071B.

Zhang et al., demonstrated that 13.56 MHz RFID sensors can detect corrosion, but in this experiment it was in the presence of Iron (III) chloride. This research was limited in that the steel samples investigated were not large and were limited to mild steel [2]. They did not address during their investigation whether large samples size can be used and the impact of the absence of Iron (III) chloride was also not addressed.

Sunny et al., studied the atmospheric corrosion characteristics of steel samples using Low Frequency RFID sending system with exposure duration ranging from1month to12 months. [11].

This investigation considered both coated and non-coated mild steel samples and an LF (125KHz) RFID reader was used for this experiment.

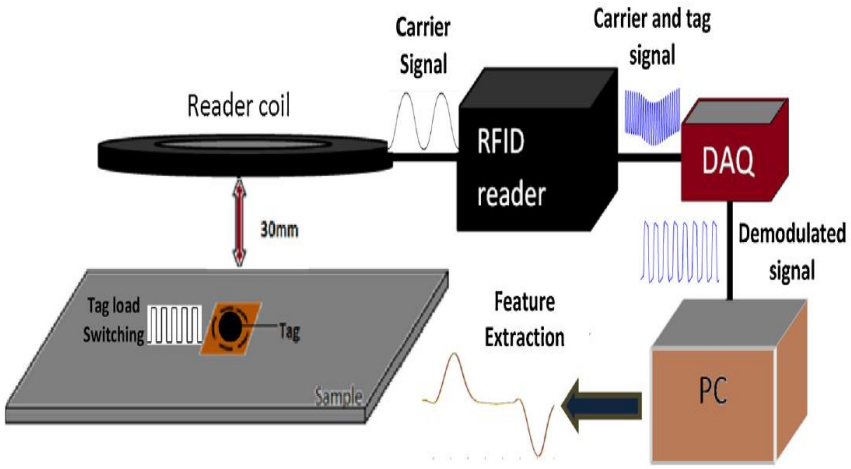

Figure 3. RFID system diagram.

Figure 3. shows a schematic of their experimental set up. In this figure an RFID tag mounted on a steel sample is 30mm away from the reader coil which generated RFID carrier signals. The RFID carrier signals are read by the RFID reader. Through the data acquisition system (DAQ), carrier signals and tag signals are demodulated, the demodulated signal is displayed on a computer screen, and this signal provided the basis for corrosion to be determined. Sunny et. al. concluded that for coated and non-coated steel samples, corrosion on mild steel could be verified. This diagram in *Figure 3.* shows RFID set up of Sunny et al [11].

2.1.2 Acoustic Emission

Acoustic emission is a commonly employed method that may be used to verify Stress Corrosion Cracking (SCC) in real time [3]. The acoustic emission method measures energy waves that are elastic and released suddenly by a test sample as cracks form during the initial

stages of SCC or from some other deformation [12]. An AMSY-6 Vallen acoustic emission system, which had an 8-channel acoustic emission system, was used to measure acoustic emissions. Parametric channels were used to monitor displacement and force. The information collected from the parametric channels (displacement and force) are correlated with the acoustic emission information for SCC evaluation.

These systems may also had piezoelectric sensors with preamplification and band filters [13]. Noise pertaining to these systems can be attenuated by making sure that the peak amplitude signals do not go beyond a prefixed level known as the threshold level. There was a load level where there were no cracks, known as the Crack Growth (CG) threshold and it was important to set the threshold correctly to avoid recording noise or attenuating the desired signal [13].

After recording the Acoustic Emission signal, parameters such as the peak amplitude signal, rise time, or the energy content can be analyzed. The Strain Energy Release Rate (SERR) SERR is expressed as:

$$G = \frac{3Pd}{2wa}$$

Where *P* is the force, *d* is the displacement, *w* is the width of the sample under test and *a* is length of the crack [13].

Hwang et al., conducted a study for 304 stainless steel in the presence of high pressure and temperature in a corrosive environment. The corrosive aqueous solution that the steel was immersed in was 1M Na_2S and 4M NaOH. This study investigated stress corrosion cracking using acoustic emissions [3]. The Acoustic Emission test rig consisted of a four-channel data collection instrument with sensors that had a 400 Hz resonance frequency with high temperature operating at 500℃ [3]. To introduce SCC, the AISI 304 stainless steel tube was mounted on a

system designed to mimic conditions that prevail in a nuclear power plant. The outer surface of the steel tube was heated using heating coils that had a maximum pressure and temperature of 73 bar and 383℃ respectively. The corrosive media introduced fractures within 3,200 seconds hence it was evaluated that the material had already been subjected to SCC attack prior to the accelerated fracture [3]. The variation of cumulative AE counts indicated that, as the count increased over time, it was shown that the AE signals generated were impacted by the cracks in the steel [3].

Ali et al., conducted an experiment on fault detection of valves in a reciprocating compressor system and base line data was taken on valves that are in good conditions. The test rig consisted of a compressor, motor, and AE sensors and data acquisition system with software for acoustic data analysis [14]. The flow rate and speed varied for different test scenarios and corrosion was introduced to two valves that were installed at the suction and discharge of the compressor. Although the type of corrosion introduced was not evaluated during this experiment, they concluded that the model can be used with high accuracy to determine valve conditions. [14].

Gang Du et al., also conducted studies of SCC corrosion on 304 stainless steel immersed in NaCl solution [5]. A stainless-steel plate placed in the bottom of a cell with electrolyte and sealed with silicone rubber at a constant load of 164.0 MPa . The experimental set up for acoustic emissions testing consisted of three AE sensors used to monitor acoustic emission count with an emission noise around 20dB [5]. Two of the sensors were used to monitor AE measurements and the third AE sensor was used to monitor noise from the background. Filters were used to ensure that mechanical disturbances and electromagnetic interferences were kept to a minimum [5]. SCC occurred in austenitic steel in NaCl solution as the potential decreased

during the early stages of the investigation [5]. Stress corrosion cracking was illustrated using acoustic emission counts over time and it was shown that there were three regions of corrosion [5].

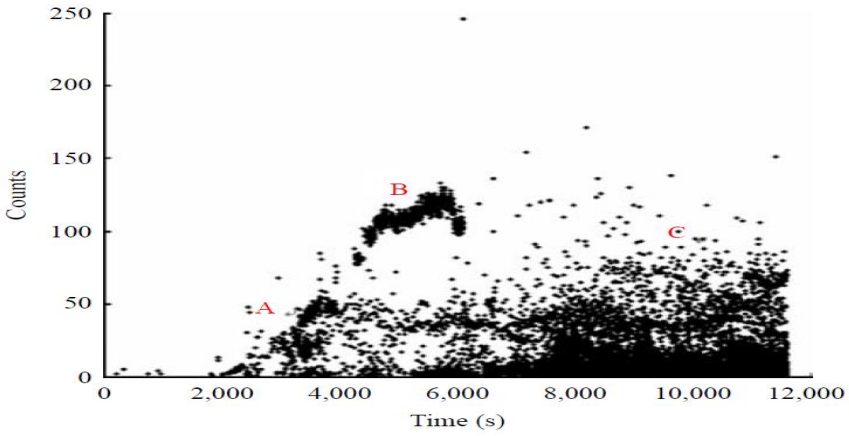

Figure 4. AE ring-down count distribution.

Figure 4. Shows the acoustic counts over time. The counts are ranged from 0 to 250 on the y-axis a time in seconds on the x-axis. AE ring-down count distribution with time. The graph's region A shows the area with localized corrosion, region B shows where cracks started to propagate in the material under test, and region C shows the area that combines general corrosion and pitting. Region C was also general corrosion region that is known as crack propagation with pitting [5].

2.1.3 Electrochemical Noise Measurement

Electrochemical noise is a reliable method to evaluate corrosion by the determination of noise resistance from the current (ampere) noise and potential (volts) noise amplitudes. Electrochemical noise measurement is a nondestructive and nonintrusive method used to evaluate the nature of electrochemical activity during corrosion. It takes into consideration the current that fluctuates during this reaction [15]. For example:

$$2Fe \rightarrow 2Fe + 4e$$

$$2H_2O + O_2 + 4e \rightarrow 4OH^-$$

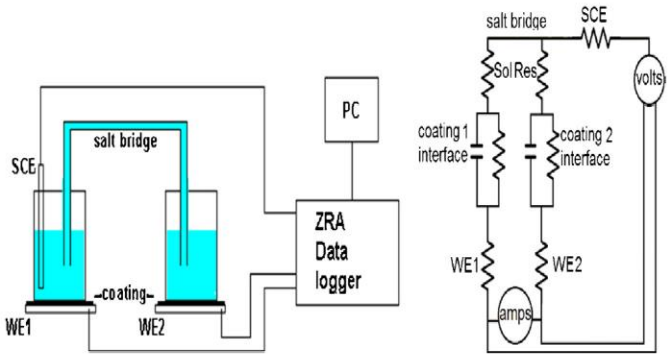

Figure 5. Salt bridge experiment.

A standard salt bridge setup is shown on the left in *Figure 5.* This salt bridge arrangement was used to measure electrochemical noise for two coated (organically) metal surfaces. Its equivalent electrical circuit is shown on the right in *Figure 5* using Randles circuit modelling. Considering the setup, *WE1* and *WE2* refer to working electrode one and working electrode two [15]. To analyze these systems, it is necessary to develop the Equivalent Electrical Circuit (EEC). Randles circuit illustrates the EEC with RC being the time constant of the circuit [15]. The right side of *Figure 5* shows standard salt bridge arrangement to measure electrochemical noise.

Hou et al., monitored the corrosion of the carbon steel sample in an aqueous solution using the electrochemical noise method. The corrosion types that were investigated was uniform, pitting and passivation [16]. The Electrochemical noise measurement was implemented by using the setup shown in *Figure 6.*

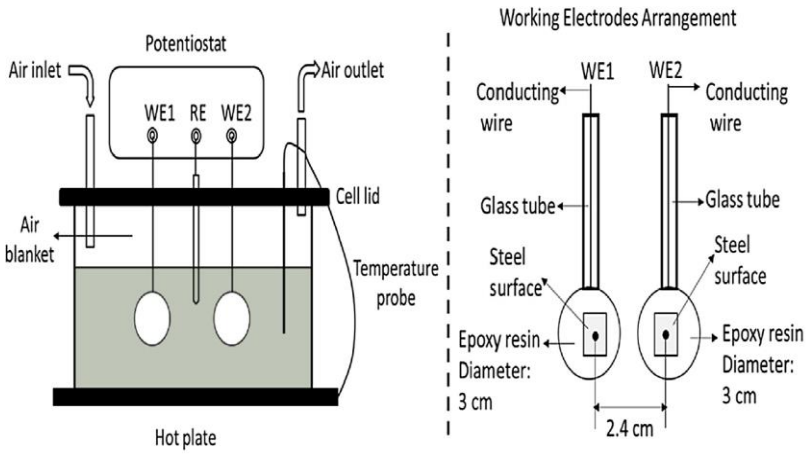

Figure 6. Electrochemical noise measurements.

The EN data shown related to testing pertaining to the type of corrosion, i.e. uniform, pitting and passivation. Hou et al. also suggested areas of improvement for this experiment [16]. An example suggested was that the data needed to be recorded in real time under normal operation conditions and that more data was needed to be collected for analysis. In their study Hou et al. determined corrosion impacts for uniform, pitting and passivation. Current and potential noise amplitudes were used to perform these evaluations. It was evident that for the testing period for uniform corrosion, high frequency fluctuations where observed for both the current and potential noises. The maximum amplitude observed for potential noise was $12mV$ while the maximum observed for current was close to $12\mu A$. Pitting current noise amplitude was $0.02\mu A$ while potential noise showed similar outcomes the amplitude was not stated. The passivation system changed with a very low frequency with an amplitudes for the current noise at $0.02\mu A$ and $12mV$ for the potential noise [16].

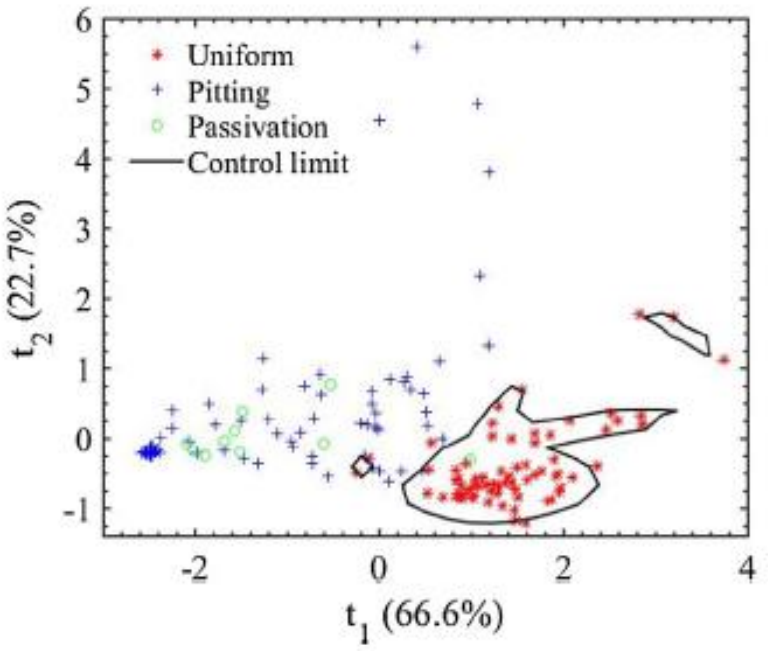

Figure 7. Principal score plot for Uniform Corrosion, Pitting and Passivation.

*F*igure *7* shows a principal component score plot of three corrosion types. The plot consists of uniform corrosion labeled red, pitting marked blue and passivation marked green. The data used in this model was very small particularly for the passivation data collected. The two principal components consisted of 89.3% of the variance of the data. The map has a control limit of 95% with the assumption of five -kernel Gaussian mixture model and can be used for monitoring corrosion in real time [16].

Estupiñán-López et al., used electrochemical noise to study the onset of pitting corrosion of 2205 stainless steel immersed in F_3Cl_3 and NaCl solutions [4]. This method, which is mainly electrochemical, emits electrical charges on to the electrodes when anode and cathode reactions are present. Electrochemical noise is measured under potentiostatically-polarized situations where corrosion is ongoing and the method is non-destructive in nature [4].

Fluctuations in potential differences between the anode and cathode, can be detected with this method. The fluctuations can be used to detect pitting corrosion. The Electrochemical noise is inversely proportional to the frequency of oscillation, and corrosion is determined by analysis of these fluctuations between the current and the potential difference of the electrodes and electrolyte with the circuit in open situation. An increase in exposure suggests that pit formation also increased [4].

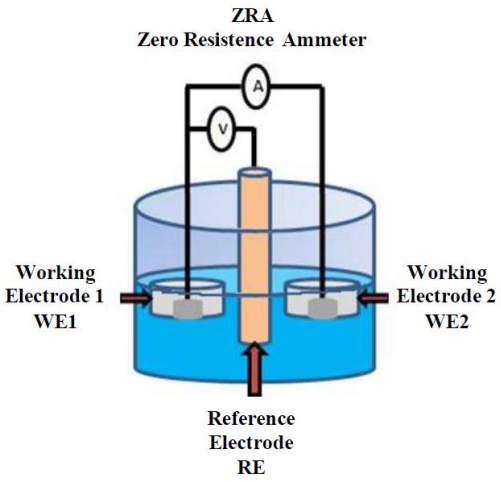

Figure 8. Experimental setup used for electrochemical testing.

Figure 8 shows the various component parts for electrochemical testing using electrodes. The set up consisted of two working electrodes WE1, WE2, a reference electrode, RE and a voltmeter and an ammeter with zero resistance. Current noise amplitude is measured between each working electrode and the reference RE. The set provided the ability to measure current noise and voltage noise in the system [4].

Aljoboury et al., studied SCC in S32750 and UNS 531603 steel, which are usually used for brine pump construction. Their investigation was geared towards mechanical, metallurgical and electrochemical impacts of these two types of steel when it is subjected to SCC. The testing

considered was metallographic, hardness testing, electrochemical long-term potential measurement and cyclic sweep [17]. SCC was tested for samples immersed in brine solution at 140°F with a *pH* of 8.31 for an hour before starting the test for a duration of a day and then started to collect potential measurements. Their SCC designed test rig consisted of a proof ring SCC testing chamber and a camera [17] as seen in *Figure 9.*

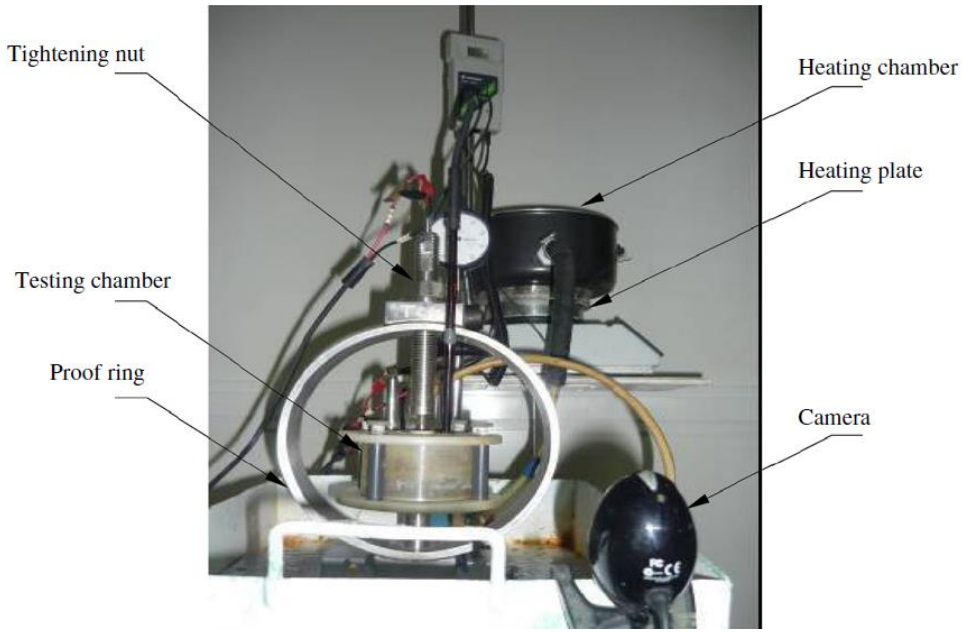

Figure 9. Stress Corrosion Cracking test set up.

The brine was heated at 55℃ and 60℃ and was free to move via gravity. The camera in *Figure 9* was installed as part of the SCC rig monitors, that detects the movement of the dial indicator which represents the failure of the material under testing [17]. The two samples were put through a constant load of 8403N and after 14 days, a fracture was detected and the test was suspended [17]. The samples that fractured during the test were compared to new samples that have not been subjected to SCC yet. The tests proved that austenitic steel was much more ductile when compared to super duplex steel. Austenitic UNS S31603 had 52% elongation, 73%

reduction in area with a yield strength of 284 N/mm^2 and super duplex UNS S32750 had 35% elongation, 68% reduction in area with a yield strength of 608 N/mm^2. *Figure 10* shows SCC test rig designed to follow ASTM and NACE Type A testing methods.

Amann et al., performed an analysis of cavitation erosion of steel in saltwater solution using electrochemical methods. Cavitation erosion corrosion creates damage in centrifugal pumps, water turbines, control valves, and motors [18]. A sonotrode was used to create bubbles that collapsed on the surface of the steel sample used for the experiment, while open circuit potential measurements were taken with cavitation erosion corrosion quantified for three different steel samples 1.4125, 1.3505 and tempered 1.3505T in 0.6M NaCl solution at room temperature [18]. Electrochemical evaluation proved that the free surface exhibited high corrosion current density [18].

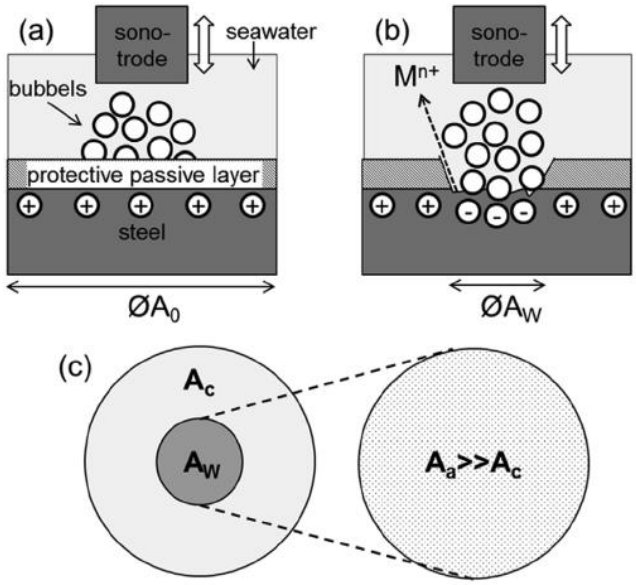

Figure 10. Sonotrode used to generate cavitation.

Figure 10 above shows: (a) Sonotrode in seawater generates cavitation bubbles that collapsed on the steel surface; (b) Cavitation erosion whereby complete removal of protective

passive layer by cavitation. Erosion and corrosion of fresh surface results in the dissolution of metal ions in NaCl solution. *Figure 10* shows mechanically removed static corrosion present and the depiction of synergistic effects; and, (c) A defined part of the total cavitation area (A_W) within the complete surface area (A_0) is considered as the anode (A_a), and the residual area in this case acted as cathode (A_C) [18].

2.1.4 Electrochemical Frequency Modulation

The nonlinear characteristics of a system that is corroding can be measured by using Electrochemical Frequency Modulation (EFM) [19] which also has the ability to monitor corrosion online [19]. When two sine waves are applied to a surface of a material that is corroding, electric current responses can be generated at various frequencies and compared to the frequency of the signal applied [19].

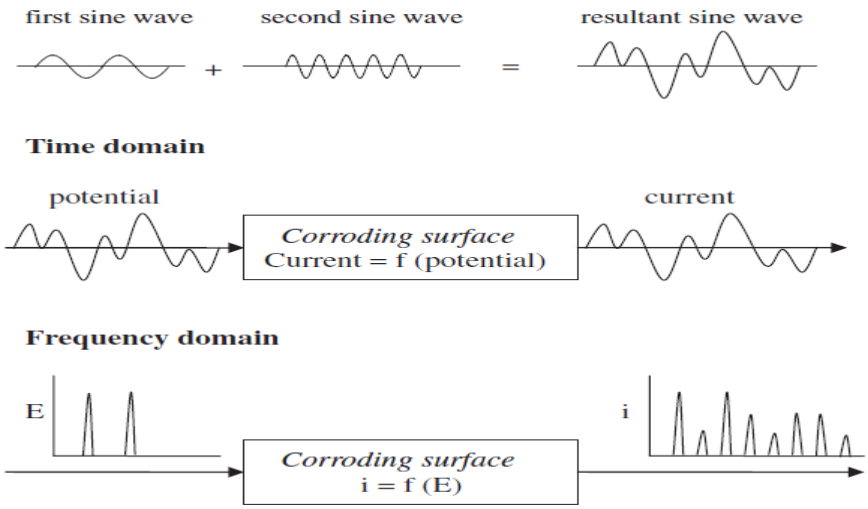

Figure 11. Principle of the Electrochemical Frequency Modulation technique.

*F*igure *11* shows the signal steps involved for electrochemical frequency modulation. A signal consisted of two sine waves superimposed on a material surface in time and frequency domains.

The two sinewaves are summed up and the resultant potential wave is impressed on the material that is corroding. The high harmonic content in the sine waves due to the applied voltage signal detected pitting in the material tested for corrosion. A mathematical evaluation of the current components and various frequency provided corrosion rate of the material [19].

There is no need to have information of the Tafel parameters with the electrochemical frequency modulation approach because, the rate of corrosive tendencies, Tafel parameters, and the factors related to causality can be evaluated in a single test using the EFM method. This technique has been used to evaluate pitting corrosion [19]. A potential perturbation signal consisting of two sine waves are impressed on a surface that is corroding and analysis of the current components at various frequencies can provide an insight into the corrosion rate and Tafel parameters for the sample under test [19]. The following equations characterize the determination of corrosion current density and Tafel parameters [19].

$$i_{corr} = \frac{i_{\omega 1}^2}{\sqrt{48(2i_{\omega 1}i_{3\omega 1} - i_{2\omega 1}^2)}}$$

$$\beta_a = \frac{i_{\omega 1}U_0}{2\sqrt{3(2i_{\omega 1}i_{3\omega 1} - i_{2\omega 1}^2) + 2i_{2\omega 1}}}$$

$$\beta_c = \frac{i_{\omega 1}U_0}{2\sqrt{3(2i_{\omega 1}i_{3\omega 1} - i_{2\omega 1}^2) - 2i_{2\omega 1}}}$$

Where i_{corr} is the corrosion current density, U_0 is the amplitude of the applied signal, and β_a is the anodic Tafel parameter, and β_c is the cathodic Tafel parameter. Causality factors are expressed as a ratio of components of current response at harmonic values and

intermodulation frequencies as an example [19]. Harmonic component $i_2\ w_1$ is measured at a frequency $2w_1$ so intermodulation components of $iw_2 \pm w_1$ is measured at $w_2 \pm w_1$,

Hence, Causality factor 2,

$$= \frac{(iw_2 \pm w_1)}{i_2\ w_1},$$

and Causality factor 3,

$$= \frac{(iw_2 \pm w_1)}{i_3\ w_1},$$

Hang and Song carried out experiments using 3 electrodes cell, 2 of which were similar and represented working electrodes placed in seawater and the method used to examine corrosion was electrochemical frequency modulation technique [6]. Testing was conducted at different frequencies and amplitudes on Q235 steel after it was placed in a 0.6mol/L NaCl solution for 24 hours [6].

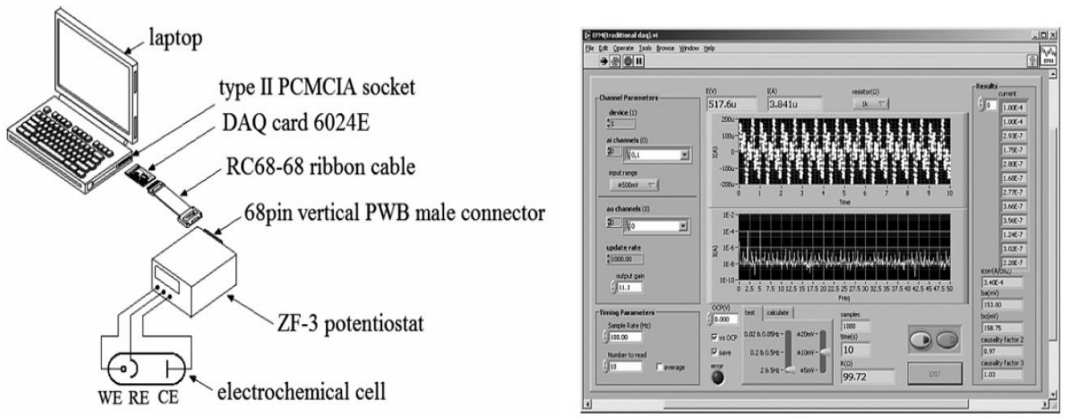

Figure 12. Virtual electrochemical frequency modulation.

*F*igure *12* shows the hardware setup and software panel of a virtual EFM system. An electrochemical cell was connected to a potentiostat and these interfaced with a computer screen.

An EFM data collected at different frequencies with resistor values of $1K\Omega$ and a $220\mu F$ capacitor with a pure resistor that has an impedance which is not dependent on frequency. The experiment was conducted on Q235 steel in 0.6 mol/L NaCl aqueous solution for 24 hours and it was observed that for reliable corrosion rates when EFM is used, low frequencies of perturbation are desired to minimize capacitance which can introduce error in corrosion rates. The result from this experiment is consistent with other research that has been conducted in the past using electrochemical frequency modulation technique . Although the Hang and Song investigation employed electrochemical frequency modulation to measure corrosion rates, the corrosion studies did not distinguish the different modes of corrosion [6].

2.1.5 Self-Diagnostics Methods

Kim et al., studied how to apply self-diagnostic methods to detect the failure of a valve due to corrosion. The system employed retrieved information from an Air Operated Valve (AOV) system with sensors, and the information collected was processed and saved into a database. A decision-making algorithm was used to develop various faults into a fault library [8].

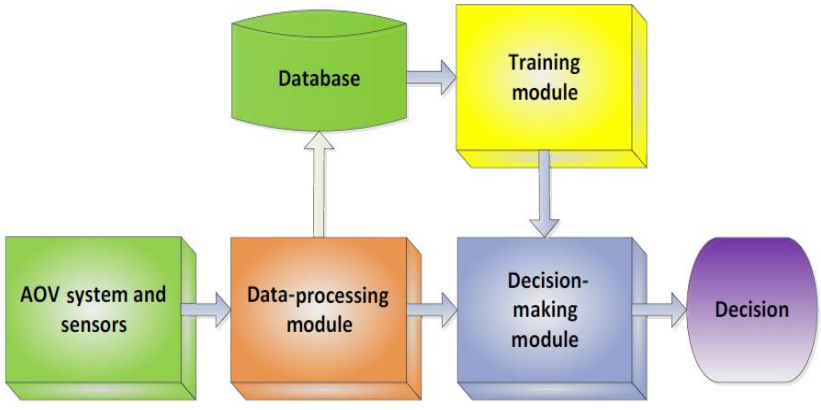

Figure 13. Self-diagnostic system.

Figure 13 shows a block diagram of the self-diagnostic monitoring system for air operated valve. The system consisted of an AOV system and sensor; the data is then sent into a data processing module. The raw data from the data processing module is stored in database after images of the data are collected. The data gathered are both analog and digital data forms. The training module retrieved the data and used it in decision making via algorithms [8].

Although corrosion was mentioned as one of the causes of degradation of equipment, the decision-making algorithm did not evaluate any faults related to corrosion. There are different types of air operated valves, however, and Kim et al. did not mention the type of air operated valve in this experiment [8].

2.1.6 Constant Load Method

While studying the impact of SCC on 316 Austenitic steel immersed in a NaCl solution at room temperature where the stress on the material under test was held constant [7]. Elsariti et al., reported that Austenitic stainless steel will crack at some point when the material is exposed to a corrosive situation where chlorides are present. The test was performed by using NaCl dissolved in tap water [7]. The experiment was constrained by the fact that they could not reproduce cracks for the 316 Austenitic stainless steel after 404 hours. They also noted in their investigation that this material was resistant to surface attack, which implies that the material was corrosion resistant and for that reason, a longer duration was needed to verify the result of corrosion [7].

After 1,244 hours and 1,678 hours during the same test, cracks started to appear on the 316 stainless steel while the strain on the steel was kept at a constant load. The results showed that, although there was no crack in the first stage of the experiment with 3.5wt% NaCl solution, the data gathered was consistent with already published data. The experiment also showed how

challenging it is to investigate SCC when the corrosive solution is not a true representation of a corrosive environment such as seawater. Elsariti et al., concluded that to yield better results when using a low concentration solution of NaCl, a longer period is needed i.e. greater than two months [7].

2.1.7 Scanning Electron Microscopy Study

A Scanning Electron Microscope (SEM) was equipped with a detector system that collects electrons [20]. The microscope can be used in pressures less than 133 Pa to access imaging of samples that are under beams full of charge [21].

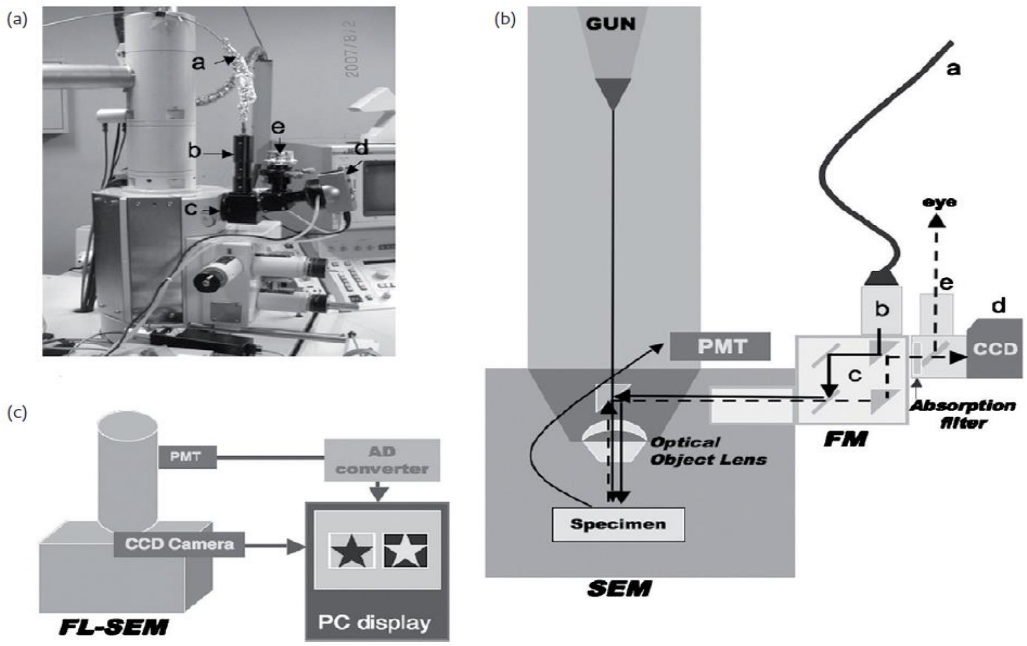

Figure 14. Scanned Electron Microscopy.

Figure 14 shows (a) a view of the fluorescence SEM (FL-SEM) including a 473nm laser light source (b) a schematic diagram with view of the FL-SEM, consisting of the SEM and the fluorescence microscope (FM) units, (c) a diagram that reveals the flow of SEM and FM image signals displayed on a personal computer. The system consisted of a prism and mirror, and an

external Charge Coupled Device (CCD) camera, an eye piece, and a photomultiplier tube (PMT) [20].

Figure 14 show a scanned electron microscope set up for corrosion examination. The FL-SEM beam of electrons penetrates small holes which were at the center of a mirror and the lens that views the object which made it possible to view the specimen . The images of the SEM were sent to a converter through the photo multiplier (PM). The specimen's fluorescence emissions were projected on to a CCD camera. Practically the FM produced images were retrieved before the SEM images so as to avoid possible fluorescence damage during the process. The FM and SEM images were displayed on computer screens via the CCD camera. The image produced by the SEM is in a panchromatic form [21]. *Figure 14* shows a setup of SEM system for scanned electronic microscopy.

Anikeev et al., investigated the hydrogen sulfide corrosion of stainless-steel clad carbon steel valves. [9]. They drew the conclusion that there were no macrostructural or micro structural defects when the welded overlay was introduced on to a sample of a cylindrical isolation valve, made of low alloy steel using optical and electron microscopy study [9].

Subari et al., presented a report of corrosive behavior when 316L steel was placed in the molten salt solution and using scanning Electron Microscope (SEM) to conduct morphological analyses to verify when corrosion took place [10]. The sample was left in a molded cup and soldered stainless steel 316L was placed in the cup, which consisted of a working electrode and auxiliary electrodes [10].

Before testing the steel, samples were cleaned with distilled water and subsequently ultrasonically washed in 95.6% ethanol. The corrosion analysis was in the form of weight loss

measurements. The test suggested that stainless steel 316L was less susceptible to corrosion when immersed in 20% NaCl solution [10]. The corrosion rate calculated was -0.5865 (mmPYx10000) and the rate of corrosion increased as the NaCl concentration increased. Subari et al., concluded that NaCl was a good candidate that encourages corrosion in eutectic salt solutions [10].

2.1.8 Ultrasonic Technique

Saluja et al., noted in their literature that current technologies for corrosion monitoring are intrusive and generally not a direct reflection of the weight loss of material. Corrosion control measures can save as much as 20-25% annually for the cost of corrosion mitigation. A commonly used technique to monitor corrosion is ultrasonic, where the sound velocity is used to estimate wall thickness and loss based on the time of flight ultrasonic technology as shown in *Figure 15* [22].

Measuring the wall thickness can be done even in the presence of low or high temperatures and with coating over the material in the case of piping. Righttrax is a tool used to measure or demonstrate the measurement of wall thickness. Data acquisition methods with software are used to analyze wall loss and wall thickness [22].

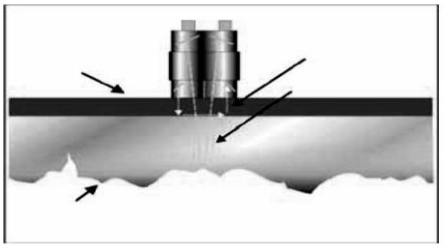

Figure 15. Ultrasonic time of flight technology.

Figure 15 shows the ultrasonic time of flight technique to monitor wall thickness using ultrasonic sensor. This is a non-intrusive technique where a transducer is mounted on a pipe to measure wall thickness of the pipe. The ultrasonic sensor is calibrated to the sound velocity of material of the pipe. Depending on the material of the surface this method can be used for high temperature surfaces [22].

2.2 Literature Gap

The method Hwang et. al, used could help make a difference between damages that may occur due to crack distorted AE signals, and normal AE signals. Hwang et al., also pointed out how other methods such as radiographic analysis and ultrasonic have certain limitations. However, there was no elaboration of these limitations as it relates to their study [3].

Estupiñán-López et al., demonstrated that pitting corrosion can be found on the surfaces of 2205 duplex stainless steel in an NaCl solution [4]. Du et al., acknowledged the fact that their findings could be used to identify the degree of ongoing corrosion when stainless steel is used in a nuclear power plant environment [5]. It is worth mentioning that, anti-corrosion studies can also be investigated using acoustic emissions measurement methods and techniques [5]. Comparing austenitic steel and super duplex stainless steel, the literature reviewed showed that duplex stainless steels are better suited for brine and sea water pump components [17].

Further studies are needed to verify SCC and its behavior in low concentration NaCl solutions as evident in the literature review. Especially the incubation periods need to be increased in excess of two months for SCC of evaluation [7]. The behavior of stainless steel 316L needs further analysis to understand different behaviors in different salt conditions [10]. Suggestions of studying high frequency RFID systems to detect corrosion on more dedicated

steel samples are recommended [2]. Sunny et al., also recommended further studies to introduce small transponders which could enhance the sensitivity for industrial applications of RFIDs [11].

Electrochemical frequency modulation techniques are a possible method that can be employed to further investigate corrosion monitoring and to evaluate forms of corrosion in the future [6]. Although Amann et, al., recognized that cavitation erosion corrosion is prominent in centrifugal pumps, water turbines, control valves and motors, they did not investigate cavitation erosion corrosion for such equipment [18].

2.3 Literature Review Conclusion and Problems to Address

The literature reviewed shows that there have been studies of different grades of steel in NaCl solutions, using various detection methods to monitor several corrosion mechanisms. Methods including RFID, AE, EN, EFM, self-diagnostic method, constant load and SEM were used in these investigations in the literature reviewed. The review of these literature also confirmed that most of the testing was conducted with steel samples that are not part of a process such as a chemical plant or in an actual component such as ball valves.

It is very important that future work focuses on investigations that will replicate environments that are close to actual chemical plant conditions. An investigation involving actual components i.e. a valve, within a hydraulic loop, with a corrosive media transported through the system is essential to the knowledge in the field.

Although several gaps were identified in the literature reviewed as describe above, not all will be investigated in this research. This research considered a flow loop in an environment where flow rates, temperature, pressure and ambient conditions are variables that can be monitored, with sodium chloride and acetic acid mixtures were present as the corrosive media. It

is proposed to monitor the wall thickness of a valve subjected to simulated process conditions using an ultrasonic sensor.

The research investigated the following topics using a hydraulic loop:

- Installed ultrasonic sensing transducers on a valve body and accessed how practical it was in the presence of sodium chloride and acetic acid solutions to monitor thickness loss or gain of the valve body.
- Investigated the possibility of verifying corrosion of a ball valve body via ultrasonic technology in the presence of sodium chloride and acetic acid.
- Observed and documented ambient conditions and its impacts to ultrasonic thickness measurements.
- Evaluated constraints of embedding ultrasonic technology on a ball valve for corrosion monitoring.

CHAPTER III

CORROSION CONCEPTS AND ULTRASONIC TECHNOLOGY

3.1 Corrosion Background

When metals are destroyed by electrochemical reactions, it is known as corrosion while physical destruction of metals can be grouped into erosion, galling or wear. A combination of physical and electrochemical degradation can also occur. These include erosion corrosion, and corrosive wear or fretting corrosion. When iron is involved, the term rust is used to describe the corrosive product or compound [23]. Metals such as iron will corrode when they are exposed to corrosive environment. This happens because metals tend to take their original form ores. The likelihood for a chemical reaction to happen is measured by the change in Gibbs free energy. Change in Gibbs free energy (ΔG) is an indication of the feasibility of a chemical reaction. The more negative the Gibbs free energy the greater the likelihood of a reaction. It is important to note that the likelihood to corrode is not a measure of reaction rate [23].

The corrosion phenomenon can be explained by the redox reaction namely, oxidation and reduction. Oxidation is the process of taking away electrons from an atom and reduction is the process where there is a decrease in positive charges of an atom [24]. Corrosion is very important because of its economics factors, safety, and conservation of natural resources. Economic factors dictate the considerable investment research in the field of corrosion study. In the US alone, economic losses amounting to 3.1% of the Gross Domestic Product (GDP) can be attributed to corrosion or approximately $276 Billion for 1999 and 2001 [23].

Corrosion can be grouped into low temperature or high temperature subgroups. There are other descriptions such as wet and dry corrosion. Vapor and gaseous conditions can also cause corrosion, and these are described as dry type when high temperatures are present [25].

Wet corrosion occurs when there is an electrolyte or liquid present. Research has proven that corrosion is prevalent when the relative humidity is greater than 60%. This condition presents a situation where water vapor will adsorb onto the surface of the metal [26].The rate of thinning of metals is generally quantified in mils per year (mpy) given by:

$$mpy = \frac{534W}{DAT}$$

Where *W* describes the weight loss of material in mg, *D* describes the density material in g/cm^3, and *A* is the area of the material that is corroding in in^2. The *T* in the formula is the amount of time that the material was exposed to corrosive situation or environment [25].

3.2 Forms of Corrosion

There are multiple mechanisms through which several of the corrosion mechanisms can be identified via visualization techniques and others that cannot be visually identified unless other methods or tools are used to help with identification.

Figure 16 shows images of several corrosion modes. These images are grouped into three. The first group is the type that can be seen by visual inspection. These are uniform corrosion, pitting corrosion, crevice corrosion and galvanic corrosion. The second group are the corrosion modes that may require the use of special tools to help identify. These include erosion corrosion, cavitation fretting, intergranular, exfoliation and de-alloying.

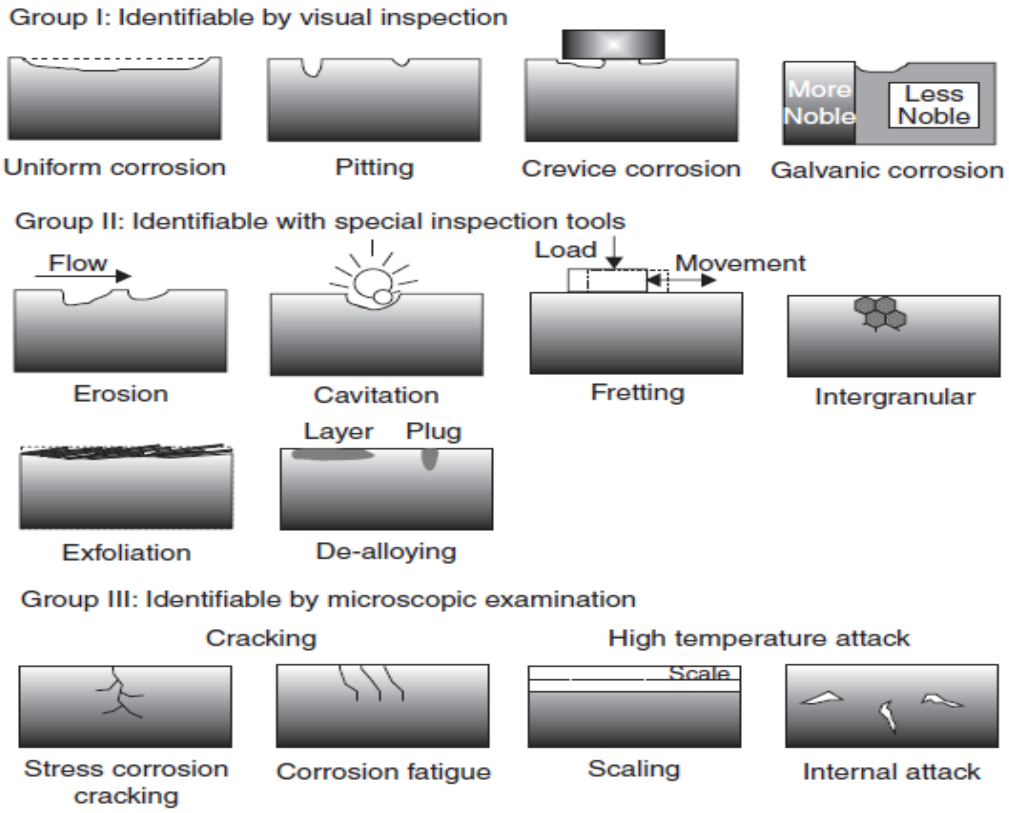

Figure 16. Forms of corrosion in groups.

The third group is a corrosion type that may require a microscope to help analyze. These include stress corrosion cracking, corrosion as a result of fatigue, scaling and internal corrosion attack [24].

3.2.1 General Attack (Uniform Corrosion)

When metals are generally exposed to an atmosphere where chlorides are present, a general type of corrosion may occur, and some examples are moisture, oxidizers and oxygen . This type of corrosion can be predicted, and with visual inspection, can be analyzed and quantified. Uniform corrosion is usually seen in pipelines and it has been an industry practice during design to introduce corrosion allowances to help reduce the impact of uniform corrosion [24].

3.2.2 Pitting Corrosion

Pitting is a form of localized corrosion where portions of the material are affected by material loss and the surfaces of the material will develop pits or crates that may be visible during inspection. Pitting corrosion tends to occur where there are liquids that are moving slowly in a pipe or liquids that are not moving at all such as in a vessel. Pitting corrosion can often be diagnosed by visual inspection. It is quite a challenge to model or predict when compared to uniform corrosion [24].

The pit depth probability function can be expressed as a probability function [F(x)] where λ represents location and α represents scaling factor.

$$F(x) = exp(-exp)\left[-\frac{x-\lambda}{\alpha}\right]$$

Gumbel had proposed the use of Extreme Value Statistics (EVS) to analyze pit depth and how these depths are distributed. There have been other statistical analyses proposed but Gumbel was credited for originally developing of the Extreme Value Statistics (EVS) [24]. Practically and in previous research where the Gumbel distribution was applied there was not enough pitting corrosion data available to construct the Gumbel line. Notwithstanding the validity question around Gumbel distribution, there seem to be some support for it use for pitting corrosion [27].

3.2.3 Crevice Corrosion

Stainless steels that are exposed to seawater may develop deep pits in a short period of time (months). These pits create crevices also known as stagnant electrolyte. Crevices will develop usually between cracks of metals surfaces and this happen to metals that are dissimilar and similar metals as well [23]. The sequence in crevice corrosion (*Figure 17.* (a)) initiated when

there is a difference in aeration between the crevice microenvironment and the external surface of the material. Dissolved oxygen reacts with the metal.

Figure 17 below shows (b) oxygen prevented from diffusing creating a differential aeration cell between the crevice microenvironment and the external surface of the material. Oxygen in the bulk solution becomes relatively cathodic while crevice becomes anodic. *Figure 17* (c) shows how the corrosion products decreases the pH around the anode leading to even greater corrosion rates within the crevice [24]. It is very likely that the pH in the crevice area maintained high acidity due to the production of metal ions from the anodic reaction.

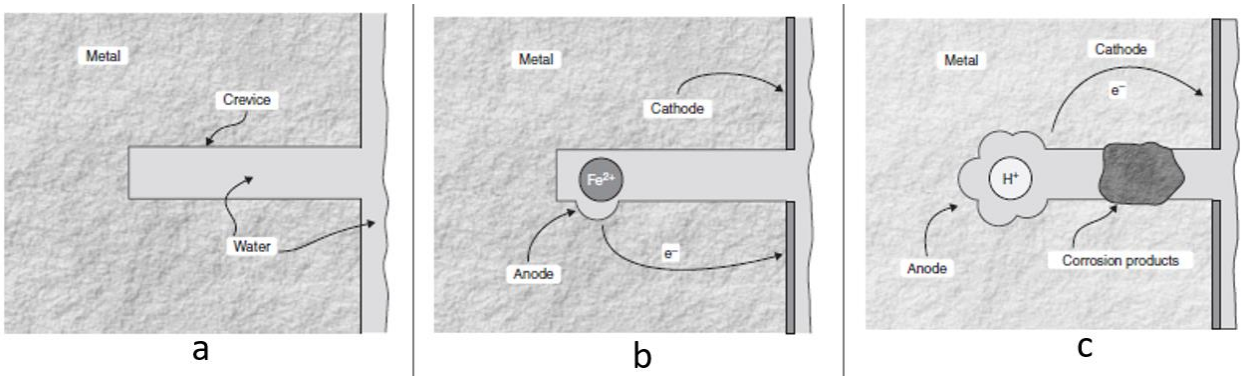

Figure 17. Stages of Crevice Corrosion.

The corrosion products will dominate and create a seal in the crevice. Some examples of crevices are corrosion under insulation (CUI), steel deck corrosion under phenolic roofing insulation, corrosion of double-pane wand poultice corrosion in cars [24].

3.2.4 The Nernst Equation

When a metal is present in its own ion solution with activity that is equal to unity then the standard electrode potential can be applied E^0. This situation is not always the case and it is not very common. The Nernst equation is used to calculate half-cell potential different concentration in the standard electrode potential form and used to construct the pourbaix diagram.

In a general form of electrochemical reaction,

$$aA + bB \leftrightarrows cC + dD$$

Where a represent number of moles of reactant *A* and b represent number of moles of *B* reactant. Then,

$$\Delta G^0 = \sum_i v_i u_i^0 \, (products) - \sum_i v_i u_i^0 \, (rectants)$$

Incorporating temperature the Nernst equation is represented as,

$$E = E^0 - \frac{2.303RT}{nF} log \frac{a_C^c a_D^d}{a_A^a a_B^b} \quad \text{at } 25℃$$

Where,

$$K = \frac{a_C^c a_D^d}{a_A^a a_B^b}$$

is defined as the equilibrium constant of the electrochemical reaction [26].

3.4 Corrosion Kinetics

Pourbaix diagrams are used to determine corrosion behavior but do not yield the rates of corrosion. This diagram can give an initial understanding of a corroding system but will not define the rate at which the corrosion is happening. Methods used to determine corrosion rates are weight loss, weight gain, and chemical analysis of solution. Some other methods are gasometrical principles, where a reaction within the system is producing gas, thickness measurements, electrical resistance probes, inert marker method and electrochemical principles.

Among the methods mentioned, thickness measurements give a practical understanding of the rate of corrosion overtime of a system that is in a corrosion environment. For example, this

method is used to understand corrosion rates of a railway hopper cars, tanks for bulk chemical storage and pipelines. [26]. This research as described focused on thickness measurement for a chemical process system that is running over a considerable period, and monitoring corrosion of a valve using ultrasonic sensing technology.

3.5 Ultrasonic Background

Ultrasonic testing has been used in science and engineering application for a very long time and the technology and its uses have grown over the years. The technology has an advantage in that it can be used for nondestructive or non-intrusive sensing [32]. Ultrasonic waves will propagate in solids, liquids and gases. Ultrasonic energy will interact with a sample and information collected can be used for data analysis. This section will discuss the principles and fundamentals of ultrasonic technology, how this energy is initiated and characteristics of ultrasonic [32].

Humans can hear sounds at frequencies around 20 Hz to 20,000 Hz (cycles per second). Ultrasonic waves are above these frequencies. Consider a medium that is continuous, ultrasonic may be described as the equilibrium between inertia forces and the elastic deformation. Ultrasonic energy velocity is a function of the properties of the material and geometry of the medium. The relationship between stress σ, and particle velocity is $\sigma = zv$, where z is known as the acoustic impedance of the ultrasonic waves [32].

$$z = \frac{\sigma}{v} = \rho c$$

Where ρ describes the density of the material and wavelength is denoted by c. The acoustic impedance is the resistance that a material offers to the vibration when force is applied.

Suppose the acoustic impedance are the same for any two media, transmitting ultrasonic wave within these two media will be at the maximum [32].

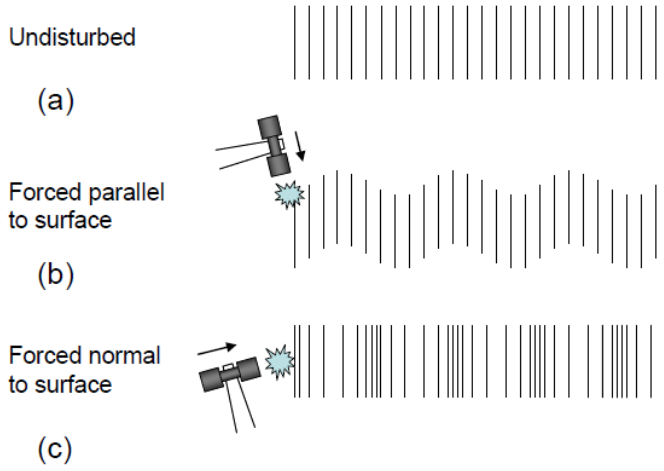

Figure 18. Images of ultrasonic waves where bulk specimen is present.

Figure 18 illustrates waves images when a bulk specimen is exposed to ultrasonic waves (a) Shows state of equilibrium where disturbances are not present. (b) Shows forces parallel to surface waves are considered to be shear or transverse vibration (c) Shows forces to normal surface where the waves are described as vibrations in the longitudinal form. [32].

3.5.1 Characteristics of Ultrasonic Waves

The type of wave used for ultrasonic testing can be expressed by the solution of the wave equation and wave equation predicts the behavior of the type of ultrasonic wave. There are two types of waves, bulk waves which are fundamental waves that propagate within an object but do not depend on shape or boundary and guided waves which propagate along the interface of a material or the surface of an object. There are two types of bulk waves isotropic i.e. longitudinal (also known as dilatational, or compression, or primary) and shear (also known as distortional, or transverse, or secondary) [32]. Longitudinal waves are waves where the particle motion is

parallel to the wave propagation while shear waves are waves where the particle motion is perpendicular to the wave propagation. Both shear and isotropic waves can exist within solids since solids are rigid and hence resistant to shear and compressive loads [32].

Depending on the boundaries or the shape that the object has, three forms of guided wave may be present. These are Surface Acoustic Waves (SAW), plate waves and rod waves. SAW will propagate on a surface and its disturbance amplitude exponentially will decay depending on the object. SAWs come in different forms like Rayleigh, Scholte, Stoneley, and Love waves [32]. Rayleigh waves are the most well-known wave and Rayleigh waves are also referred to as SAW. Rayleigh waves are waves whose particle motion is elliptical, and the depth of penetration is in the order of one wave length [32].

Plate waves occurs when ultrasonic waves propagate through a plate which has a finite medium. The wave will resonate in this type of medium. Lamb waves occurs when there are multiple layers associated with the object that ultrasonic wave is propagating through. Guided wave propagation is a function of the plate thickness, and the frequency. The frequency is also a function of the wave velocity and this frequency is known as the frequency of dispersion [32].

3.5.2 Wave and Sound Velocity

The wave velocity of an ultrasonic wave can be deduced from the wave equation. The wave equation for isotropic, longitudinal and shear is expressed as:

$$v_1 = \left(\frac{E}{\rho} * \frac{1-v}{(1+v)(1-2v)}\right)^{1/2}$$

$$v_s = \left(\frac{E}{\rho} * \frac{1}{2(1+v)}\right)^{1/2} = (G/\rho)^{1/2}$$

Where v_1 and v_S are the longitudinal and shear waves respectively. *E* is the Young Modulus, *v* is the poisson's ratio *G* is the shear stress and ρ is the density of the object [32]. In a finite medium when considering bulk waves, the phase velocity is constant for a given medium but will vary depending on thermodynamics influences including compressibility, density, external pressure, and temperature among others [33].

3.5.3 Ultrasonic Work and Signal Attenuation

There are losses as the signal propagates through a medium and factors that normally contribute to attenuation are the viscosity and thermal conductivity. In a molecular process, acoustic energy may change to become molecular energy. In fluids, these changes are expressed as a phase difference between the acoustic pressure and how the medium changes as a result of density or volume. Signal attenuation of an ultrasonic wave happens when the amplitude of the wave decreases as the signal propagates through a medium.

Assuming the pressure *P* and the volume *V* changes due to acoustic wave, the work done $W = -\int pdV$. Therefore, work done is the area under the curve of the acoustic system as shown in *Figure 19.* Losses within the system changes along the path when expansion is taking place from A to B, and compression occurs from B to A.

Figure 19 shows (a) Reversible transformation from A to B and from B to A in a lossless medium; (b)Transformation from A to B and from B to A in a lossy medium.

For a displacement *u* of a wave,

$$u = u_0 expj(wt - kx)$$

When there is no dissipation of wave energy, $I \propto u^2$ for a plane wave. Assuming that dissipation is prevalent then wave vector $k \rightarrow \beta - j\alpha$ a complex expression where α is the attenuation coefficient. Then,

$$u = u_0 expj(wt + \beta x)\exp(-\alpha x)$$

Suppose there is a plane wave where $I \propto u^2$ and acoustic intensity decays to $\exp(-2\alpha x)$.

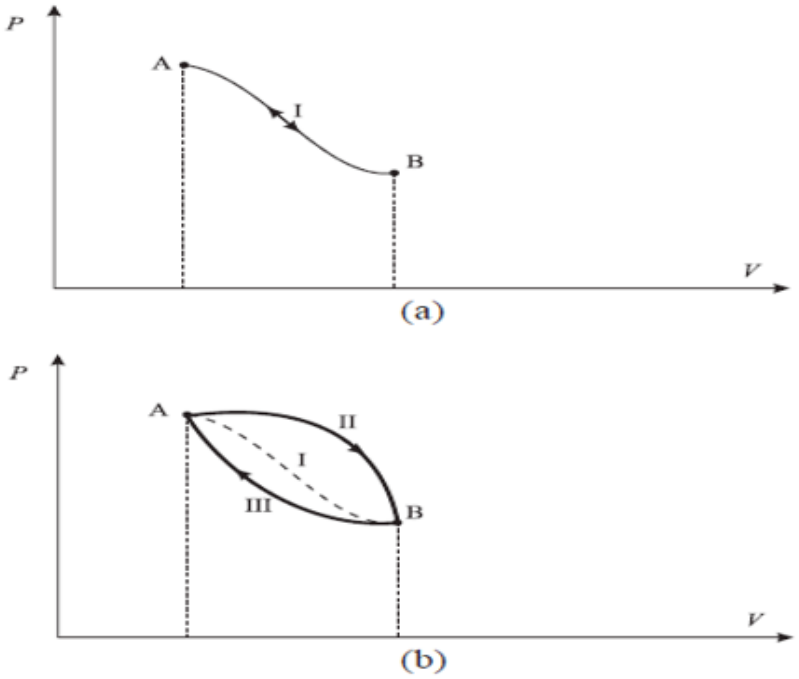

Figure 19. P-V diagram and system reversibility.

Practically the attenuation factor for the amplitude of the wave is ration r_{12} for a wave located at a position x_1 and x_2 [33].

And,

$$r_{12} = expa(x_2 - x_1)$$

Attenuation (unit in Nepers),

$$\equiv \ln(r_{12}) = \alpha(x_2 - x_1)$$

Some other factors that may influence attenuation are when beams are spreading, energy is absorbed, when non-linearity is present , transmission occurring at interfaces, inclusion due to scattering or defects, and tendencies of Doppler effect [32].

Attenuation *A* can be described quantitatively with the attenuation coefficient α using the following equation

$$A = A_0 * e^{-\alpha x}$$

Where *A* is the peak of the amplitude of the wave at a distance *x*, the propagation of the wave α is given as dB/m or Neper/m or Np/m and A_0 is the initial peak amplitude of the wave. The attenuation coefficient has a relationship between the peak variation and the propagation distance [32]. Decibel (dB) is typically used to express attenuation (dB) as:

$$= 10log_{10}(r_{12}^2)$$

$$= 20(log_{10}e)\alpha(x_2 - x_1)dB$$

Where, $\alpha = dB/m$ relationship between dB Neper,

$$\alpha\left(\frac{dB}{m}\right) = 20(log_{10}e)\alpha\left(\frac{Np}{m}\right) = 8.6686\alpha\left(\frac{Np}{m}\right)$$

3.5.4 Wavelength

Distances travelled by the ultrasonic wave during a cycle is the distance from a compression area to another, which is also known as wavelength. Frequency is the number of waves that are transmitted in a second [34]. The wavelength is expressed as $\lambda = v/f$, where v is the velocity (m/s) of the ultrasonic wave and f is the frequency (cycles per second, Hz). Wavelength (in meters) is very key and an important parameter in the evaluation of ultrasonic waves [32].

3.6 Reflection and Transmission

In the presence of two media, as shown in *Figure 20,* ultrasonic waves will reflect when they propagate via the interface. Parts of the waves are reflected to medium 1 and the rest will propagate through medium 2. The amplitude of the reflected wave is A_R and the incident wave is A_I and these can be expressed as the reflection coefficients and transmission coefficients respectively below where R is the reflected coefficient and T is the transmitted coefficients [32]:

$$R = \frac{A_R}{A_I} = \frac{Z_1 - Z_2}{Z_1 + Z_2}$$

$$T = \frac{A_R}{A_I} = \frac{(2Z)_1}{(Z_{1+}Z_2)}$$

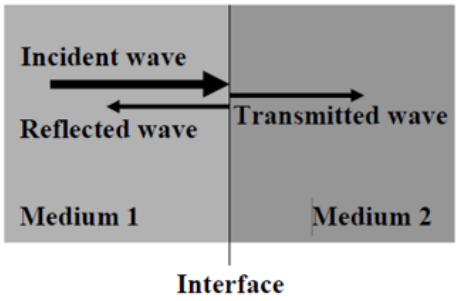

Figure 20. Wave interface diagram.

Subscript 1 and 2 represented in the equation are for medium 1 and medium 2, and Z is the acoustic impedance. When the impedance of both media are equal, that is when the wave propagation is at the maximum [32].

3.6.1 Ultrasonic Wave Refraction and Mode Conversion

An oblique impingement of the ultrasonic wave on medium 2 (see *Figure 21 and 22.)* interface may create a refraction where there is a difference between the incident and the transmitted wave. This refraction is a result of the velocity differences at both ends of the media interface. This is an expression that can be deduced from Snell's Law [32].

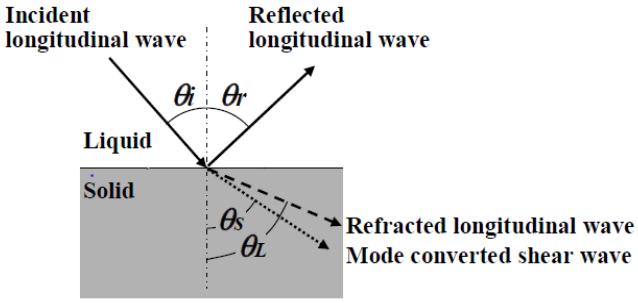

Figure 21. Wave reflection and refraction diagram.

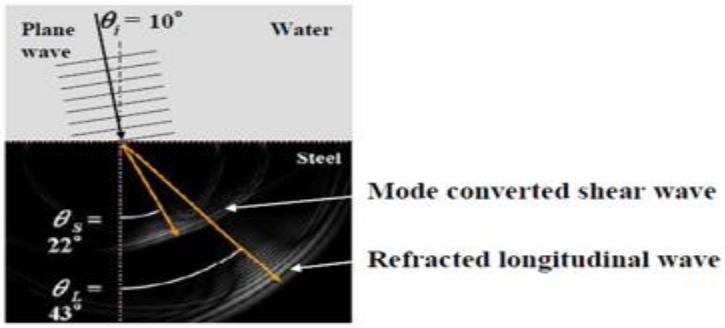

Figure 22. Simulated refraction and mode.

Mode conversion is when one type of wave is converted to another during refraction. If for example, a wave that is longitudinal incidents on an interface where the medium is a liquid, and solid, there is a partial transmission, (refracted longitudinal waves) and also shear wave in the solid [32]. *Figure 22*. shows the results and mode conversion and it can be seen that an incident wave of 10° in water is refracted at an angle of 43° in steel and then changed to shear wave at an angle of 22° of refraction [32].

3.7 Ultrasonic Measurements

3.7.1 Ultrasonic Contacting Transducers

The transducer changes electrical energy to mechanical energy and this energy is inferred as an ultrasonic vibration. Piezoelectric materials with crystalline characteristics, for example

quartz, can be used. The piezoelectric material produces electrical energy when subjected to mechanical stress and for this reason piezoelectric materials are used to detect ultrasonic waves. Materials in the forms of barium titanate $B_aT_iO_3$, lead metaniobate $P_bN_b2O_3$ and lead zirconate titanate (PZT) are known to have piezoelectric effects [32].

The supply to the piezoelectric element operates at the resonant frequency of the piezoelectric material. Polyvinylidene fluoride (PVDF) is a polymer that produces piezoelectric effects and can be used to make ultrasonic transducers [32]. PVDF has a very low coupling factor, low impedance, and low dielectric constant. These reasons make PVDF suitable for high oscillation frequency applications of up to 100MHZ [35].

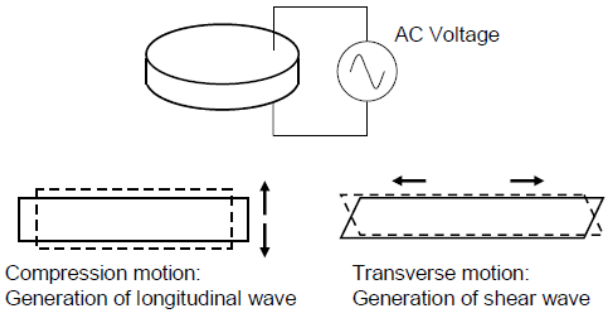

Figure 23. Diagram of piezoelectric plate.

Figure 23 shows a diagram of a piezoelectric element energized through an ac voltage that is supplied to the plate. A compression motion will generate longitudinal waves that will that can be measured as a voltage signal and a transverse motion will generate shear waves. On the other hand, voltage supplied to the plate will yield vibrations.

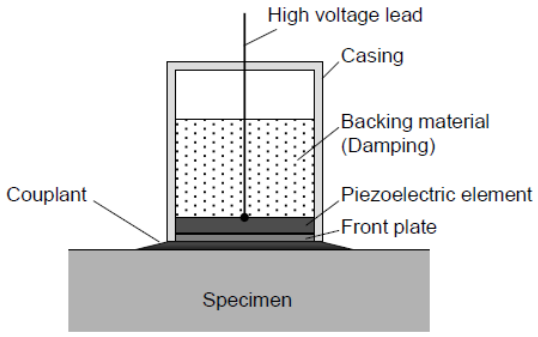

Figure 24. Piezoelectric transducer and coupling.

Figure 24 shows the construction of a piezoelectric material and the element is protected against external and environmental stresses. The specimen is coupled to the casing which contains the piezoelectric element, high voltage leads and a damping material. To maximize the ultrasonic energy, it must behave as an impedance matching device which means that maximum ultrasonic waves are transferred from the transducer through the specimen with impedance as close to zero as possible. The back wall acts as a damper, changing the resonant frequency so that ultrasonic waves reflection from the backwall can be deleted [32].

One of the drawbacks of piezoelectric and magneto-strictive effect is the decrease in signal effectiveness as temperature increases as the effect will no longer exist at curie (some material will lose their magnetic properties) temperature [32]. Sometimes, coupling medium such as gel, liquids, or grease are used to create better ultrasonic wave transmission. Without the coupling medium, a large air gap may exist which increases the acoustic impedance between the specimen material and ultrasonic transducers. This is a significantly huge practical drawback for contact type transducers in ultrasonic technology applications [32].

3.7.2 Non-Contact Transducers

The methods that exist for non-contacting are optical, electromagnetic and air coupled. An irradiated high energy pulse on the surface of the specimen creates thermoelastic and ablative effects. Longitudinal, shear and guided waves can be produced at varying frequencies by altering the laser irradiation. Ultrasonic energy waves are therefore detected by this method by quantifying the displacement caused by the ultrasonic energy. This method can be used for large distance and high temperature applications as well [32].

Electromagnetic Acoustic Transducers (EMAT) is another method that is used to generate ultrasonic energy and receive it where no coupling medium is required between the specimen under test and the ultrasonic transducer [32]. A stack consisting a of coil and magnet are used in an environment where electrical conductivity is present. Placing the coil near the surface of a material to be tested creates pulse currents at an ultrasonic frequency. An eddy current is then induced into the material surface by means of electromagnetic induction due to the static magnetic field developed [32]:

$$Lorentz\ force\ \ F = J * B$$

Figure 25 show a permanent magnet with north and south pole and an illustration of how Lorentz force is used in a magnetized condition to generate ultrasonic waves. Where *J* is the eddy current and *B* denotes the static magnetic field. This force produces high frequency vibrations. EMAT are able to generate and receive ultrasonic signals simultaneously [32]. Coupling is not needed because, on the surfaces between the transducer and specimen, there is electro- mechanical conversion due to electromagnetism. This method can be used for moving specimens, rough surfaces, vacuum conditions and situations where hazards are present [32].

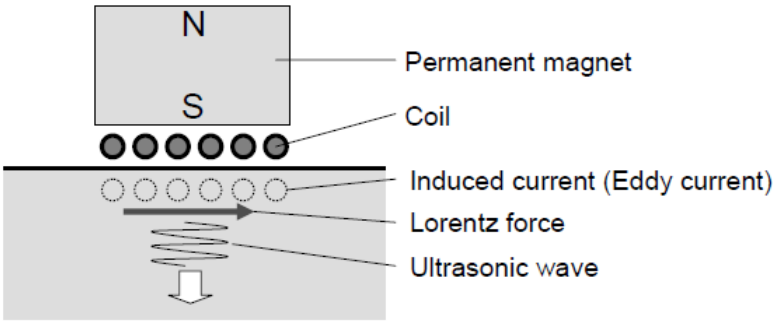

Figure 25. Acoustic transducer wave generation.

Air coupling is a method used for non-contacting ultrasonic, but it has a high attenuation coefficient due to the air used as a medium between the transducer and the specimen under test. When a capacitor type air coupled transducer is used it provides much more effective coupling with a wider frequency band when compared to the frequency of the air coupling applications. The frequency for the capacitor type is between 100KHz to 2MHz [32].

3.7.3 The Ultrasonic Measuring System

Figure 26 shows a block diagram of an ultrasonic system. The synchronization generator initiates the trigger with 1,000 per second. The pulse-generating element is known as the pulser. The pulser generates electrical voltage to the transducer and then, ultrasonic waves are created at an equal rate of repetition. The reflected signal is detected by the transducer which is amplified and displayed for data analysis **[32]**.

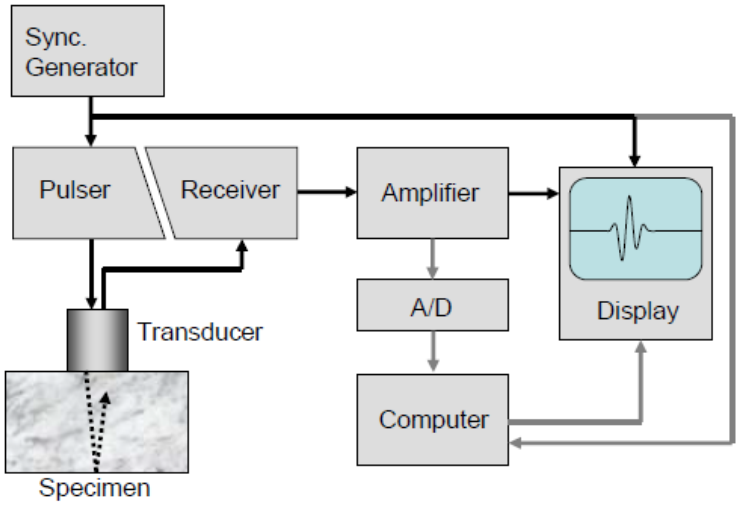

Figure 26. Ultrasonic measuring principles.

Figure 26 shows construction of basic ultrasonic measuring system used for generating and detecting ultrasonic waves.

3.7.4 Ultrasonic Transducer Configuration

Figure 27 below show how ultrasonic transducers can be configured. (a) Is the most widely used to measure reflected waves from a defect or the opposite side of the specimen. Through-transmission where two transducers seen in (b) is probably the second most widely used configuration. The third configuration is known as pitch-catch configuration where two transducers are located on the same side of the specimen as shown in (c).

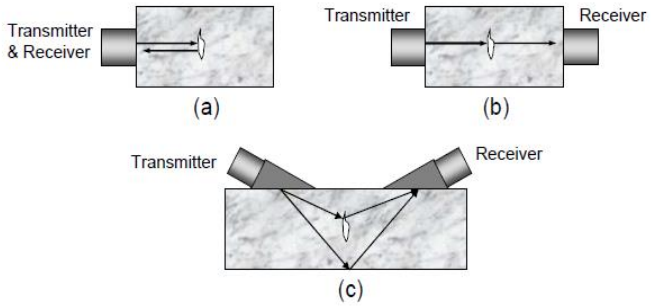

Figure 27. Ultrasonic transducer configuration.

The pitch catch configuration can be of benefit in the case where the back wall is not parallel to the front wall or there is some challenge to use normal incidence ultrasonic beams [32]. *Figure 27* shows three types of ultrasonic transducer configurations used for ultrasonic measurements [22].

3.8 Ultrasonic Technology Applications

Ultrasonic transducers have many applications such as in logging wells in the oil and gas industry. There are also applications in transportation and health industry. Ultrasonic transducers have been used in instrument measurements such as level measurement, concentration and thickness. Other application for ultrasonic transducers are industrial cleaning, welding application, and are used for fuel measurements of gasoline, diesel and natural gas in automobile [36].

Ultrasonic technology is used to prepare nanomaterials by using an ultrasonic spray pyrolysis method. Ultrasonic Spray Pyrolysis (USP) is a process where droplets are generated by ultrasonic waves to synthesis nanoparticles and deposition of thin films. This is a new and promising method that is used in laboratories around the world [37].

Membrane Bioreactor can be used for wastewater treatment and are, a combination of a biological sludge treatment with a filtration system. Fouling is a challenge for the membrane in these reactors and therefore applications has been limited for membrane bioreactors in wastewater applications. The type of fouling present in a membrane bioreactor system are organic fouling, biofouling and inorganic fouling. Cleaning of the fouling in the membrane can be achieved by using ultrasonication which can be performed while the reactor in-situ or ex-situ. The liquid in the reactor is exposed to ultrasound was creating low pressure and high pressure

when the ultrasonic waves expand and compress which produce a cavitation phenomenon on the surface of the membranes in effect cleaning the surface of the membranes of the reactor.

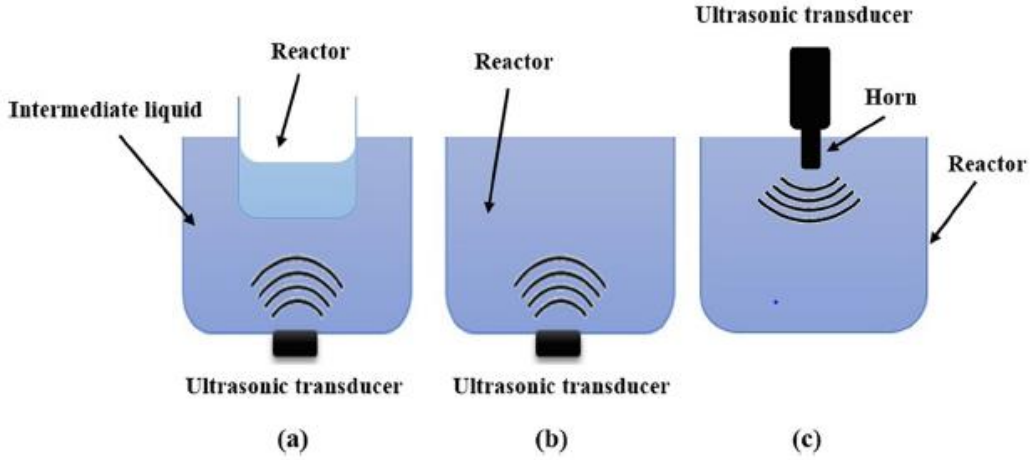

Figure 28. Ultrasonic transducer position and irradiation.

Figure 28 shows how ultrasonication is applied in cleaning a reactor through indirect (a) Indirect ultrasonic irradiation, (b) direct ultrasonic irradiation in bath and (c) direct ultrasonic. With the indirect irradiation the produced ultrasound goes through the fluid. In the case of the direct irradiation the ultrasonic transducer is in direct contact with the reactor or the transducer can be mounted inside of the vessel [38].

Ultrasonic technology has been used in the processing of metals in manufacturing for welding or to improve product quality through inspection. The impact that ultrasonic energy has on metals can be compared to heat energy used to soften a material. The ultrasonic energy that is needed to soften a material is about 10^7 times less when compared to traditional methods for softening a material. Ultrasonic is very clean, cost effective and does not require pre welding or post welding evaluation. Ultrasonic welding use high frequency vibrations and pressure to create joints for dissimilar metals with different and significantly large melting points [39].

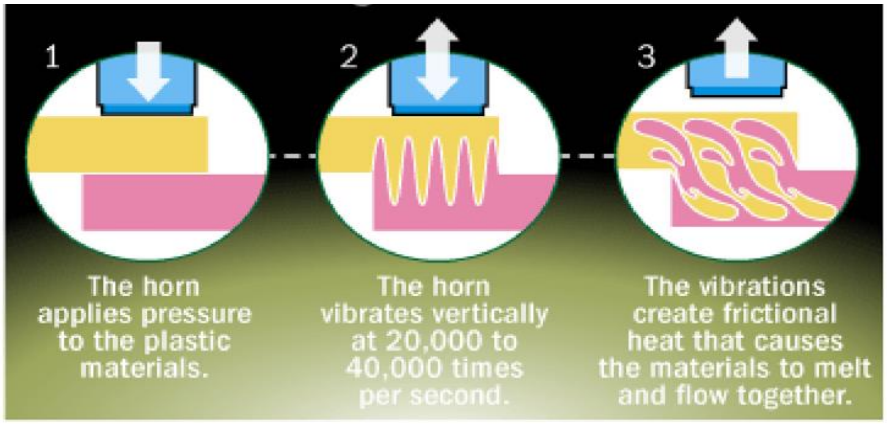

Figure 29. Stages of ultrasonic welding.

Figure 29 shows the stages of ultrasonic welding and during the process of ultrasonic welding, a horn is used to introduce ultrasonic vibrations via ultrasonic energy applying pressure to the materials that is been welded, the vibration occurs at a rate of 20,000 to 40,000 times per second. A frictional heat is created in the process which causes the material to soften and flow [39].

One of the practical applications for ultrasonic technology is to measure distance for various process media that ultrasonic waves are exposed to. This distance measurements are based on the discontinuity of the ultrasonic waves at boundaries between dissimilar fluids. Ultrasonic signals are transmitted and received such that the distance measurement is derived from the time the signal is transmitted and the time the ultrasonic signal is received at the source. Such applications are found in snow layer measurements to determine snow fall levels [40].

Accurate measurements such as flow rates are needed in the petrochemical, oil and gas, irrigation. Varieties of flow meters are made available today by using ultrasonic technology. These flowmeters are either installed in-situ or ex-situ for flow measurements. Where two phase mixtures are present in a reactor vessel ultrasonic technology can used to determine the level of

each mixture [41]. In the transportation industry for railway safety wheels are integral part of the safety system. Ultrasonic technology is used to inspect railcar wheels to identify wear. The application of ultrasonic technology is integral part of nondestructive testing methods to ensure railway safety [42].

CHAPTER IV

RESEARCH METHODOLGY

4.1 Corrosion Monitoring of Carbon Steel Ball Valve in Sodium Chloride Solution

4.1.1 System and Component Description

The basis for the hydraulic system design was to have a flow loop that was almost a closed loop except for a few openings on top of the tank. The system consisted of a stainless-steel ball valve 1- inch in size and was manually operated to control flow within the system.

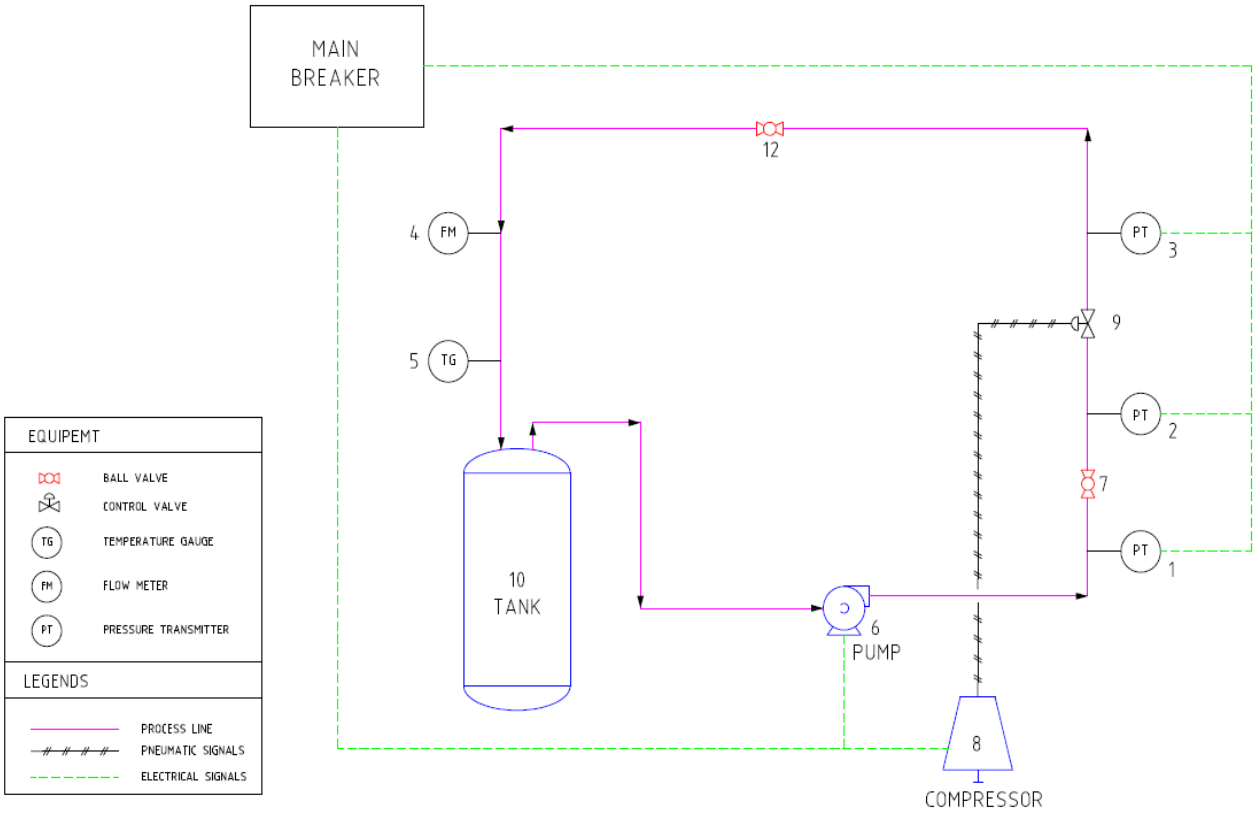

Figure 30. Hydraulic loop schematic diagram.

Figure 30 shows the schematic diagram of the hydraulic loop with major equipment. The main breaker also provides control voltage at 24 volts to the instruments and the control valve. The ball valve had a smart positioner that was used to control the position of the control valve as needed. A 30-gallon plastic tank was used to hold the process fluid with a pump for circulation of consisted of 6.8% sodium chloride in water solution. An air compressor was installed to supply air to the actuator of the 1-inch control ball valve when needed.

Figure 30 shows pressure instruments PT 2 and PT 3 that monitored pressure across the inlet and outlets locations of the valve. A Coriolis flow instrument FM installed within the loop measured the flow within the system and the interconnecting piping for the system was a 1-inch PVC piping. The entire system required a supply voltage of 120 Volts suitable to draw power from a 20-ampere breaker outlet. The components within the system were supported with plywood to ensure that components were adequately held in place and vibration was kept to a minimum.

4.1.2 System Pump

The system pump motor had a 1.1Kw (1.5 Hp) motor. The pump was capable of delivering 70 GPM and was thermally protected with an internal switch that cut off the motor when the operating temperature exceeded 40℃ of surrounding temperature. The supply to the pump was 115 Volts alternating current (AC) 60-Hz supply.

4.1.3 Coriolis Flow Meter

The flow meter in the system was a 1-inch Endress+Hauser Coriolis flow meter with Cl.150 raised flange (RF), 1.4404/316/316L, flange American Society of Mechanical Engineers (ASME) B16.5 standard. The measuring tubes were made of non-polished stainless steel and it

could output a $4mA$ to $20mA$. This instrument could measure flows up to 40,000 lb./hr. The Coriolis flow meter was pressure tested by the manufacturer and had an aluminum housing for the electronics with an electronic digital display. The electrical connection had a threaded 1/2-inch NPT connection. The Coriolis flow meter measured and displayed temperature of the recirculated fluid, mass flow rate, volumetric flow rate, and density of the fluid.

4.1.4 Smart Pressure Instruments

The smart electronic pressure transmitters were installed to measure the pressure across the valve monitored for corrosion. These pressure transmitters had a maximum working pressure of 10,500PSI for each transmitter and these transmitters determined the pressure drop across the valve monitored for corrosion. These transmitters were calibrated to accurately read the pressures within the system.

4.1.5 Fasteners, Fitting and PVC Piping

The interconnecting fasteners, fitting, and polyvinyl chloride (PVC) piping were made of 5/8-11X3 stud bolts ASTM-A193 B7 Teflon coated blue bolts, 5/8-11 heavy HEX nuts A194 grade 2H Teflon coated blue. One-inch Schedule 40 clear PVC pipe, 1-inch PVC socket flange, socket tee, 1”x1/2” PVC reducing bushing, and 1/2" PVC industrial compact socket ball valve used as a drain valve for the system.

4.1.6 Instrument Air Compressor

The instrument air compressor had a single-phase induction motor which required a 120 Volts alternating current (AC) 60 Hertz supply for operating it. This compressor does not require oil for lubrication, and it is used to supply air to modulate the control valve under corrosion monitoring if modulation is needed.

4.1.7 Carbon Steel Body Ball Valve

The control ball valve that was monitored for corrosion was a 1-inch ball valve. The ball was constructed of chrome, but the body of the valve was carbon steel. Other details of the control ball valve are: 150 American National Standards Institute (ANSI) metal seated ball valve, 1-inch Face to Face is 6.5 inches. raised face flange (RF), internal model of construction series, standard construction with Live Loaded packing, WCB body, Hard Chrome ball with XM19 shaft, metal seat with Polytetrafluoroethylene (PTFE) back seals – Max 440°F, hard faced cobalt coated 316 seat material, PTFE packing, live loaded, B7 bolting with a class 6 shutoff [56].

Figure 31 shows the surface of the body of the valve prepared so that the ultrasonic sensor could be seated on the valve body to record thickness measurements. The ultrasonic thickness meter was not permanently installed on the control valve for this experiment. The body of the valve was leveled with a grinder and a general-purpose adhesive was used to hold stainless-steel washer to the body of the control valve. These were the location of the valve body where thickness measurements were taken in inches using the ultrasonic thickness meter.

Figure 31. Valve body and surface preparation

Figure 32. Experimental hydraulic loop system set up.

Figure 32 shows a close look at the system with all the major components connected. They include pressure transmitters (1), (2) and (3), Coriolis flow meter (4) Coriolis flow meter measuring temperature, density, volumetric flows and mass flows, temperature gauge (5), system pump (6), manual valve (7) for throttling inlet flow, air compressor (8) supplying air to the control ball valve that is under corrosion monitoring when needed. The other components in the system were, control valve being monitored for corrosion (9), a holding tank (10) with NaCl and tap water solution.

Figure 33 shows the return manifold connected to the return section of the system. The figure also shows how the return manifold was physically built. The return manifold was designed and installed into the system to ensure that turbulence in the tank was diffused as the NaCl entered the tank.

Figure 33. Hydraulic loop return manifold.

Figure 33. shows Return Manifold, (1) manifold installed in the tank, (2) complete manifold and (3) suction line.

4.1.8 Ultrasonic Thickness Meter

There were various material options for measurement such as steel, PVC, cast iron, aluminum, red copper, zinc, quartz glass, polyethylene, gray cast iron and nodular cast iron. The ultrasonic thickness meter was calibrated to the measure thickness of steel from of 1.0 mm to 200 mm. The thickness meter TM 8812 had a resolution of 0.1mm/0.001inch with an accuracy of $\pm 0.5\% n + 0.1$. The range for the sound velocity is 500 m/s to 9000 m/s and the measuring frequency was 5 MHz [58].

Four AAA batteries were used to supply voltage for this meter. which had an operation temperature of 0℃ to 50℃. The thickness gauge tolerated humidity greater than 80%. The circuitry employed a micro-computer large scale integrated circuit to provide high accuracy of measurements [49].

Figure 34 shows how the ultrasonic thickness meter was used to collect the thickness of the valve body daily. *Figure 34* shows, (1) glycerin was used as a coupling gel when taking ultrasonic thickness measurement, (2) readings off the ultrasonic thickness meter, and (3) ultrasonic thickness measurement set up. It was very important to eliminate surface variation while carrying out thickness testing on the surface of the valve.

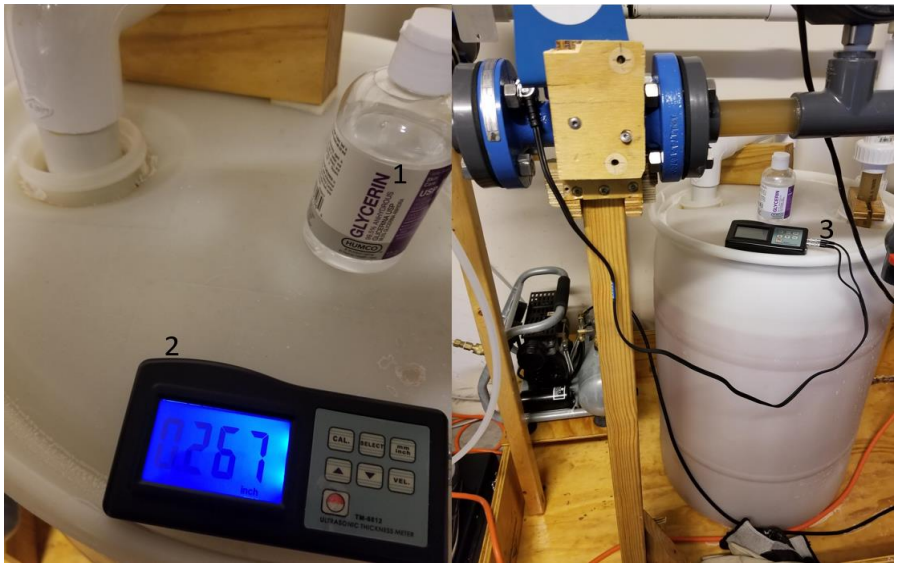

Figure 34. Ultrasonic thickness monitoring.

The standard deviation of glycerin, when compared to other coupling gel that is ultra-gel, petroleum jelly and Dow Corning high vacuum grease, was 0.0484 when weight was not introduced on the ultrasonic transducer, and 0.0783 when weight is introduced on the transducer. Glycerin was used in this experiment because it helped produce more repeatable values of thickness readings [43].

4.1.9 Experimental Procedure

The system total dissolved solids (TDS) was measured throughout the experiment duration. The initial TDS of tap water that was used to mix with NaCl was 356 ppm at 29℃ (84.2°F) and the pH of the tap water at the time of mixing was 7.90. The initial TDS of

the sodium chloride solution was 6610 ppm after mixing with 25 gallons of tap water. Process variables measured were temperature, differential pressure across the ball valve, pH of the process, TDS of the process liquid, volumetric flow rate, density of the process liquid, thickness changes of the valve body and temperature of the fluid when returning to the holding tank.

The sodium chloride solution started to turn reddish brown in color after 24 hours of use. The system set up was a continuously ran system with the ball valve monitored for corrosion 100% opened during the experiment. The total dissolved solids were also monitored. Total dissolved solids measurements were taken using an electronic TDS meter. The Coriolis flow meter installed in the system was capable of measuring volumetric flow rate every day throughout the period of experiment.

The system temperature was measured at several points. The Coriolis meter and control valves measured temperature. The return line had a temperature instrument installed to monitor temperature of the liquid going back to the tank, and an electronic TDS meter had the option to display the temperature of the process fluid while taking readings for the TDS. After 336 hours of continuous run time, the water level was increased in the holding tank and the NaCl content increased from 6.9 kg to 13.61kg to increase corrosion rates.

$$\text{ppm} = \frac{\text{Mass of Solute (g)}}{\text{Mass of Solution (g)}} * 10^6$$

The salt solute in NaCl solution was 13,072 ppm after the water quantity had increased from 25 gallons to 27.5 gallons.

The mass flow rate at inlet and exit are given as m_i, m_e and specific heat c_v [31]:

Then,

$$\frac{dm_i}{dt} - \frac{dm_e}{dt} = \frac{dm_{cv}}{dt}$$

An energy balance on the fluid yielded:

$$(Q - W) + \sum E_i - \sum E_e = \triangle E_{CV}$$

$$E_i = \int_0^t m_i \, (h_i + c_i^2 + gz_i) dt$$

$$E_e = \int_0^t m_e \, (h_e + c_e^2 + gz_e) dt$$

Then,

$$(Q - W) + \sum m_i (h_i + C_i^2/2 + gz_i) - \sum m_e (h_e + C_e^2/2 + gz_e)$$

$$= m_{final} * u_{final} - m_{initial} * u_{initial}$$

Where *m* is mass flow rate, (kg/min), *z* is elevation (m), *Q* is the heat energy (BTU), *W* is the shaft work (Joules), *C* is the velocity (m/s), h is the enthalpy $H = U - PV$, *V* is the specific volume (m^3/kg), *U* is the internal energy (J/kg), *P* is the pressure (N/m^2). Suppose there was a uniform control volume state, uniform fluid properties, and a steady flow in and out of the hydraulic loop, then the energy balance can be used for unsteady flows analysis.

4.1.10 Valve Body Material Composition

Table 1 shows the weight per cent of welded carbon steel grades (WCB) for the valve body that is been monitored for corrosion. WCB are ASTM designation that define the welded carbon steel casting as a grade of B. It also defines the mechanical properties such as yield strength, tensile strength and elongation of the valve body [44].

Table 1 Chemical Composition of WCB

Standard Designation	Type, Grade	UNS Number	Weight %							
			C	Mn	Si	P	S	Cr	Ni	Mo
ASTM A 216	WCB	J03002	0.30	1.00	0.60	0.04	0.045	0.50	0.50	0.20

Note. Table shows the content of the carbon steel for the valve body.

An ultrasonic thickness meter was used to collect thickness measurements once daily for 1,152 hours of continuous run time. Specific locations on the inlet and outlet of the valve were monitored to validate valve body thickness loss. The initial ultrasonic reading for the inlet and outlet locations where readings were taken was 0.238 inches and 0.267 inches respectively. These values changed between 0 hours and 1,152 hours and discussed in detail in the results and discussions section.

4.2 Corrosion Monitoring of Carbon Steel Ball Valve in Sodium Chloride and Acetic Acid

4.2.1 System Description

This experiment used an acetic acid, NaCl and water and NaCl mixture and was conducted as seen in *Figure 32*. The changes that were made was to drain 15 gallons of NaCl solution in the holding tank and to replace it with acetic acid diluted to 5% acidity. The system pH attained was less than 4 and this was done to speed up corrosion within the valve. Two new valves were installed one was monitored in the loop for 408 hours and the other valve monitored for 240 hours respectively. The two new manual ball valves had the same specifications i.e. a 1-inch flanged carbon Steel body ball valve 300 PSI ANSI 4-bolt flanged ends, 2-Piece A216 carbon steel body, with full-port. These valves were a class 300 (300 PSI), 316SS trim, and met NACE MR-01-75, Fire Safe API 607 5th Edition specification [55].

Table 2 Shows the chemical composition of carbon steel manual ball valve body

Standard Designation	Type, Grade	UNS Number	Weight %							
			C	Mn	Si	P	S	Cr	Ni	Mo
ASTM A 216	WCB	J03002	0.30	1.00	0.60	0.04	0.045	0.50	0.50	0.20

Note. Table show the content of the carbon steel for the valve body [44].

A flexible nylon cable tie with a loop tensile strength of 334 N (75 lbf) for indoor use with an operating temperature of -40°F to 185℉ was used to tie down the ultrasonic transducer on the valve body. A hand mixed steel reinforced non-rusting epoxy, which after curing, formed an industrial grade polymer compound was used to form a groove to hold the acoustic coupling gel in place on the valve body. This coupling compound is a high temperature coupling gel with a range of 35℉ to 700℉. The compound SONO 600 meets API, ASME, and AWS specifications with a tensile strength of 900 PSI, which is also compatible with metals and most composites. The SONO 600 gel is very thick and contains no silicon or glycerin but instead, contain propylene glycol and less than 50 ppm of sulfur and halogens. The SONO 600 high temperature ultrasonic coupling compound was not water soluble [48].

4.3 Experimental Procedure

After 1,152 hours of consecutive runtime using NaCl solution acetic acid was introduced. A quantity of 15 gallons of NaCl solution was drained from the system and 15 gallons of acetic acid that consisted of 5% acidity was introduced into the loop. The reason for introducing acetic acid was to increase the rate of corrosion of the valve being monitored for corrosion.

The inlet manual valve was kept 100% fully open and the carbon steel ball valve that was in the flow loop for corrosion monitoring was also 100% fully open for these experiments.

4.3.1 Valve body Surface Preparation

Figure 35 below shows how the surface of the valve body was prepared to mount the ultrasonic transducers on the valve body for thickness measurement. *Figure 35* (1) shows ultrasonic thickness meter monitoring thickness readings for the valve inlet and outlet.

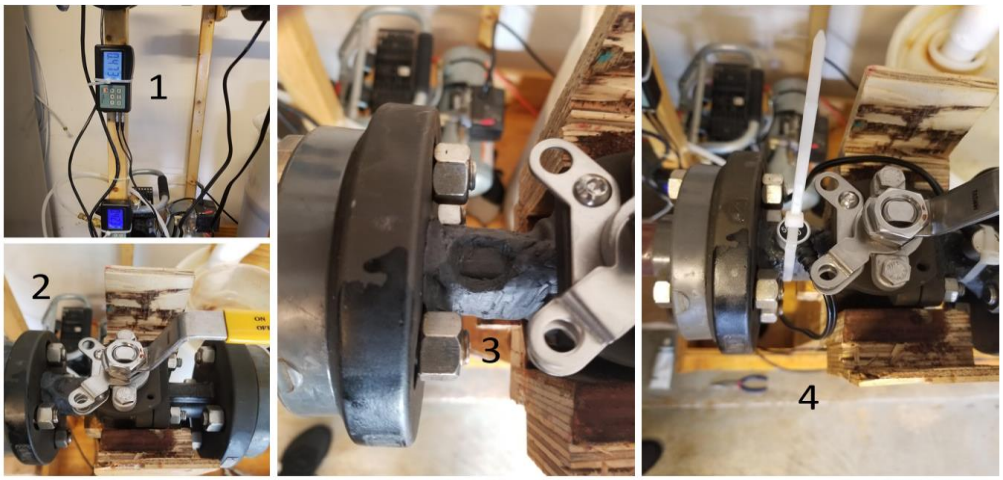

Figure 35. Valve body surface preparation and mounting.

(2) shows epoxy compound used to form a groove on the valve surface. The groove held the coupling gel used to reduce acoustic impedance for better contact between the valve surface and the ultrasonic transducers. (3) shows a closer view of the epoxy on the body of the valve and (4) shows a view of the ultrasonic transducers mounted in the groove created on the body of the valve. The ultrasonic transducer in *Figure 35* was secured with a tie wrap to ensure that it was firmly held on the valve body.

4.3.2 Thickness Evaluation

Considering that this experiment was simply a normal low frequency incident thickness measurement, the intent was to irradiate a thin layer situated between the surface of the ultrasonic transducer and the surface of the valve body. Assuming there were no losses, acoustic impedance $Zs = \rho V_S$. Where h represent the thickness been determined for the valve body and

the acoustic impedance $Z = \rho V_l$. V_l= Longitudinal propagation velocity [m/s] and ρ= Density [kg/m^3].

Then transmission amplitude coefficient T was given by:

$$T = \frac{2}{2cosKh + j\left(\frac{Z_s}{Z} + \frac{Z}{Z_s}\right) sinKh}$$

Where,

$$K = \omega / V_l$$

The energy that permeates through the transmission coefficient:

$$\sqrt{t} = |T|$$

Therefore,

$$\left|\frac{R}{T}\right| = \sqrt{\frac{1-t}{t}} = \frac{sinKh}{2}\left|\frac{Z_s}{Z} - \frac{Z}{Z_S}\right|$$

If the layer becomes so thin that $Kh \ll 1$. Then,

$$\left|\frac{R}{T}\right| = \sqrt{\frac{1-t}{t}} \approx \frac{sinKh}{2}\left|\frac{Z_s}{Z} - \frac{Z}{Z_S}\right|$$

Where R is the amplitude reflection coefficient of the substrate interface. The relationship is applicable to longitudinal and shear wave when the incident ray is normal. For a high impedance layer where $Z \gg Z_S$: $\left|\frac{R}{T}\right| \approx \frac{\pi}{Z_s}\rho h f$

The relationship neglects bulk wave velocity in the layer. Therefore, if the density is known, then the thickness of the body of the valve can be determined [33].

CHAPTER V

RESULTS AND DISCUSSIONS

5.1 NaCl Fluid Condition Corrosion Data Analysis

Figure 36. shows a close image of the system with NaCl recirculated through the system. The transparent PVC tubing showed that corrosion was ongoing, and the PVC was discolored at both the inlet and outlet of the valve under test. This change was evident during the first 24 hours of running the experiment although the discoloring of the transparent PVC did not increase after the 24 hours.

Figure 36. Interconnecting piping with visible oxides.

*F*igure *36* shows evidence of oxides when carbon steel valve body started to corrode in the presence of NaCl mixed with tap water. The blues circles 1 and 2 show where the transparent

PVC discolored. The experiment was conducted with the system fluid recirculated continuously for a period of 1,152 hours without any break in the operation of the system. During the experiment the process variables were documented daily. *Figure 36* shows (1) the inlet of the control valve and (2) the outlet of the valve under corrosion monitoring, temperatures, pressures, flows, valve thickness to verify loss of material in the inlet and outlet location on the valve.

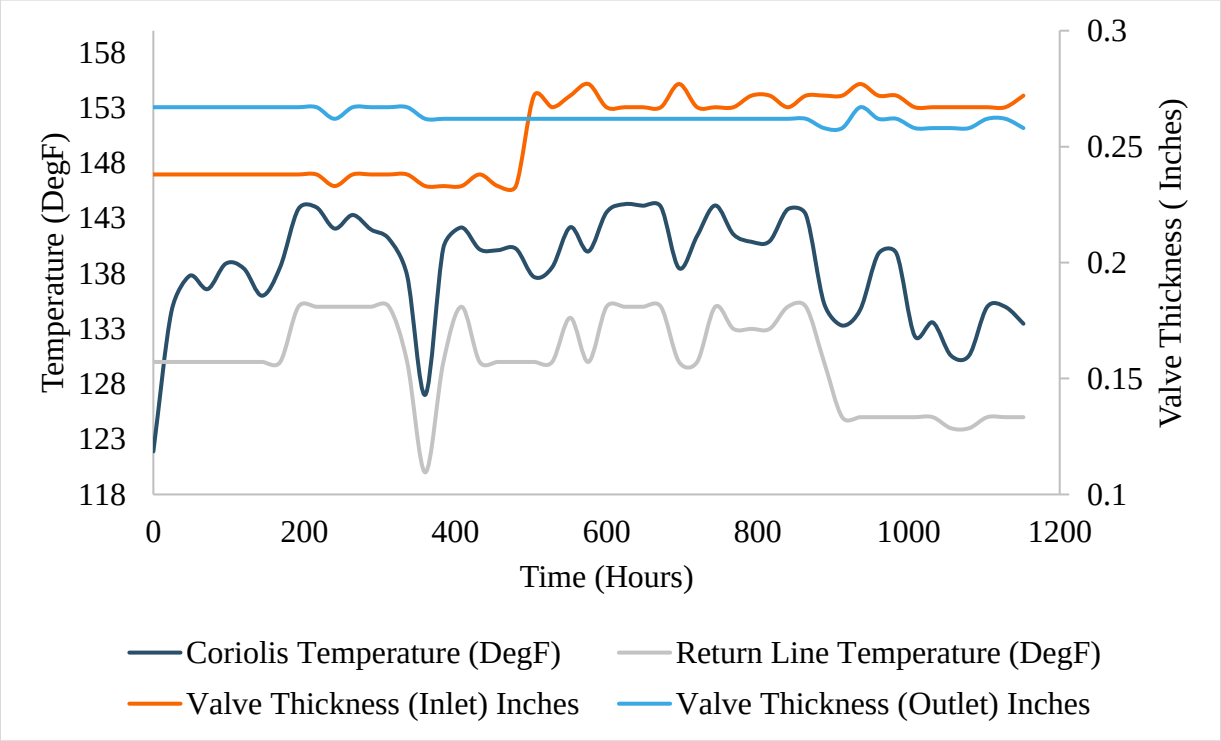

Figure 37. Temperature and valve thickness graph.

Figure 37 shows the relationship between the temperature been monitored by the Coriolis flow meter and the return line temperature and valve thickness overtime. There was an average difference in temperature of 8.25°F between the Coriolis flow meter and the return line temperature. The large difference may be attributed to the accuracy of the return line temperature gauge. There was a difference between the inlet thickness and outlet thickness measured in

inches after a continuous run of the system for 1,152 hours. The actual difference in thickness average measured was 0.0074 inches (0.19 mm) over the continuous run period.

These overall measurements indicated that, over this period of continuous run, there was a change in valve body thickness loss that could be collected using the handheld ultrasonic meter. Material thickness was much more stable and the accuracy was better when using multi-channel type ultrasonic monitoring system under Flow Accelerated Corrosion [45]. The ultrasonic thickness meter used was not permanently installed on the valve body for the thickness measurements. The control valve body surface needed to be prepared to adequately secure the ultrasonic thickness meter on the valve to minimize error in measurement.

Figure 38 shows the relationship between the flow rate in gallons per minute, and the differential pressure measured in PSI across the control valve monitored for corrosion over time. At these approximately constant flow rates, the pressure drop across the control valve was between 0 PSI to 2 PSI. The pressure differential did not exceed 2 PSI for the period that the system recirculated process fluid.

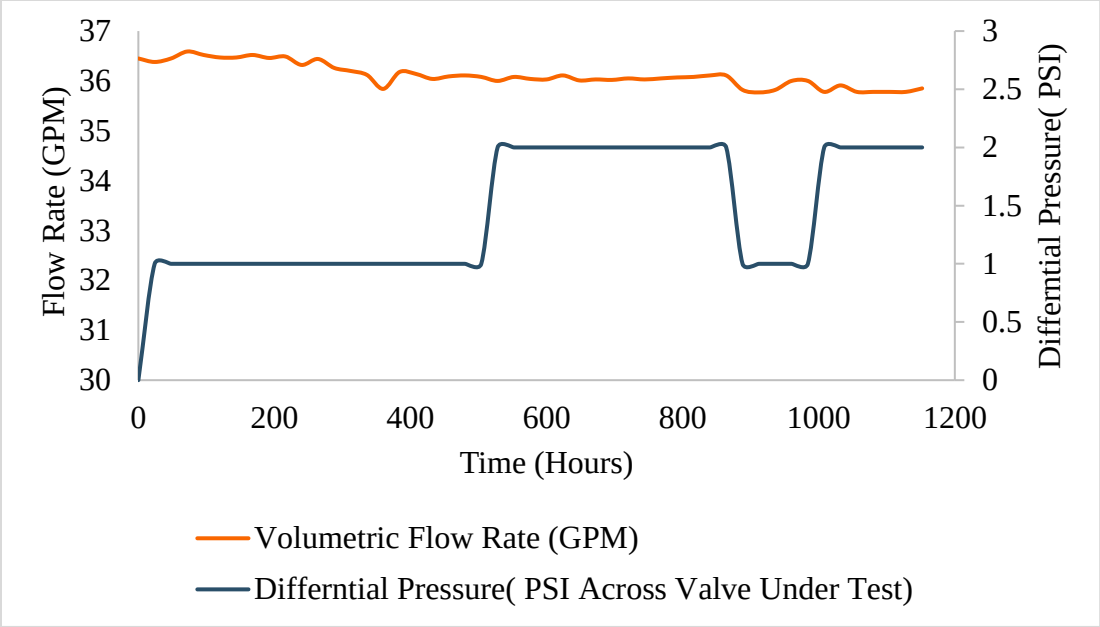

Figure 38. Flow rate and differential pressure graph.

Figure 38 shows the relationship of flow rate and differential pressure over time. The small pressure drop indicates a lack of severe damage in the internals of the valve. The volumetric flow rate was largely constant between 35.84 GPM and 36.59 GPM over the period that the test was conducted. The pressure differential is the difference between the inlet pressure and the outlet pressure instruments directly mounted across the control valve monitored for corrosion.

Figure 39 below shows the relationship between the Total Dissolved Solids (TDS) and the flow rate in Gallon Per Minute (GPM). During the experiment, black particles were seen in the samples , which were an indication of internal deterioration of the test valve and in addition, the process solution changed color to brown as observed. *Figure 39* shows the relationship between total dissolved solids and flow rate overtime. Signs of deterioration of the internals of the valve are shown in *Figure 40* with images of the control valve before and after 1,152 hours. *Figure 40*. shows (1) a sample jar, (2) System fluid after 1152 hours. Note the presence of iron

oxides (3) view of the control valve before running process fluid through it and (4) shows control valve after 1,152 hours of continuous recirculation of process fluid.

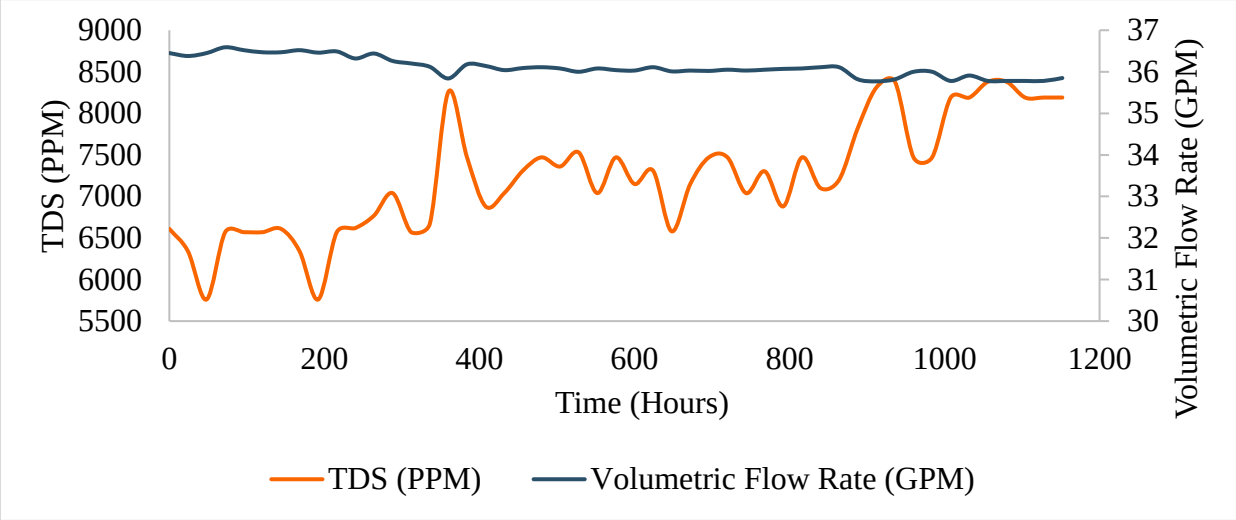

Figure 39. TDS and flow rate graph.

The pictures in *Figure 40* showed oxygen was present on the surface of the control valve under corrosion monitoring. Using the thickness measurements the rate of corrosion during the experiment was expected to be $8.3\mu m\ to\ 16.67\mu m$ per month [46].

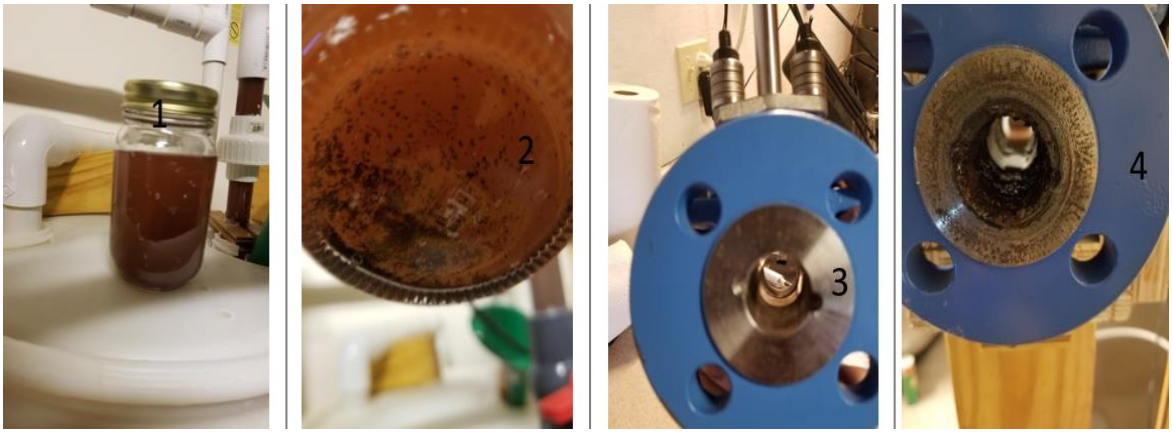

Figure 40. Samples and valve deterioration.

Figure 40. shows samples used to test for pH, TDS and temperature and physical images of control valve before and after 1,152 hours.

Figure 41 shows the relationship between the power of hydrogen (pH) of the system and density when the system recirculated NaCl for 1,152 hours. The pH and the density of the system remained constant without much change during the runtime of 1152 hours. Figure 41. shows the relationship between pH and density over 1152 hours. The flow rate can influence the corrosion rates per month increasing it by a factor of 100 depending on the velocity present within the system and this could be as high as 40 m/s [46].

The volumetric flow rate measured within the system given by:

$$\dot{V} = \boldsymbol{V} A = \int \boldsymbol{V_{Local}}\, dA$$

So that the mass flow rate of the system with sodium chloride as the process fluid is given by :

$$\dot{m} = \rho_{avg} \dot{V} = \dot{V}/v = \int (\boldsymbol{V_{Local}}/\boldsymbol{v})\, dA = \boldsymbol{V} A/v$$

Where A is the area of the pipe, $\boldsymbol{V_{Local}}$ is the local velocity of the process fluid, ρ_{avg} average density of the process fluid and v is the volume [47].

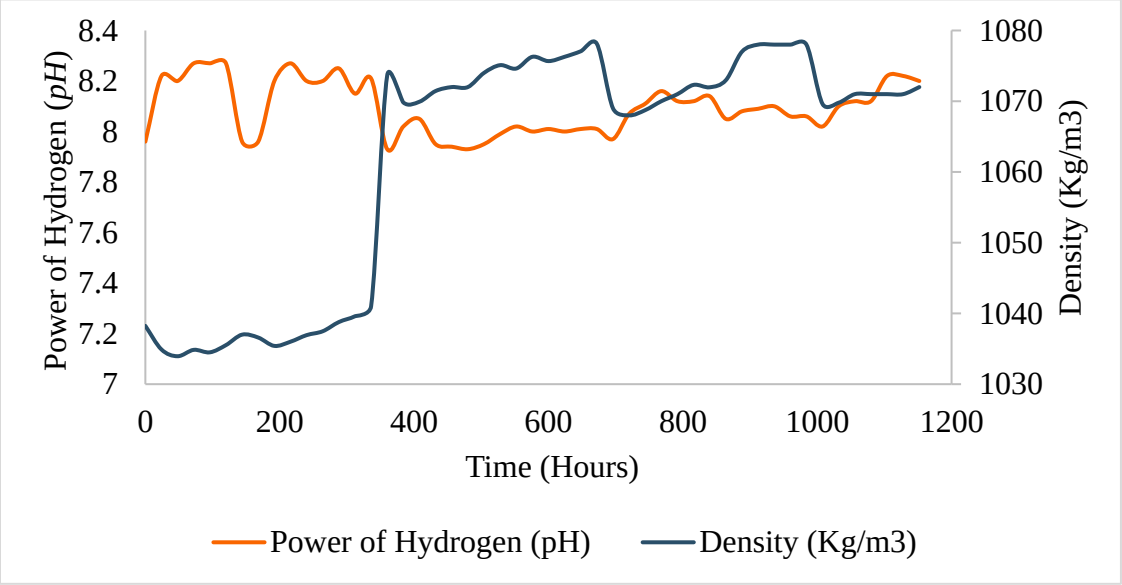

Figure 41. pH and density graph.

Evaporation of the water and topping up the NaCl solution with water to maintain solution levels in the tank, was a contributing factor to the changes in temperature seen in the graph in *Figure 42*. The liquid became denser when the level started to fall in the tank and these levels were physically observed on the transparent tank. Some heat contributing to the system was due to the shaft work from the motor pump that introduced heat. *Figure 42* shows the relationship between system temperatures, mass flow rate in kg/min overtime. However, the mass flow rate and the volumetric flow rate did not vary much over the time.

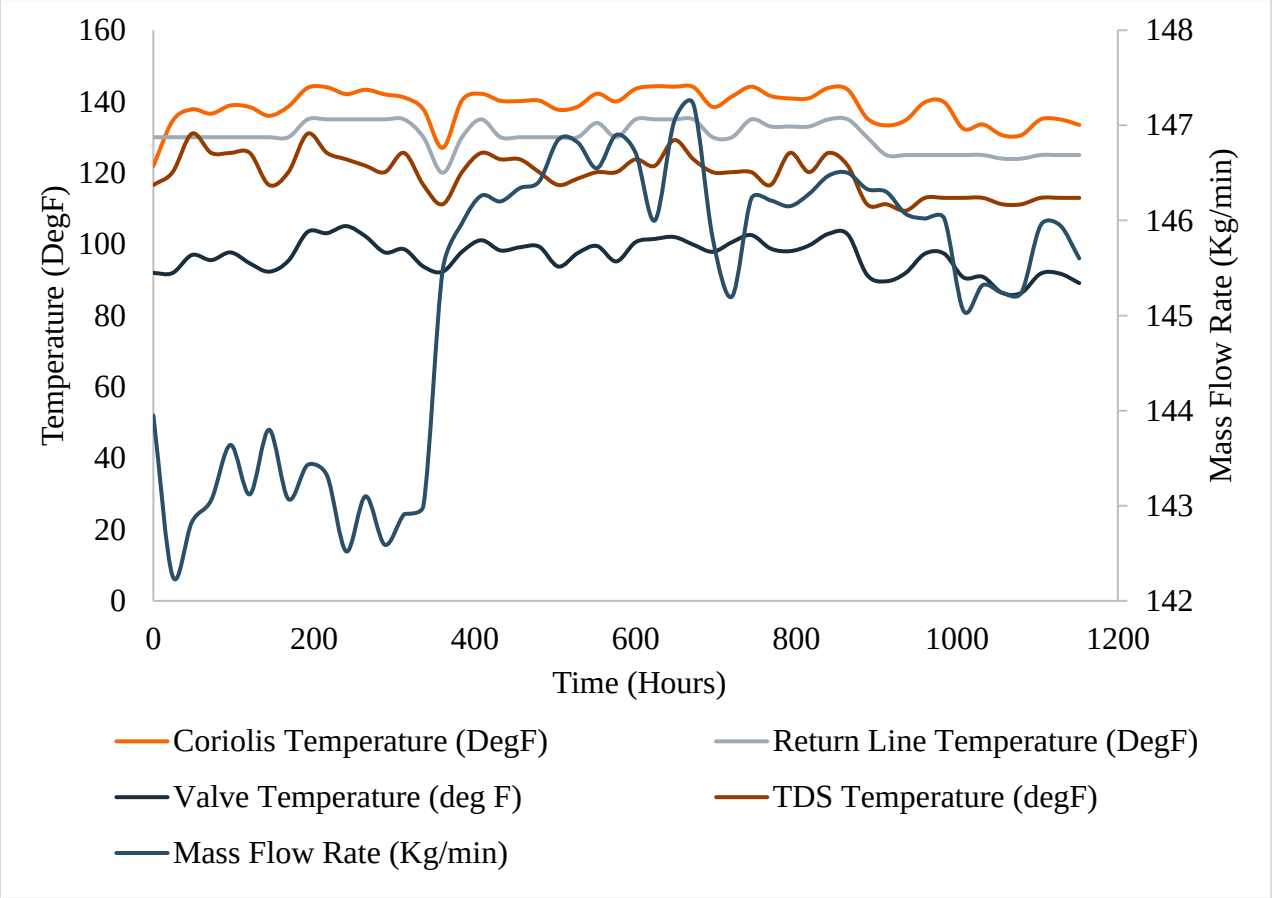

Figure 42. System temperature and mass flow rate graph.

Figure 42. shows relationship between various temperatures and mass flow rate over 1152 hours during the 1152 hours of continuous recirculation of the sodium chloride solution.

Corrosion of carbon steel (iron) occurs aqueous salt solutions via an electrochemical mechanism. Corrosion continued because the metal oxide formed did not have the ability to protect the metal surface. Iron oxide products are very porous in the presence of an NaCl solution. The carbon steel surface of the valve realized electric current due to the NaCl solution acting as an electrolyte. The electrical forces in the NaCl solution caused the metal ions to give up their positions in the crystal, and then moved into solution to become cations [28]. This process can be expressed as,

$$Fe \rightarrow Fe^{2+} + 2e^{-}$$

During an anodic or oxidizing process the surface of the carbon steel body of the valve loses iron content degrading the metal surface [28]. The valve was maintained in the open position over the entire run. This state allowed for a maximum flow rate through the system to be achieved. *Figure 44 and Figure 45* show a digital microscopic image of the internals of the control valve monitored for corrosion. It was evident from visual inspection that the inlet side of the control valve had more deposits of iron oxide.

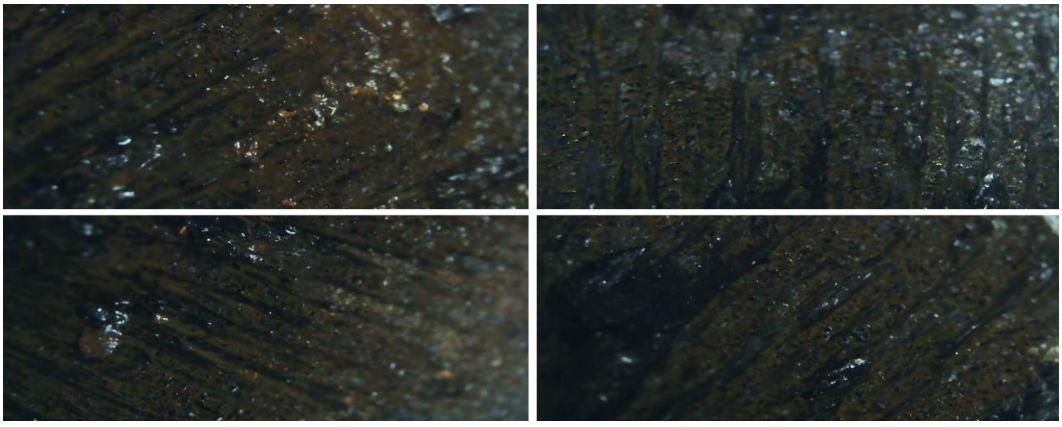

Figure 43. Inlet side of valve microscopic view.

Figure 43 shows microscopic images of control valve internals of the inlet after 1152 hours in NaCl conditions.

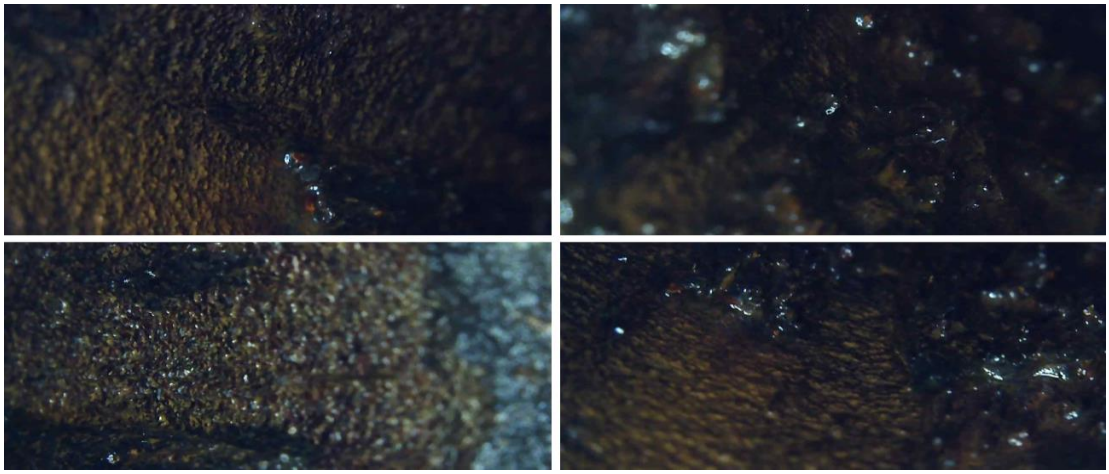

Figure 44. Outlet side of valve microscopic view.

The images show iron oxide formation, matrix formation and delaminated crater on the surfaces of the inside of the control valve inlet and outlet [48].

5.2 Acetic Acid and Sodium Chloride Solution Corrosion Data Analysis

5.2.1 Acetic Acid and Sodium Chloride Corrosion Data Analysis Condition I

In order to increase the rate of corrosion of the block valve, acetic acid was added to the fluid. The total continuous runtime was 408 hours. The results consist of physical inspection, digital microscopic images of the inlet and outlet of the block valve, and process variables that were monitored over 408 hours of continuous recirculation of NaCl and acetic acid mixture. The process variables that were monitored are pressure, temperature, flow rate, density, pH, and TDS.

Figures 45 to 47 show images of the inlet and outlet of the valve. These images are consistent with the images that were taken after NaCl and H_2O experiment. Both images show corrosion products and morphologies. *Figure 45* shows view of control valve inlet (1), view of control valve outlet (2) after 408 hours of running acetic acid through the system.

Figure 45. Valve corroded internal view.

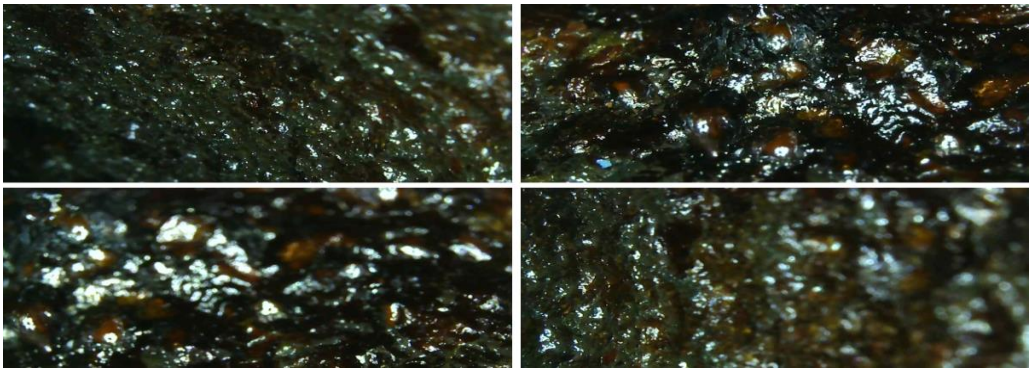

Figure 46. Internal microscopic view 408 hours inlet.

Figure 46 shows microscopic images of the inlet of the control valve after 408 hours of running mixtures of acetic acid and NaCl through the system. Figure 47. shows microscopic images of the outlet of the control valve after 408 hours of running mixtures of acetic acid and NaCl through the system.

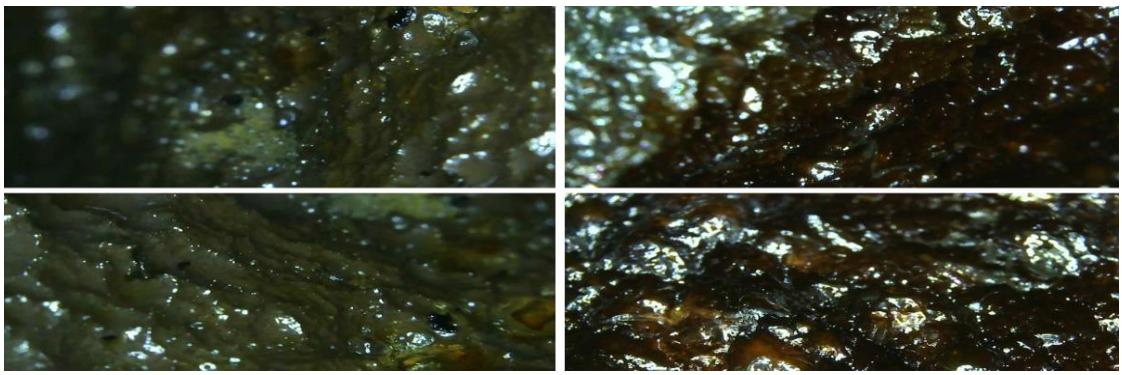

Figure 47. Internal microscopic view 408 hours outlet.

Figure 48 shows the relationship between volumetric flow and differential pressure across the valve. While the volumetric flow was relatively constant, the differential pressure measure across the valve during the 408 hours of continuous run was not large enough to alter the flow in the system. The maximum pressure drop was less than 1.4 PSI and the system volumetric flow rate was between 34.6 GPM and 36.2 GPM. The density did not change much for this period of running the system, as seen in *Figure 49.*

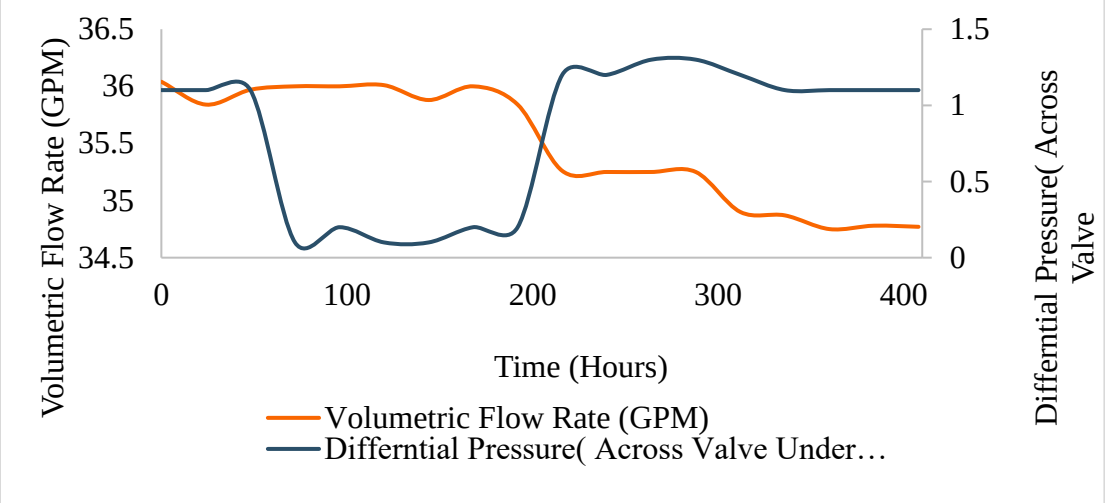

Figure 48. Volumetric flow and differential pressure graph.

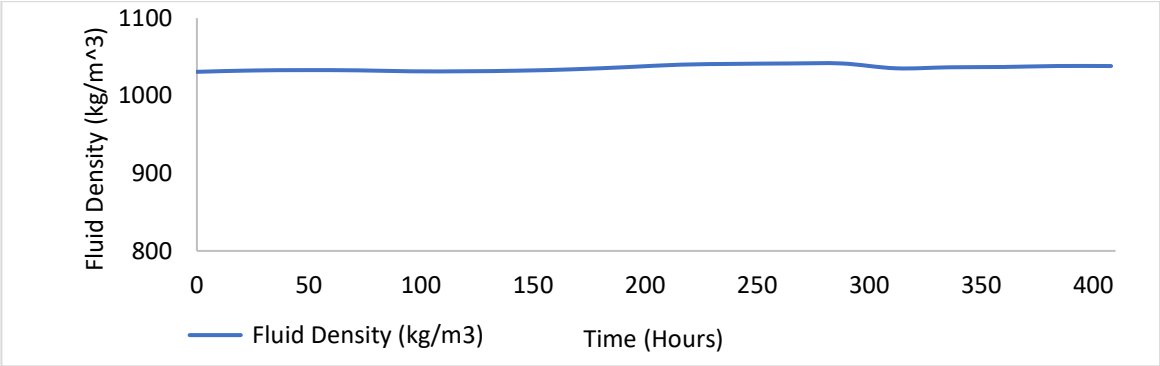

Figure 49. Fluid Density over time.

Figure 49. shows the relationship between density (kg/m^3) over 408 hours.

Figure 50. Fluid density and valve thickness graph.

Figure 50 shows the relationship between density (Kg/m^3) and valve thickness (inlet and outlet) over 408 hours. The pH for this experiment was maintained close to 4 to help accelerate corrosion rates . *Figure 50* shows how the inlet and outlet of the valve had lost material over time when acetic acid was introduced into the system. The valve position had been maintained at a 100% fully open during this experiment.

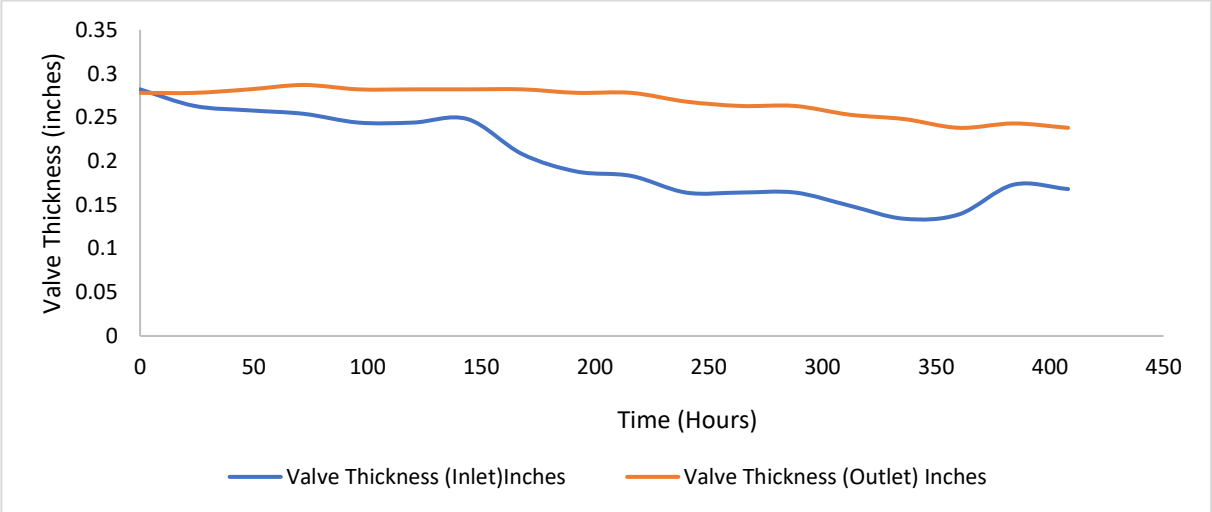

Figure 51. Valve inlet and outlet thickness over time.

Figure 51 shows the relationship between valve thickness loss our 408 hours of run time.

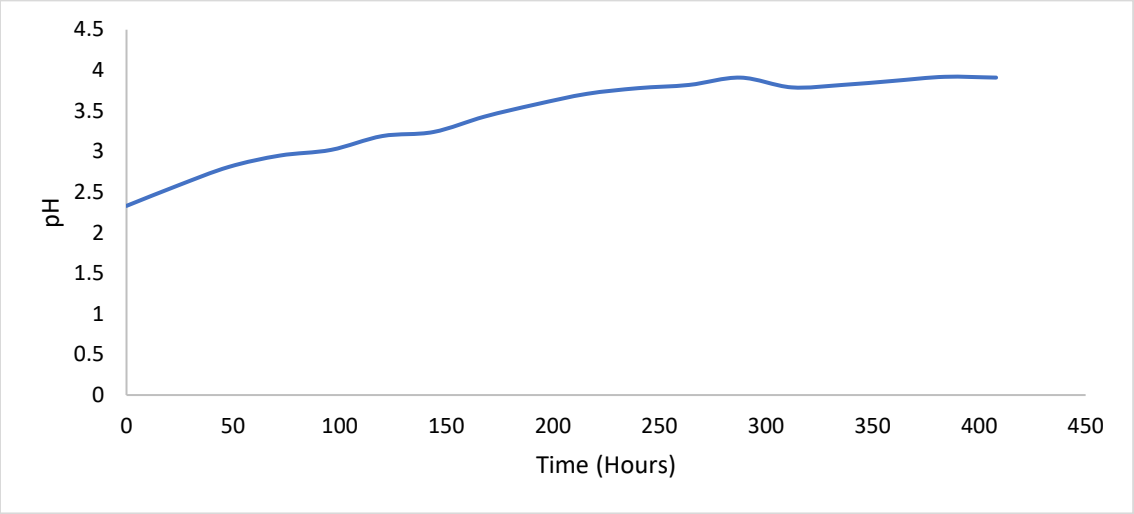

Figure 52. pH over time

Figure 52 shows the relationship between pH monitored over 408 hours. The *pH* varied between 2.33 and 3.91

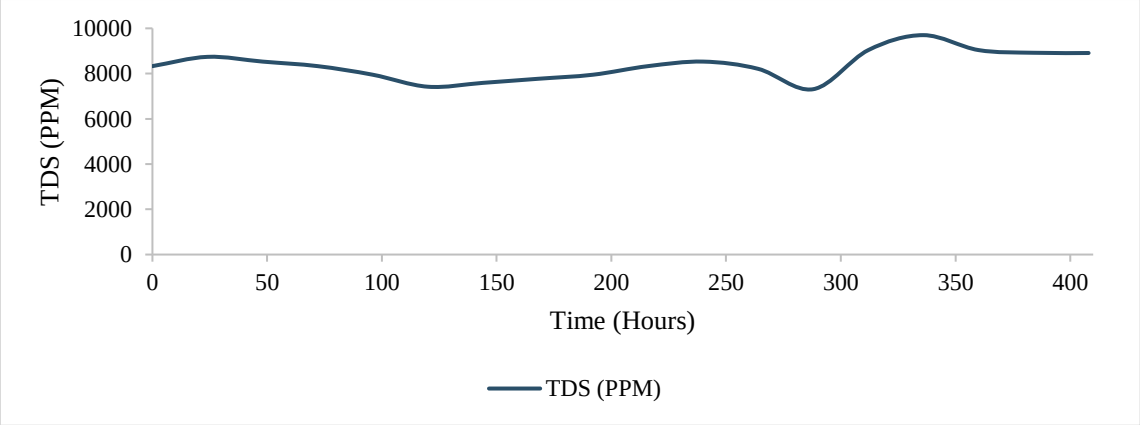

Figure 53. Valve inlet and outlet thickness over time.

Figure 53 shows the relationships the TDS over 408 hours of continuous runtime. The total dissolved solids for the period of 408 hours was between 7000 ppm and 9700 ppm. The temperature was largely constant at about 115°F. Changes in the temperature are attributed to changes in ambient temperature.

5.2.2 Acetic Acid and Sodium Chloride Corrosion Data Analysis Condition II

This condition had the system recirculating acetic acid and sodium chloride mixtures continuously for period of 240. *Figure 54* shows the relationship between the flow rate which remained constant throughout 240 hours and the fluid density of the process. There were no significant changes in the density. *Figure 54* shows the relationship between density and volumetric flow rate over 240 hours.

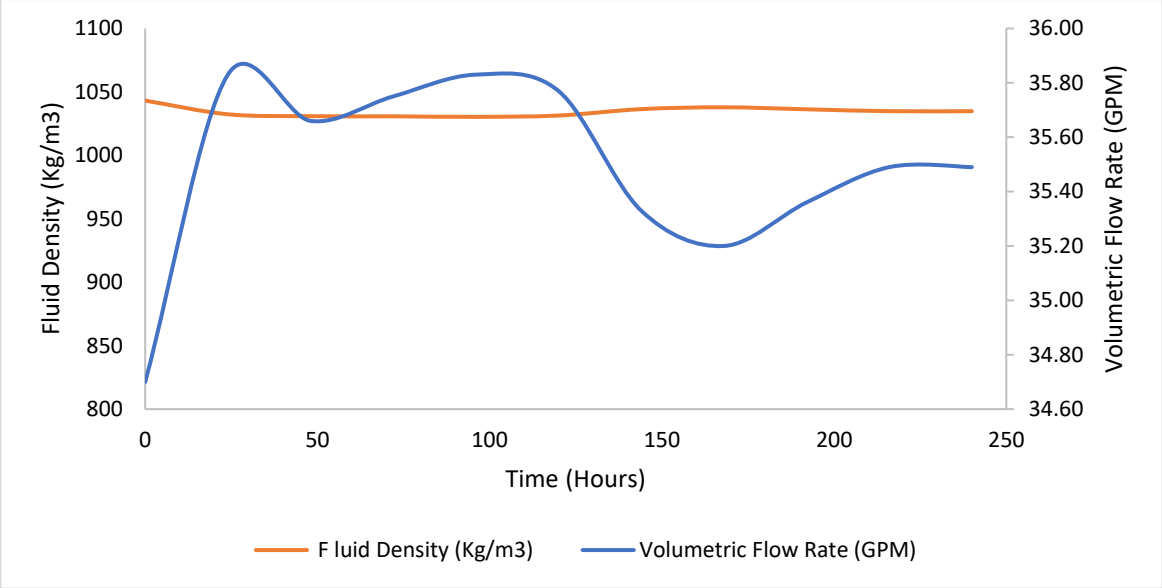

Figure 54. Density and volumetric flow graph.

While the mass flow rate was almost constant, the temperature varied up to 131°F. This change was monitored over a period of 240 hours while the system was continuously running. This change in temperature was attributed to changes in the ambient temperature.

Figure 55 shows relationship between Coriolis temperature and mass flow rate over 240 hours. The temperature as seen in *Figure 56* increased the first 20 hours and then remained constant while the mass flow rate varied between 136kg/min to 138.57kg/min.

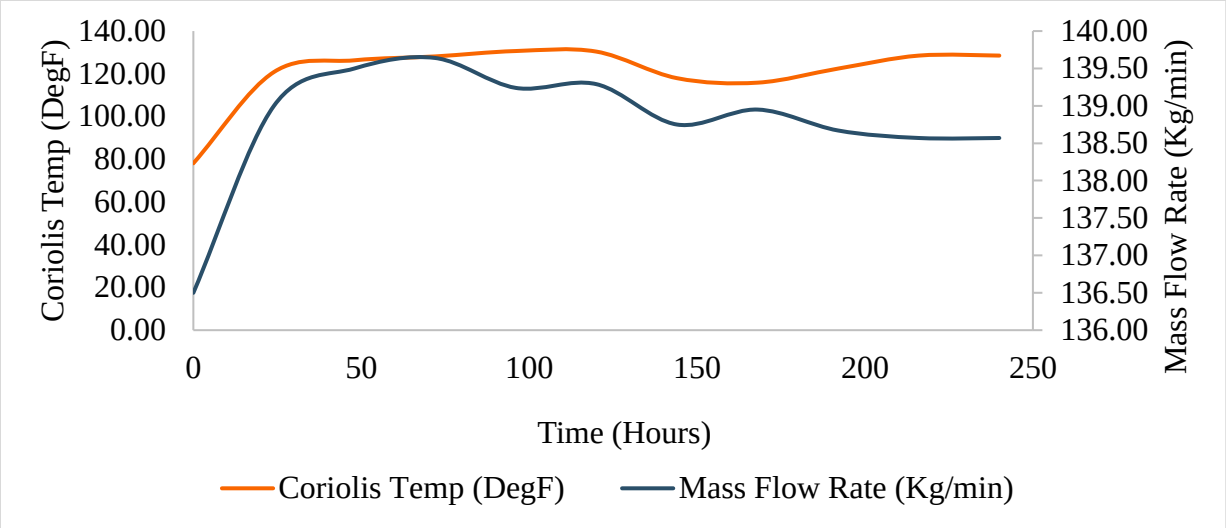

Figure 55. Coriolis temperature and mass flow graph.

Both the inlet and the outlet of the valve showed material losses when the valve was removed from the system and visually inspected. There was no significant pressure drop across the valve over this time period of 240 hours. The average pressure drop across the valve was less than 0.3 PSI over the period of continuous run of the system. The pH was maintained close to 4 to encourage corrosion reaction as the fluid flow through the valve. Iron will typically experience rapid corrosion when the fluid that it is exposed to has a pH of less than 4.

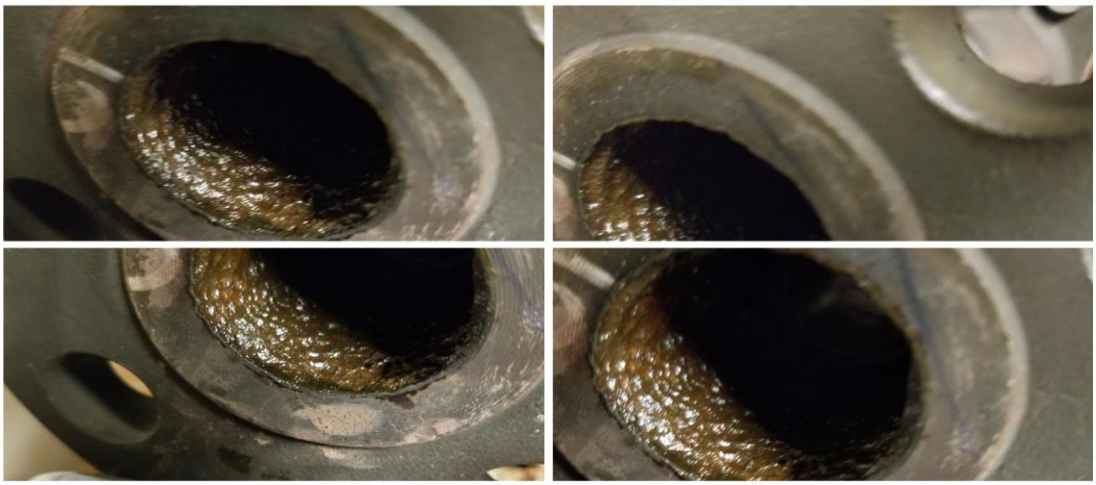

Figure 56. Inlet internal inspection view 240 hours.

Figure 57 shows how the internals of the inlet side of valve looked like by visual inspection after 240 hours.

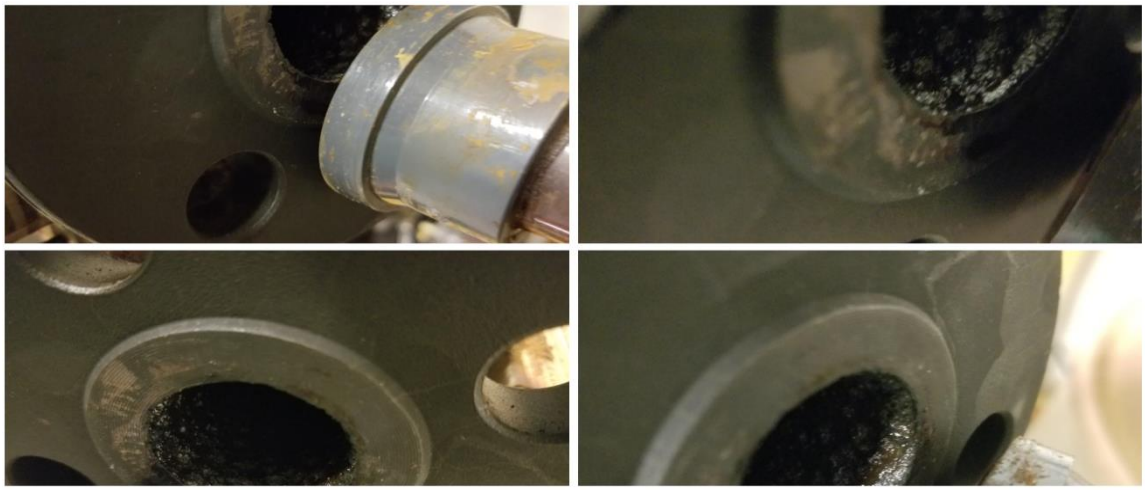

Figure 57. Outlet internal inspection view 240 hours.

Figure 57. shows how the internals of the outlet side of valve looked like by visual inspection after 240 hours.

5.3 Coupling Effect

Figure 58 and *59* show a microscopic view of the surface of the valve locations (inlet and outlet) to which the ultrasonic transducer was mounted. A leak from the split body of the valve introduced a brownish fluid from the process to the surface of the outlet area where the thickness was being monitored. Both images for the inlet and outlet show the shiny and silky compound of SONO 600 ultrasonic gel that was used for coupling.

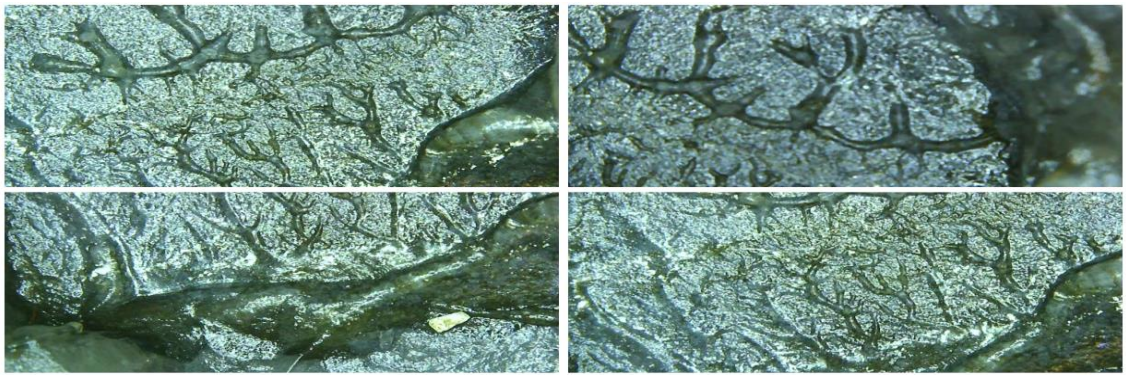

Figure 58. Inlet surface coupling view.

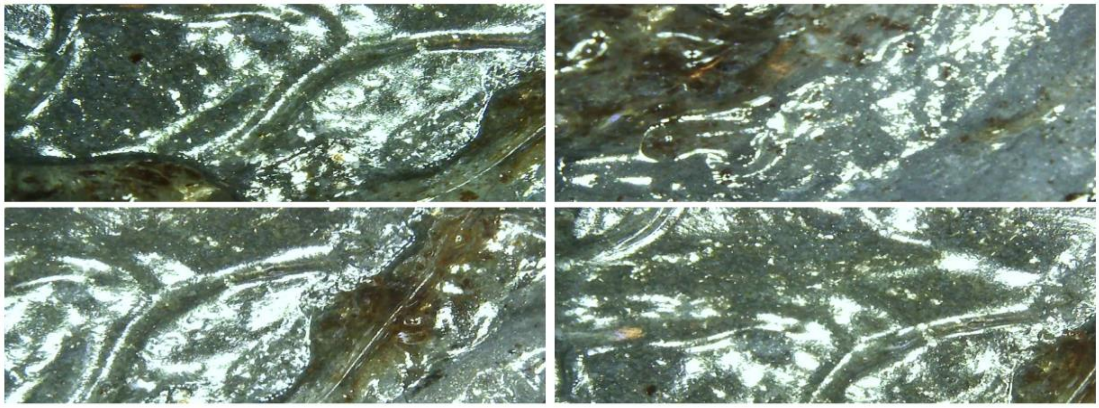

Figure 59. Outlet surface coupling view.

The coupling gel from the images shown did not deteriorate over the period of the experiment and maintained its characteristics over a period of 240 hours of continuously running the system. The highest temperature seen in this experiment was less than 140°F while the SONO 600 ultrasonic coupling gel can withstand temperature of 700°*F*. Glycerin was not used because a couple of drops of glycerin could evaporated in less than 12 hours, and also will decompose at 320°*F*, while SONO 600 ultrasonic coupling gel did not disintegrate over the entire experiment period of 240 hours.

Figure 60 shows that effective coupling of SONO 600 high temperature coupling gel after 5,567 hours. This proved that effective coupling can be maintained for more than 5000 hours. The picture in *Figure 60* shows the ultrasonic sensor indicated coupling and ultrasonic transducers still held in place after 5,567 hours.

Figure 60 shows ultrasonic transducers embedded using SONO 6000 high temperature coupling gel after 5567 hours. A microscopic image in *Figure 61.* shows pictures of the high temperature coupling gel. The blue portions of the photo were the portions of the valve body while the glossy elements were the coupling gel. The grey compounds are images of the epoxy used to create a

holding area to hold the coupling gel in place and the white area is the tie wrap used to hold the ultrasonic transducers in place.

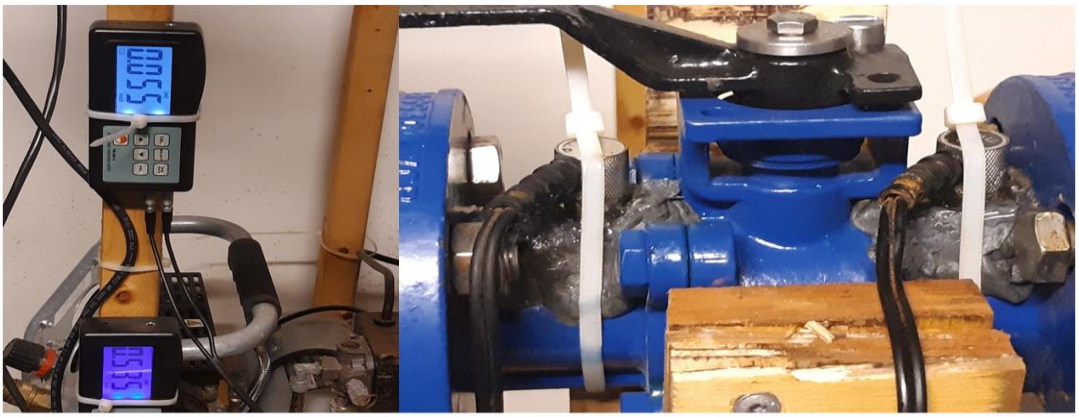

Figure 60. Transducer coupled and embedded.

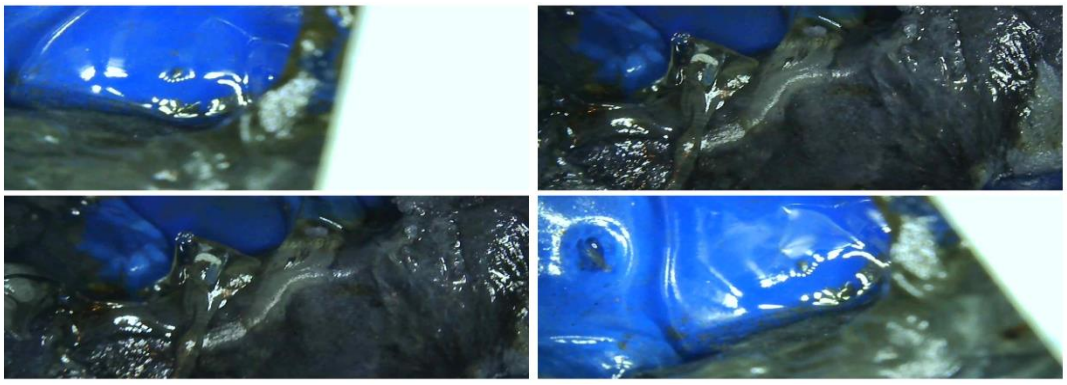

Figure 61. Inlet microscopic view of embedding area.

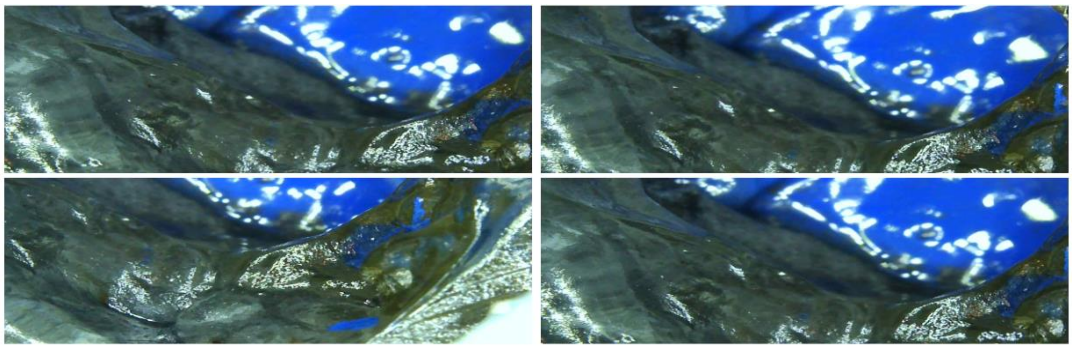

Figure 62. Outlet microscopic view of embedding area.

Figure 61 and 62 are microscopic images for the inlet portions and outlet portions respectively, of the valve body were the ultrasonic transducers were mounted.

5.4 Statistical Analysis of Thickness Measurements

5.4.1 An Overview of Statistical Distribution

There is a chance that errors may be introduced when measuring physical quantities. These errors may come from the deviations from measuring instruments or devices. Fluctuations are always evident when measuring quantities and a repeat of these experiment will always yield different results. Therefore, results from the experiments could be described as random from a probability distribution standpoint [49]. In general, there are systematic deviations or random errors which is also known as uncertainties. One source of systematic error in these experiments came from not properly calibrating the ultrasonic thickness meter.

The ultrasonic thickness meter used had a calibration block used to calibrate the thickness meter to minimize systematic errors. Random error, also known as uncertainty, were very hard to predict as these are usually caused by fluctuations that are considered natural caused by the transducers precision limitations [49]. This chapter will use statistical tools to analyze the linear relationships between observation, probability and statistical significance of the experiments.

The distribution curves within this chapter are for both the inlet and the outlet which are expressed below. Considering the experiments conducted and for these variables observed a continuous random variable with a normally distributed characteristics will have parameters μ and $\sigma^2 > 0$ if the probability density function f is expressed as:

$$f\ (x) = \frac{1}{\sigma\sqrt{2\pi}} e^{-0.5\left(\frac{x-\mu}{\sigma}\right)\text{^}2} \quad for \quad -\infty < x < \infty.$$

$$\sigma = \sqrt{\frac{\Sigma(x - \bar{x})\text{^}2}{(n-1)}}$$

Where x is the thickness values observed, $\bar{x}$ represents the mean thickness measurements observed, n represent number of observations within the sample, σ is the standard deviation, σ^2 represent the variance and μ represent the population mean. The normal distribution is denoted by $N(\mu\sigma^2)$ [50]. The standard error is represented by $\sqrt{\sigma}/n$ where n represents the total number of thickness measurements over the period of continuous run time.

5.4.2 An Overview of Least Square Estimation Analysis

The linear regression model where the regressor *x* axis is referred to as time, and the corrosion thickness on the *y* axis will follow a model,

$$y = \beta_0 + \beta_1 x + \varepsilon$$

Where β_0 is the intercept and β_1 is the slope β_0 and β_1 constants that are not known and ε is defined as the error component and ε is not related with mean of zero [51]. The probability distribution of *y* for each time *x* exists and the mean of the distribution can be expressed as,

$$E(y|x) = \beta_0 + \beta_1 x$$

Variance is also expressed as

$$Var(y|x) = Var(\beta_0 + \beta_1 x + \varepsilon) = \sigma^2$$

β_0 and β_1 are the regression coefficients and are used for Least Square Estimation. β_0 and β_1 are estimated such that the sum of the square of the differences between the thickness measurements defined as y_i and the straight line through the plot are a minimum [51].

$$y_i = \beta_0 + \beta_1 x_i + \varepsilon_i, \qquad i = 1,2,\dots,n$$

Therefore, the least square is defined as;

$$S(\beta_0, \beta_1) = \sum_{i=1}^{n} (y_i - \beta_0 - \beta_1 x_i)\text{^}2$$

The least square estimation of β_0 *and* β_1 suppose $\widehat{\beta_0}$ and $\widehat{\beta_1}$ meets,

$$\frac{\partial s}{\partial \beta_0} = -2 \sum_{i=1}^{n} (y_i - \widehat{\beta_0} - \widehat{\beta_1} x_i) = 0$$

Where,

$$\frac{\partial s}{\partial \beta_1} = -2 \sum_{i=1}^{n} (y_i - \widehat{\beta_0} - \widehat{\beta_1} x_i) = 0$$

Simplifying the above two equations yields,

$$n\widehat{\beta_0} + \widehat{\beta_1} \sum_{i=1}^{n} x_i = \sum_{i=1}^{n} y_i$$

$$\widehat{\beta_0} \sum_{i=1}^{n} x_i + \widehat{\beta_1} \sum_{i=1}^{n} x_i^2 = \sum_{i=1}^{n} y_i \, x_i$$

The solution for the above least square normal equations is,

$$\widehat{\beta_0} = \bar{y} - \widehat{\beta_1} \bar{x}$$

Where,

$$\widehat{\beta_1} = \frac{\sum_{i=1}^{n} y_i \, x_i - \frac{(\sum_{i=1}^{n} y_i)(\sum_{i=1}^{n} x_i)}{n}}{\sum_{i=1}^{n} x_i^2 - \frac{(\sum_{i=1}^{n} x_i)^2}{n}}$$

and,

$$\bar{y} = \frac{1}{n} \sum_{i=1}^{n} y_i \;\; and \; \bar{x} = \frac{1}{n} \sum_{i=1}^{n} x_i$$

Denotes the average of y_i and x_i respectively and $\widehat{\beta_0}$, $\widehat{\beta_1}$ are the least square estimators for the equation,

$$\hat{y} = \widehat{\beta_0} + \widehat{\beta_1} \bar{x}$$

The residual is expressed as,

$$e_i = y_i - \hat{y_i} = y_i - \left(\widehat{\beta_0} + \widehat{\beta_1} x_i\right), \;\; i = 1, 2, 3, \ldots, n$$

The residual is very important when looking into how adequate the model is in determining values between estimated thickness measurements and true values of thickness measurements [51].

5.4.3 Valve Thickness Statistical Analysis Sodium Chloride Condition

This section considered the thickness error characteristics when NaCl was present and run through the loop continuously for 1,152 hours. In this case, the ultrasonic transducer was not permanently installed on the body of the valve.

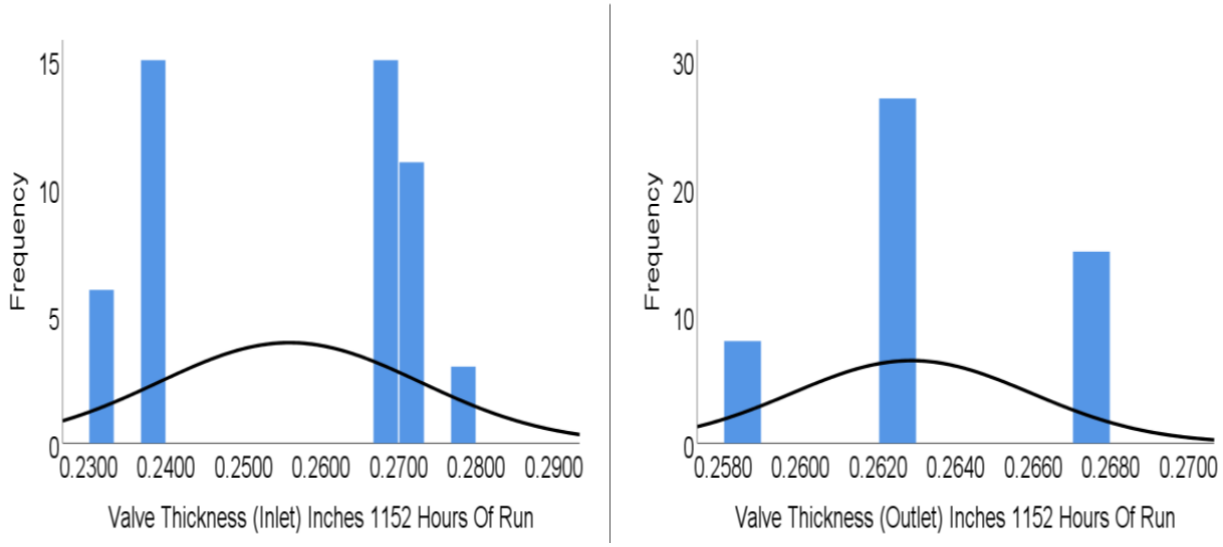

Figure 63. Inlet and outlet statistical distribution.

The graph shown in *Figure 63* was an indication that there was a decrease from the average of 0.2559 inches. There were similar data points collected over the period of 1,152 hours of experimentation with less variation in thickness loss of the inlet of the control valve been monitored for corrosion under NaCl conditions.

Figure 63 shows inlet and outlet frequency and thickness measurement of control valve body for 1152 hours continuous system. The normal curves for the inlet and outlet measurements superimposed on the histograms *Figure 63* looks very similar although the frequency in

thickness measurements were quite different. The differences came from the fact that the rate of material loss at the inlet of the valve was not the same as the rate of the material loss at the outlet of the valve. *Figure 64* shows the normal probability-probability plot of the inlet thickness measurements. The observed cumulative probability was plotted against expectation. The plot shows that data was somewhat not linear and therefore there are deviations from normal behavior. The normal distribution of the inlet and outlet looked similar in shape but differs in frequency.

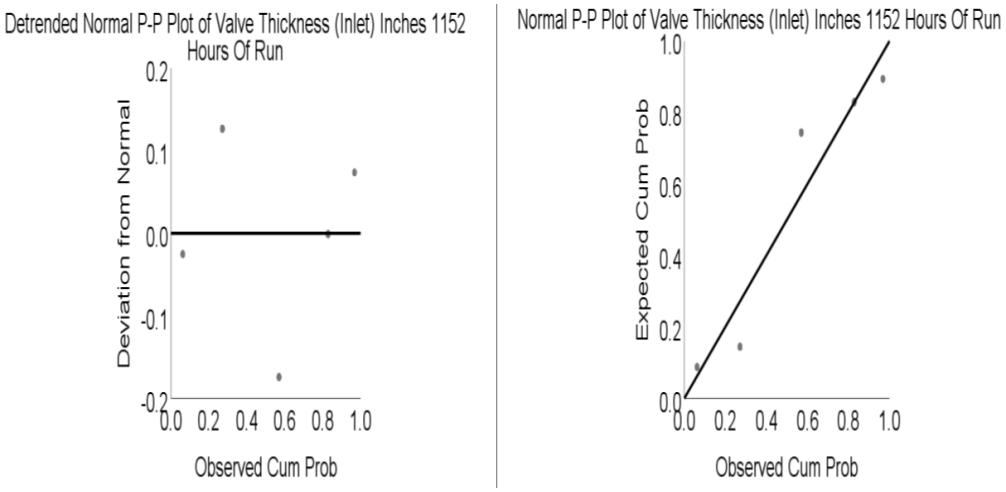

Figure 64. Inlet thickness measurements normal probability-probability graph.

Figure 64 The probability relationships for the inlet thickness for 1152 hours of continuous run time.

Figure 65 show probability relationships for the outlet thickness after 1152 hours of continuous run time. Figure 65. shows the valve outlet thickness errors when the valve was exposed continuously to NaCl solution for 1,152 hours. The mean thickness measurement was 0.2559 inches, the standard deviation of the thickness reading was 0.0169 inches and the standard error was ±0.0024 inches. These values estimated are for the inlet location of the valve when the ultrasonic transducer was not embedded on the valve body.

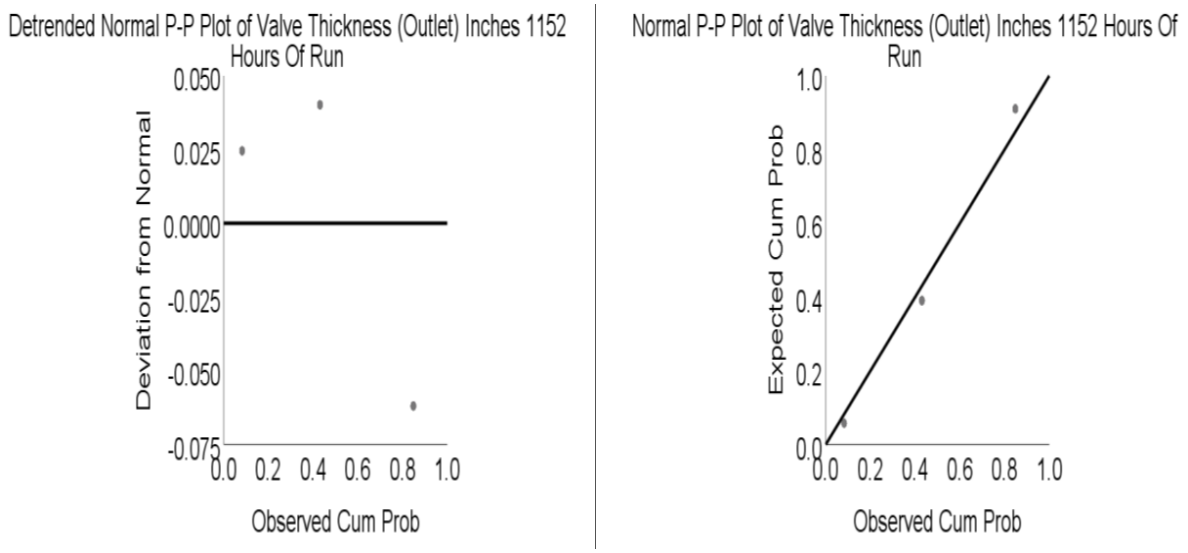

Figure 65. Outlet thickness measurements normal probability-probability graph.

The Average, standard deviation and standard error were 0.2629 inches, 0.0031inches and $\pm$0.0004 inches respectively. The valve inlet normal probability-probability in plot *Figure 65* shows a close to linear plot and therefore the model can be used with this data. The normal probability-probability plot shows that the deviation was ± 0.2 after 1,152 hours of continuous run of the system. A closer look at the detrended normal probability plot shows how much the observed cumulative probability deviated from a normal situation. The outlet had a deviation that ranged ± 0.050 and the thickness data was close to the expected normal cumulative probability after the system had run continuously for 1,152 hours. The observed thickness data per the normal probability-probability plot shows that the data is close to be linear.

Table 3 shows regression statistics for the 1,152 hours of runtime thickness measurements. The coefficient of determination R square shows that 68% of the 50 observations thickness readings fit the model for the inlet. But for the outlet an R square of 64% of the outlet thickness measurements fit the model. The thickness loss over time varied near the average are related to the time at which the thickness loss occurred.

Table 3 Regression Statistic for 1152 hours of runtime thickness measurements

Regression Statistics (Inlet 1152 Hours)		Regression Statistics (Outlet 1152 Hours)	
Multiple R	8.22E-01	Multiple R	8.02E-01
R Square	6.76E-01	R Square	6.43E-01
Adjusted R Square	6.70E-01	Adjusted R Square	6.36E-01
Standard Error	9.71E-03	Standard Error	1.86E-03
Observations	5.00E+01	Observations	5.00E+01

Note. Inlet and outlet thickness regression analysis.

Table 4 Analysis of Variance for runtime of1152 hours thickness measurements

ANOVA					
	Df	SS	MS	F	Significance F
Regression Inlet	1.00E+00	9.46E-03	9.46E-03	1.00E+02	2.42E-13
Residual Inlet	4.80E+01	4.53E-03	9.43E-05		
Total Inlet	4.90E+01	1.40E-02			
Regression Outlet	1.00E+00	3.00E-04	3.00E-04	8.65E+01	2.55E-12
Residual Outlet	4.80E+01	1.66E-04	3.46E-06		
Total Outlet	4.90E+01	4.66E-04			

Note. Inlet and outlet thickness Analysis of Variance.

Table 5 Regression Coefficients for 1152 hours of runtime thickness measurements

	Coefficients	Standard Error	t Stat	P-value	Lower 95%	Upper 95%	Lower 95.0%	Upper 95.0%
Intercept (Inlet)	0.233	0.003	85.83	3.38E-54	0.228	0.238	0.231	0.238
Time (Hours) Inlet	3.981E-05	3.98E-06	10.024	2.42E-13	3.183E-05	4.78E-05	3.18E-05	4.78E-05
Intercept (Outlet)	0.267	0.001	514.32	1.85E-91	0.266	0.268	0.266	0.268
Time (Hours) (Outlet)	-7.08E-06	7.62E-07	-9.30	2.55E-12	-8.62E-06	-5.56E-06	-8.62E-06	-5.56E-06

Note. Inlet and outlet ultrasonic transducers thickness coefficients.

Table 5 shows that there was not a significant difference between the Least Square Estimators for both the inlet and outlet thickness measurements taken. The intercept of 0.233 for the inlet

and the outlet was 0.267 for the period of 1,152 hours were recorded. The thickness loss for the inlet and outlet thickness measurements were 3.981E-05 hours and -7.087E-06 hours respectively. The *p* values recorded in table 5 are less than the significant level of 0.05.

Figure 66 shows the relationship and line fitness between the valve thickness values and predicted valve thickness measurements by the ultrasonic thickness meter for the inlet and outlet ultrasonic valve thickness measurements.

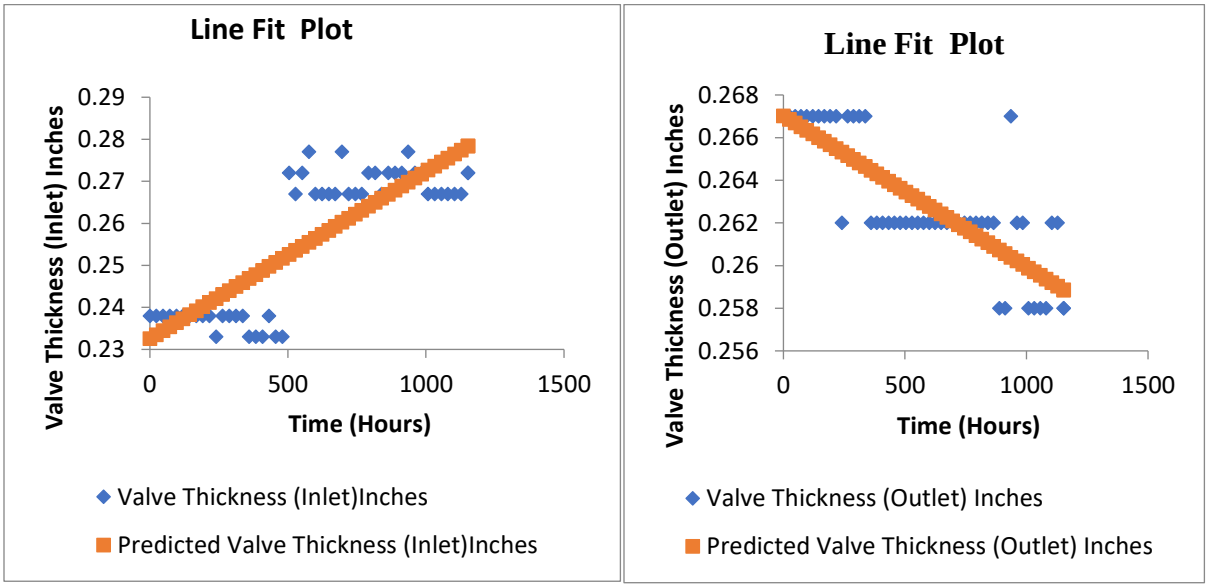

Figure 66. Line fit plot for inlet and outlet thickness.

Figure 66 shows the relationship between valve body thickness and predicted valve body thickness for both inlet and outlet thickness measurements for 1152 hours of runtime. It can be seen in the plots that the relations were not linear and most of the valve thickness measurements were not close to the predicted valve thickness. This is the case for both the inlet and outlet ultrasonic thickness measurements.

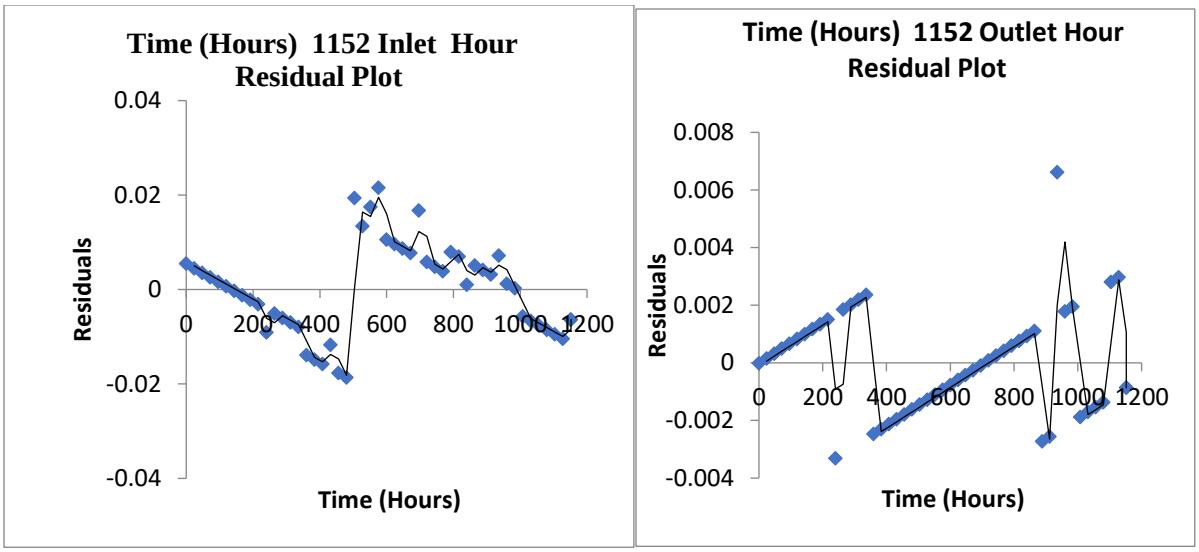

Figure 67. Residual plot for inlet and outlet thickness.

Figure 67 shows the relationship between valve body residual thickness for both inlet and outlet thickness measurements for 1152 hours of runtime. The inlet residual plots do not have traits of a trends, shifts or cycles. The residuals seem to be distributed randomly around the residual centerline. But there seems to be a point in the outlet thickness measurements which were an outlier not too far from zero.

5.4.4 NaCl Condition Sources of Error

The starting inner diameter of the valve used during the NaCl test solution was (1.3 inches) 33 mm. This valve dimension was taken from the valve specification as reported by the valve manufacturer. During the experiment for the NaCl condition there were several sources of error. One of the sources of error was each time the ultrasonic measurement was taken manually. The ultrasonic transducer was remounted for this test, introducing error due to how the ultrasonic transducer was mounted on the valve body. During the experiment for the NaCl condition, the ultrasonic transducer needed to be calibrated multiple times due to an ultrasonic technology limitation which introduced thickness measurement drift over time. These errors

were also demonstrated in the linear regression analysis that was evaluated for the 1152 hours of run.

The valve surface curvature was also a source of error because surface of the ultrasonic transducer needed to be well seated and mounted on the surface of the valve body to minimize error while transmitting and receiving ultrasonic signals. The significant amount of error exhibited in the linear regression analysis suggested that this method of testing was not viable. In order to avoid this source of error a new testing method consisting of the ultrasonic transducer mounted permanently on the valve body was developed. In order to overcome the testing limitations seen in this test, an alternative sampling method was used in all future experiments. A second change to experimental apparatus was the addition of acetic acid to increase the rate of corrosion. The starting inner diameter for theses valves was 0.98 inches. These valve dimensions where taken from the valve specification as reported by the valve manufacturer.

5.4.5 Valve Thickness Statistical Analysis NaCl and Acetic Acid Condition I

This section considers thickness error characteristics when NaCl and acetic acid was present and recirculated through the loop continuously for 408 hours. In this case, the ultrasonic transducer was permanently installed on the body of the valve. *Figure 68* shows inlet and outlet frequency and thickness measurements of the valve body for 408 hours continuous system. The normal distribution function was used to assess errors in the data taken for the inlet and outlet of the control valve under testing during 408 hours of experimental observation [50].

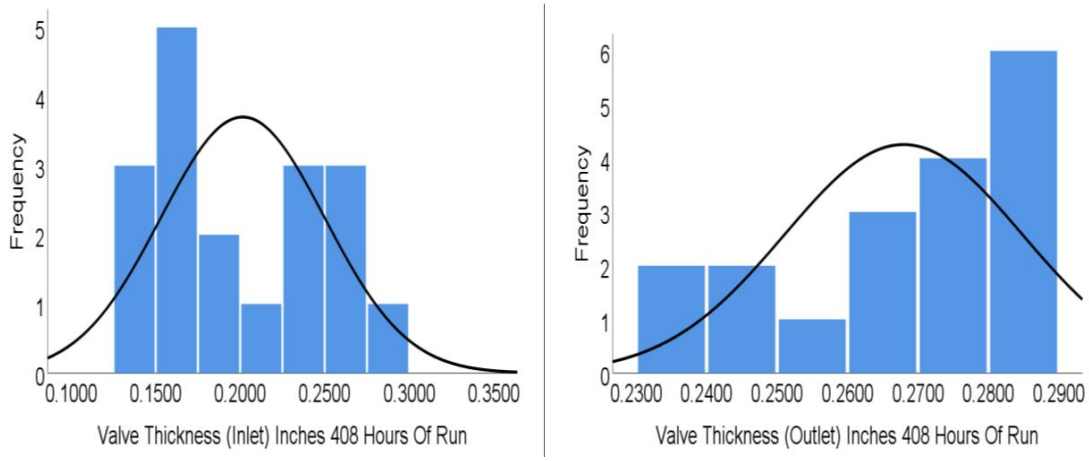

Figure 68. Inlet and outlet statistical distribution.

The inlet observations seemed to have the distribution descriptively somewhat skewed to the right, but the average of the data collected were positive. The graph indicates values that are acceptable since the decreases are in the positive direction and below the mean value of 0.202 inches. Similarly, the observation for the outlet is skewed to the left with the thickness decreasing below the average positive value of 0.278 inches.

Figure 69 shows the normal probability-probability plot for the inlet thickness measurements after 408 hours of continuous running of the system. The normal probability-Probability plot shows a deviation with a range of ± 0.15 from the normal cumulative probability. This is an indication that the readings taken were not linear [50]. *Figure 69* also shows how the observed cumulative thickness data deviated from the expected cumulative data set. The inlet mean value was 0.185 inches, standard deviation of 0.046 inches and a standard error of ± 0.011 inches. Figure 69 show probability relationships for the inlet thickness 408 hours of continuous run time.

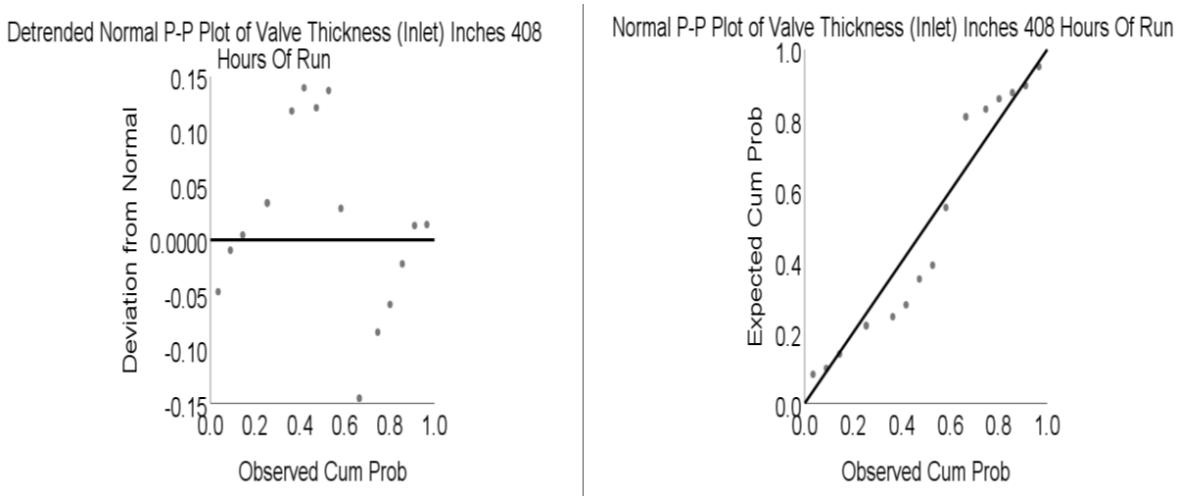

Figure 69. Inlet thickness measurements normal probability-probability graph.

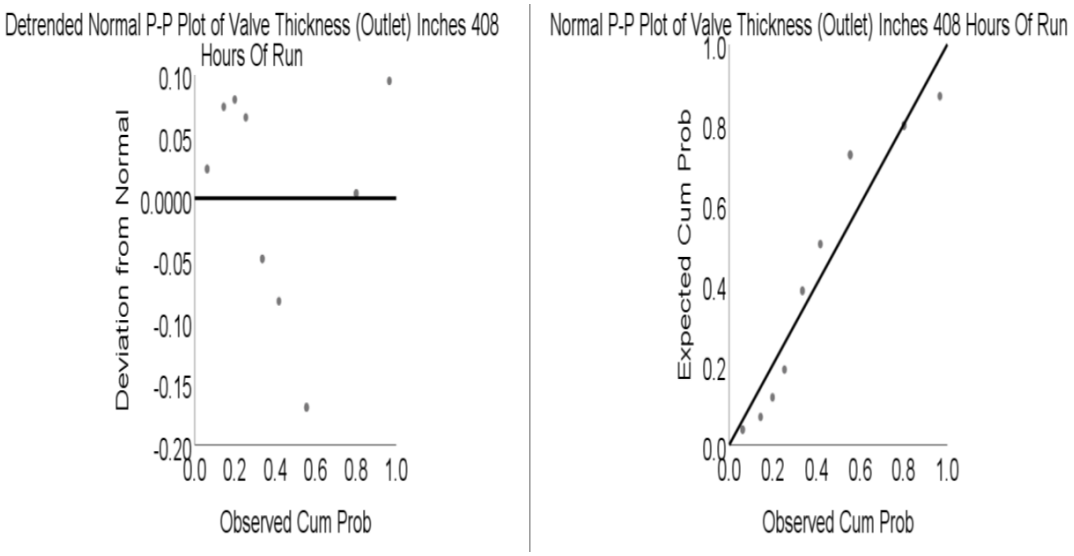

Figure 70. Outlet thickness measurements normal probability-probability Graph.

Figure 70 show the probability relationships for the outlet thickness for 408 hours of continuous run time. The outlet normal probability-probability plot is shown in Figure 70. where the deviation from normal was in the range of $-0.2\ and\ +0.10$. Meanwhile the outlet had a mean of 0.268 inches, a standard deviation 0.017 inches, and a standard error $\pm$ 0.004 inches. The observed cumulative probability for the thickness data did not form a straight line, demonstrating, the nonlinear characteristics of the data collected for the thickness readings

during the 408 hours of continuous run when the ultrasonic transducer was not permanently mounted on the body of the valve.

Table 6 shows the regression statistics for 408 hours of runtime while inlet and outlet thickness. A percentage of 85% represent the coefficient of determination, which means that 85% of the measurements fit the model for the inlet ultrasonic thickness measurements. The outlet had a coefficient of determination of 80% and therefore 80% of the data collected fits the model for the outlet thickness measurements. The number of measurements observed were 18 for this experiment with a runtime of 408 hours.

Table 6 Regression statistics for 408 hours thickness measurements

Regression Statistics (Inlet 408 Hours)		Regression Statistics (Outlet 408 Hours)	
Multiple R	9.24E-01	Multiple R	8.94E-01
R Square	8.54E-01	R Square	7.98E-01
Adjusted R Square	8.44E-01	Adjusted R Square	7.86E-01
Standard Error	1.91E-02	Standard Error	7.81E-03
Observations	1.80E+01	Observations	1.80E+01

Note. Inlet and outlet thickness regression analysis.

Table 7 Analysis of variance for 408 hour of runtime thickness measurements

ANOVA					
	Df	SS	MS	F	Significance F
Regression Inlet	1.00E+00	3.41E-02	3.41E-02	9.33E+01	4.44E-08
Residual Inlet	1.60E+01	5.84E-03	3.65E-04		
Total Inlet	1.70E+01	3.99E-02			
Regression Outlet	1.00E+00	3.87E-03	3.87E-03	6.34E+01	5.90E-07
Residual Outlet	1.60E+01	9.76E-04	6.10E-05		
Total Outlet	1.70E+01	4.84E-03			

Note. Inlet and outlet thickness Analysis of Variance.

Table 8 Regression coefficients for 408 hours runtime thickness measurements

	Coefficients	Standard Error	t Stat	P-value	Lower 95%	Upper 95%	Lower 95.0%	Upper 95.0%
Intercept Inlet	2.73E-01	8.65E-03	3.15E+01	7.76E-16	2.54E-01	2.91E-01	2.54E-01	2.91E-01
Time Hours Inlet	-3.49E-04	3.62E-05	-9.66E+00	4.44E-08	-4.26E-04	-2.73E-04	-4.26E-04	-2.73E-04
Intercept Outlet	2.92E-01	3.53E-03	8.26E+01	1.75E-22	2.84E-01	2.99E-01	2.84E-01	2.99E-01
Time Hours Outlet	-1.18E-04	1.48E-05	-7.96E+00	5.90E-07	-1.49E-04	-8.64E-05	-1.49E-04	-8.64E-05

Note. Inlet and outlet ultrasonic transducers thickness coefficients.

Table 8 show the Least Square Estimators for both the inlet and the outlet and the intercept are 2.73E-01 and 2.92E-01respectively. The time in hours for thickness changes for the inlet and the outlet measurements are -3.49E-04 and -1.18E-04 respectively. The *p* values from Table 8 for both the inlet and outlet ultrasonic thickness measurements w less than 0.05 for the runtime of 408 hours.

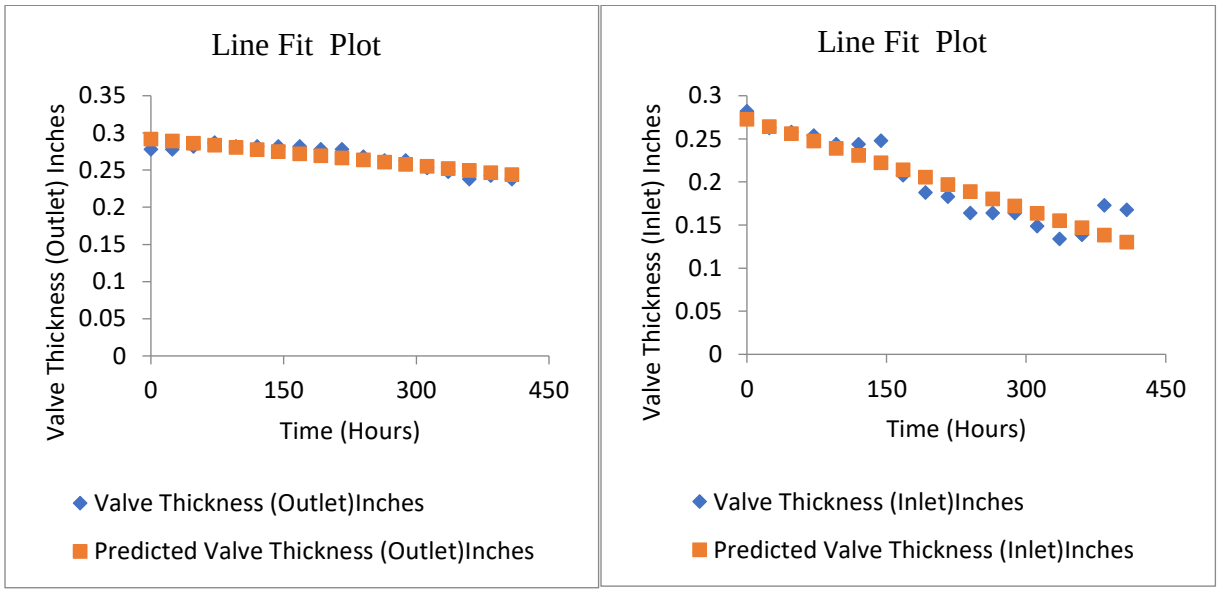

Figure 71. Line fit plot for inlet and outlet thickness.

Figure 71. shows the relationship between the valve body thickness measurements and predicted valve body thickness for both the inlet and outlet for 408 hours of runtime.

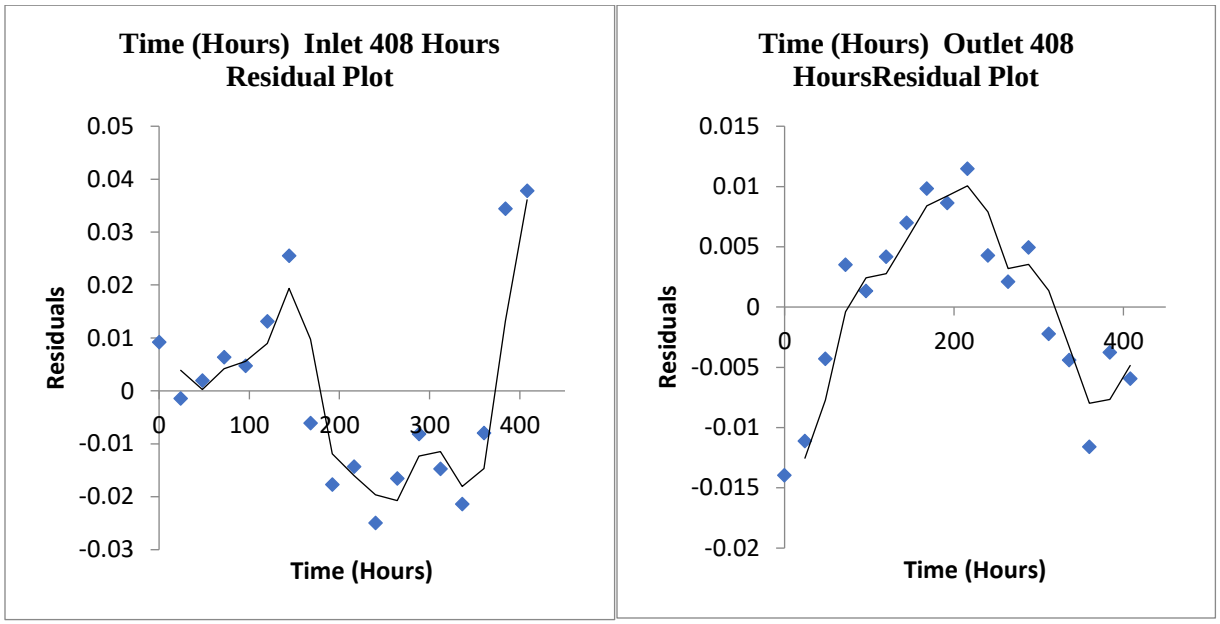

Figure 72. Residual plot for inlet and outlet thickness.

Figure 72 shows the valve body residual thickness for both inlet and outlet thickness measurements for 408 hours of runtime. *Figure 72* shows the inlet and outlet residual ultrasonic thickness relationship over 408 hours of runtime. There were no cycles, shifts or trends in the residual plots for both the inlet and outlet for this period of running the flow loop for 408 hours.

5.4.6 Valve Thickness Statistical Analysis NaCl and Acetic Acid Conditions II

This section documents the evaluation of the thickness error characteristics when NaCl and acetic acid were present and ran through the loop continuously for 240 hours. In this case, the ultrasonic transducer was permanently embedded on the body of the valve. The graphs below show a comparison of the inlet and outlet thickness measurements over a continuous run of 240 hours with the ultrasonic transducer embedded on the surface of the ball valve. *Figure 73* shows the difference in the normal distribution curves for the inlet and outlet material thickness loss.

This inlet thickness loss for 240 hours of run time has a mean of 0.441inches, a standard deviation of 0.040 inches and a standard error of $\pm$0.01 inches.

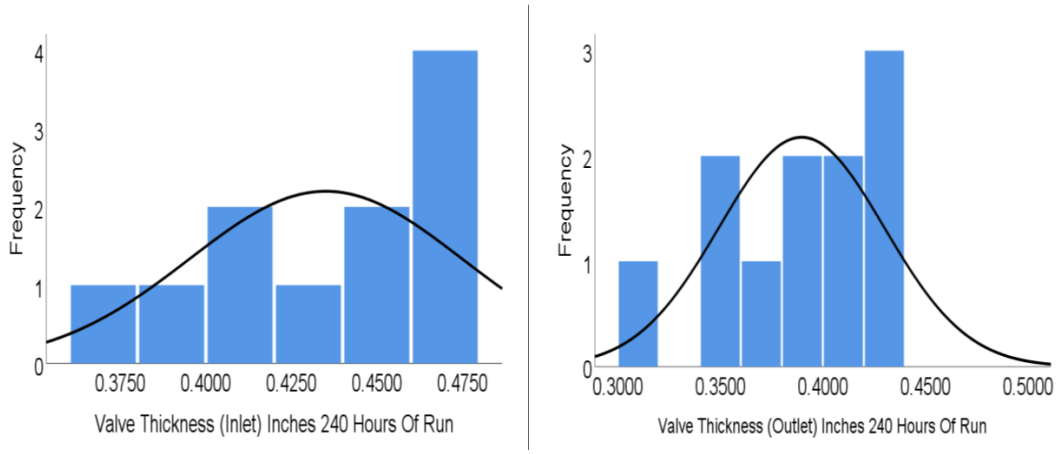

Figure 73. Inlet and outlet statistical distribution.

Figure 73 shows inlet and outlet frequency and thickness measurement of control valve body for the 240 hours continuous system. *Figure 74* compares a normal probability-probability plot with a detrended normal Probability-Probability plot for thickness readings for the embedded ultrasonic transducer at the inlet point of the valve.

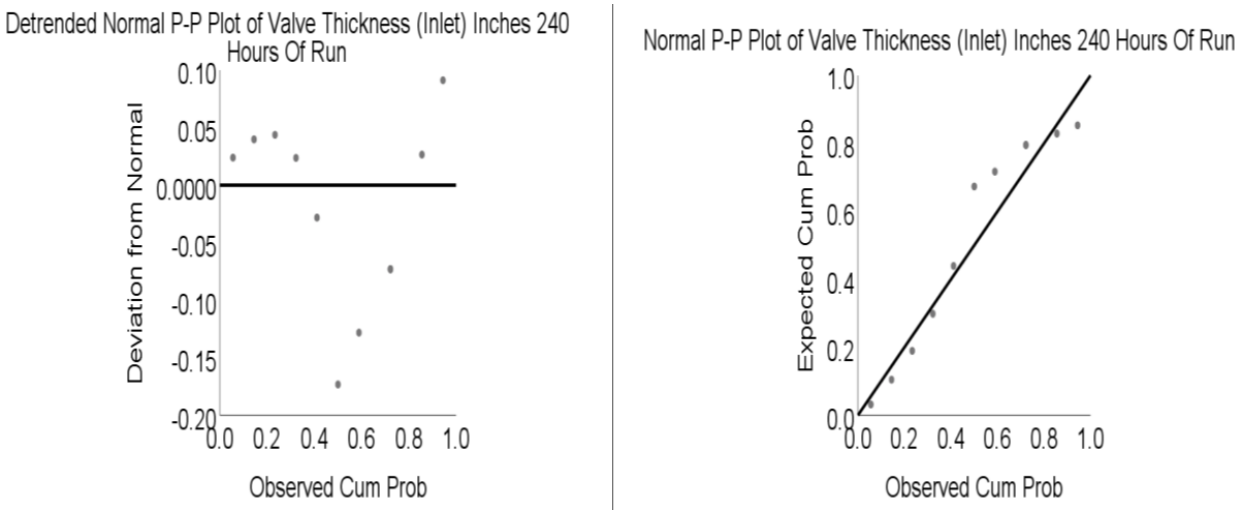

Figure 74. Inlet thickness measurements normal probability-probability graph.

Figure 74 shows the probability relationships for the inlet thickness for 240 hours of continuous run time with addition of water, acetic acid and NaCl.

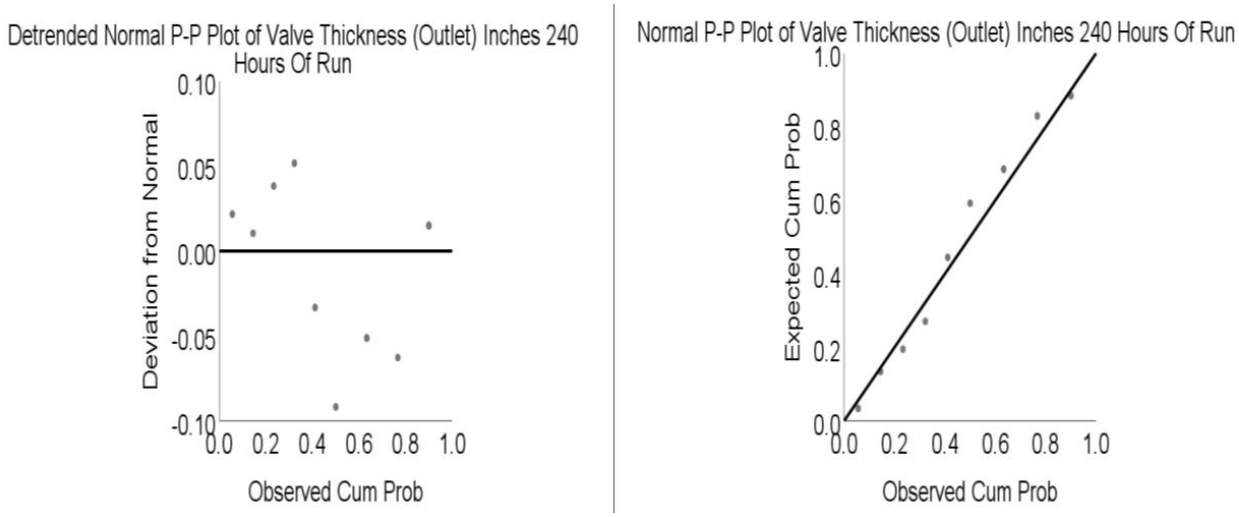

Figure 75. Outlet thickness measurements normal probability-probability graph.

As can be seen the normal probability-probability plot of observed cumulative thickness probability was close to the normal expected cumulative line. This suggests that the thickness readings taken when the transducer was embedded on the valve were close to the normal distribution with a deviation from normal between ± 0.10 as seen on the detrended normal probability-probability plot. The average outlet thickness loss measurement for the 240 hours of continuous run was 0.39 inches, with a standard deviation of 0.04 inches and a standard error ± 0.01 inches.

Table 9 below shows the regression statistics for the 240 hours of runtime for both the inlet and outlet thickness measurements. The coefficient of determination for the inlet and outlet thickness measurements are 93% and 97% respectively. The observation fits the model 96% for the inlet ultrasonic thickness measurements and 98% for the outlet ultrasonic thickness measurements.

Table 9 Regression Statistics for 240 hours thickness measurements

Regression Statistics Inlet Measurements 240 Hours of run time		Regression Statistics Outlet Measurement for 240 Hours of run time	
Multiple R	0.96	Multiple R	0.983
R Square	0.93	R Square	0.97
Adjusted R Square	0.92	Adjusted R Square	0.96
Standard Error	0.01	Standard Error	0.01
Observations	11	Observations	11

Note. Inlet and outlet thickness regression analysis.

Table 10: Analysis of Variance 240 Hours of runtime

ANOVA					
	df	SS	MS	F	Significance F
Regression Inlet Thickness	1.00E+00	1.47E-02	1.47E-02	1.12E+02	2.24E-06
Residual Inlet Thickness	9.00E+00	1.18E-03	1.32E-04		
Total Inlet Thickness	1.00E+01	1.59E-02			
Regression Outlet Thickness	1.00E+00	1.57E-02	1.57E-02	2.60E+02	6.05E-08
Residual Outlet Thickness	9.00E+00	5.44E-04	6.05E-05		
Total Outlet Thickness	1.00E+01	1.62E-02			

Note. Inlet and outlet thickness Analysis of Variance

The outlet regression coefficients from table 11 are 4.49E-01 for the intercept and -4.98E-04 for the rate at which the decrease is occurring for the outlet in hours. The *p* values for the inlet and outlet measurements are less than the significant level of 0.05**.** The lower *p* values confirmed that there is statistical significance between the thickness readings and the term.

Table 11 Regression coefficients for 240 hours runtime thickness measurements

	Coefficients	Standard Error	t Stat	P-value	Lower 95%	Upper 95%	Lower 95.0%	Upper 95.0%
Intercept (Inlet)	4.93E-01	6.47E-03	7.62E+01	5.86E-14	4.78E-01	5.08E-01	4.78E-01	5.08E-01
Time (Hours) Inlet	-4.82E-04	4.56E-05	-1.06E+01	2.24E-06	-5.85E-04	-3.79E-04	-5.85E-04	-3.79E-04
Intercept Outlet	4.49E-01	4.39E-03	1.02E+02	4.08E-15	4.39E-01	4.59E-01	4.39E-01	4.59E-01
Time (Hours) Outlet	-4.98E-04	3.09E-05	-1.61E+01	6.05E-08	-5.68E-04	-4.28E-04	-5.68E-04	-4.28E-04

Note. Inlet and outlet ultrasonic transducers thickness coefficients.

Figure 76 shows the relationship between valve body thickness and predicted valve body thickness for both inlet and outlet thickness measurements for 240 hours of runtime.

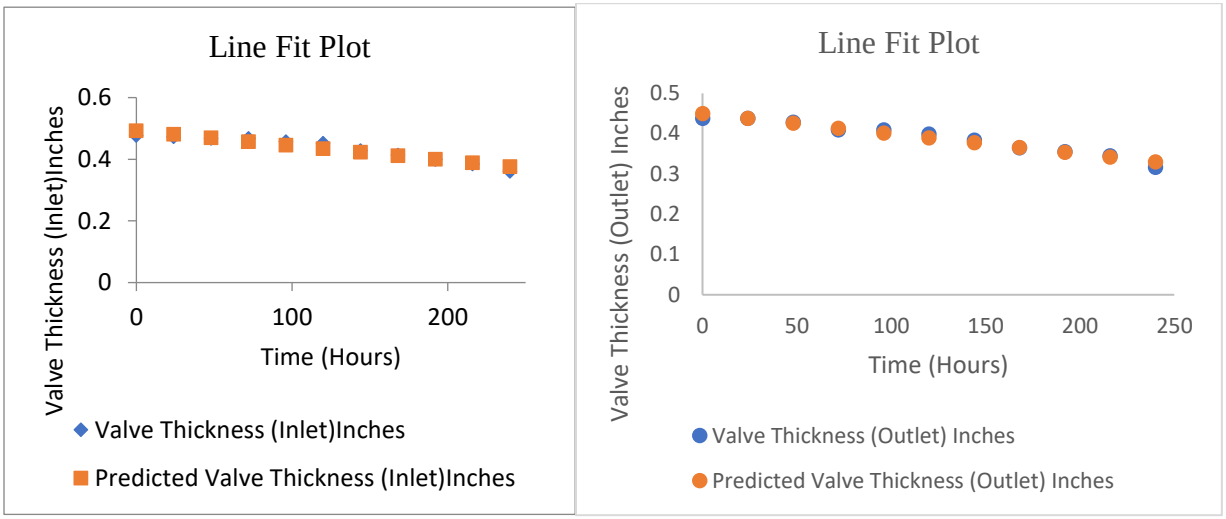

Figure 76. Line fit plot for inlet and outlet thickness.

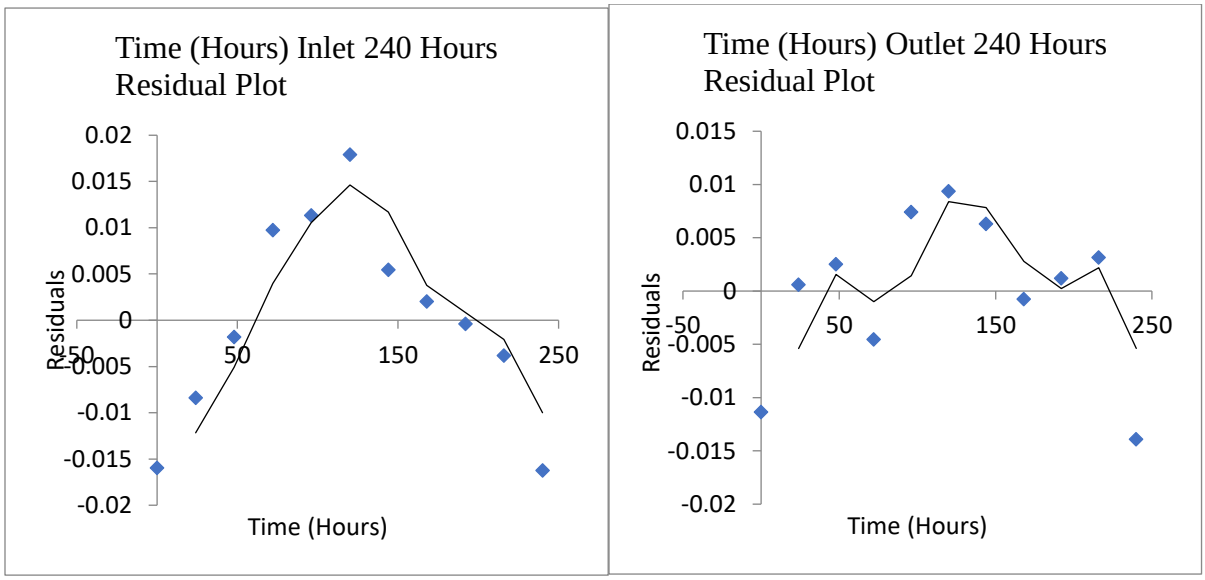

Figure 77. Residual plot for inlet and outlet thickness.

Figure 77 shows the relationship between the valve body residual thickness for both the inlet and outlet thickness measurements for 240 hours of runtime. Although there are no cycles, shifts or

trends, both residual plots show signs of outliers in the thickness measurements which are not too far away from zero.

5.5 Ambient Conditions and Valve Position Effects on Thickness Measurements

5.5.1 Ambient Conditions, Valve Positioning Overview

This section discusses how ambient conditions affected thickness measurements when ultrasonic transducers was used for thickness measurements. Ambient conditions that were considered were the inlet and outlet temperatures, vibration, noise and air pressure. The position of the valve was also changed at various percentages to observe if the readings from the ultrasonic transducers for the inlet and outlet readings were affected.

5.5.2 Ambient Temperature Effect on Ultrasonic Transducer Thickness Reading

In order to determine the impact of cold temperatures on the ultrasonic measurements, an ice pack was directly placed on the transducers and measurements were taken while the flow loop circulated fluid at a maximum flow. Temperature readings were taken while the temperature was changed and became relatively warmer during this observation. Cold temperatures did not have any adverse impact on the readings, and during this period of ambient temperature testing, acoustic coupling was maintained. *Figure 78* shows a plot of measured inlet thickness versus transducer temperature. The warmest temperature recorded of 77.9°F and the coldest temperature recorded was an inlet temperature was 11.7 °F.

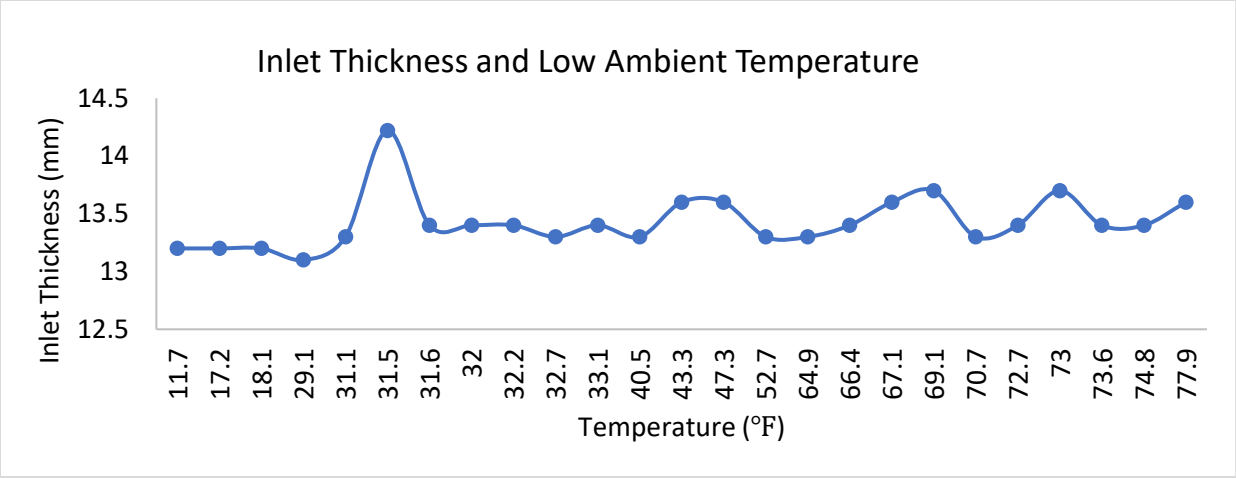

Figure 78. Relationship between the inlet thickness and low temperature.

There was a spike in thickness reading of 14.22 mm when the temperature reached 31.5 *°F*. Between 32.7*°F* and 52.7*°F* the thickness flatulated between 13.3 mm and 13.6 mm. The readings indicate that the measured thickness is somewhat dependent on temperature.

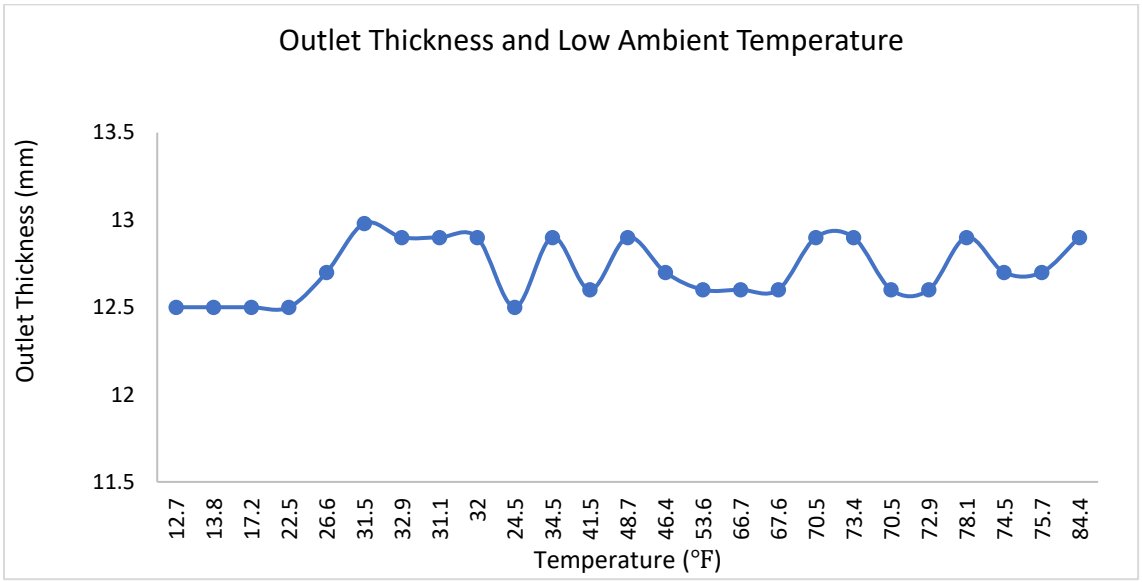

Figure 79. Relationship between outlet thickness and low ambient temperature.

Figure 79 shows outlet thickness measurements versus the ambient temperature. The outlet thickness between 12.5°F and 22.5°F remained at 12.5mm with no variation when thickness readings were observed . An electronic thermometer was used to measure these

temperatures. When the temperature reached 31.5°F the thickness reading was the highest at 12.98 mm. Between 35°F and 49°F the thickness relationship showed some variability in the data. Ultrasonic thickness readings for the outlet became stable between 46.4°F and 67.6°F at a thickness reading of between 12.7 mm and 12.6 mm.

When the temperature increased to between 67℉ and 79℉, some random variability was observed in the thickness measurements. When the temperature reached 74.5℉ a linear relationship developed until the final test ambient temperature of 84.4℉. During these temperatures, the thickness observed was between 12.7 mm and 12.9 mm. Under these ambient cold temperature conditions, thickness readings observed were not stable for both the inlet and outlet thickness measurements.

A variable heat blower was used to create a higher ambient temperature within an area of $0.016m^2$ where the ultrasonic transducer was embedded on the valve body. The initial temperature was 120℉ and this temperature was increased in 50 ℉ increments to a final temperature of 400℉. The high temperature increments were conducted within one minute of each other. The heat blower had an embedded thermometer which display the temperature readings.

Figures 80 shows thickness measurement versus the ambient temperature during the high temperature testing for both the valve inlet and outlet . As seen in *Figure 80* between 120°F and 200°F the measured thickness varied by only 0.1 mm.

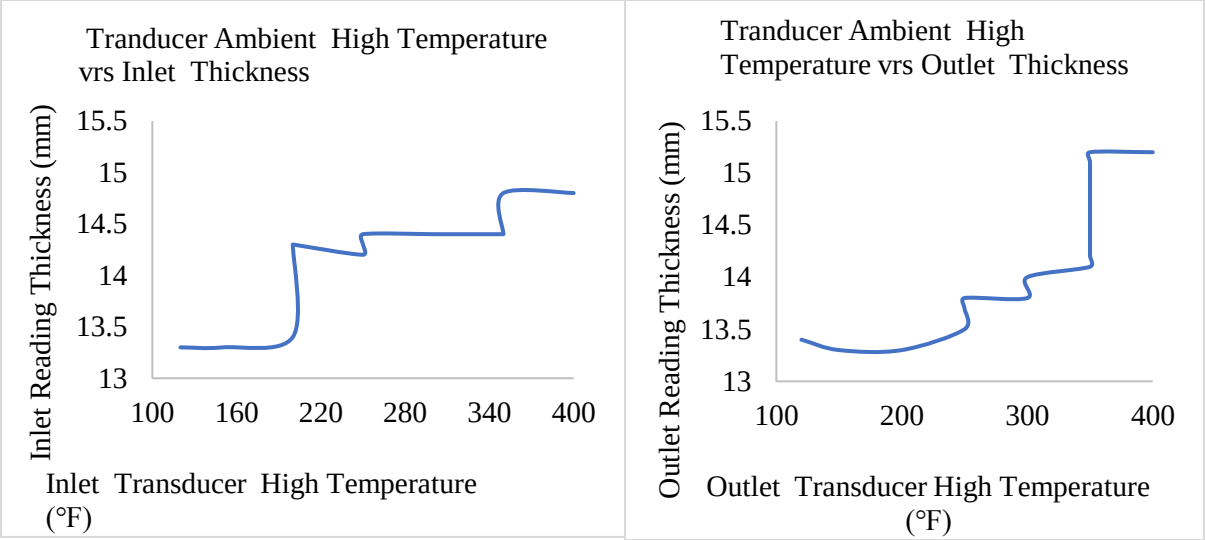

Figure 80. Transducer ambient high temperature and thicknesses.

When the ambient temperature increased to above approximately $220℉$ the thickness measurements became unreliable. The inlet ultrasonic transducer lost signal as there was no acoustic coupling at $300℉$ and the outlet transducer signal loss started at $350℉$. In both cases at these signal loss temperatures, the ultrasonic meter indicated thickness measurements but there was no acoustic coupling between the surface of the transducer and the valve body.

5.5.3 Ambient Vibration Effect on Ultrasonic Transducer Thickness Reading

The vibration was simulated by using a hand-held hammer to initiate vibration by striking the hammer on the body of the valve and a vibration meter was used to record the vibration values in $\mathrm{m/s^2}$. *Figure 81* shows the results of vibration simulated at low frequency of 1KHz for the inlet and outlet areas on the valve body where ultrasonic transducers were mounted. A hammer was used to strike the valve body and immediately after the imposition, a digital vibrometer was placed on the valve body to measure vibration. The values recorded for vibration simulated were the initial value immediately after the strike of the hammer on the valve body. When there was no flow and the flow loop was shutdown, the vibration value was $0\mathrm{m/s^2}$.

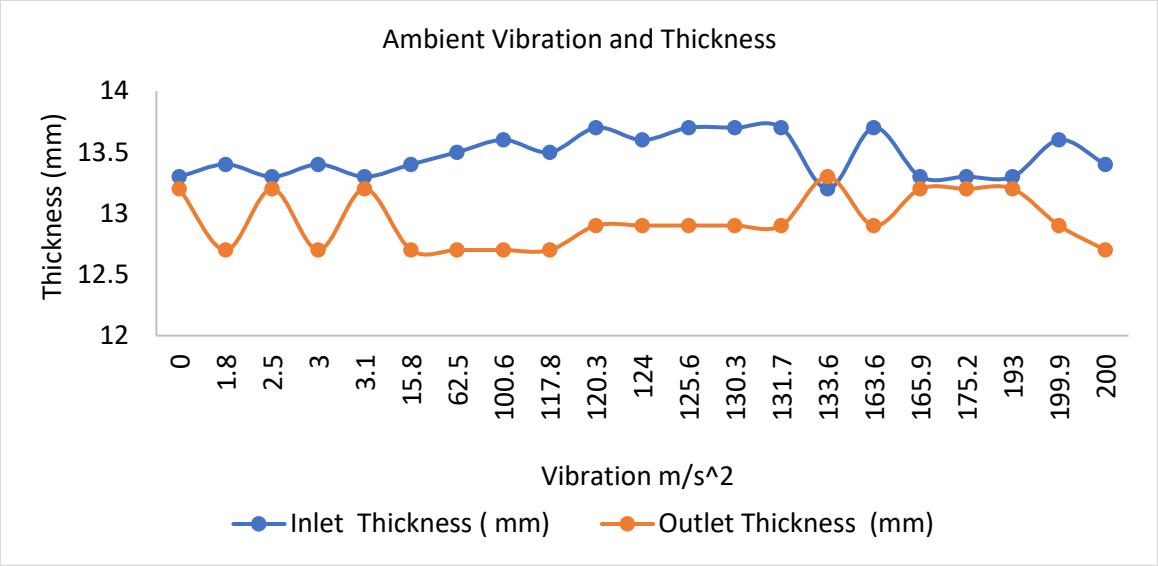

Figure 81. Thickness and ambient vibration.

Figure 81 shows the measured thickness versus the imposed vibration. *Figure 81*. shows that from zero vibration to 117.8 m/s^2 the relationship between the inlet thickness, outlet thickness was somewhat similar as seen in the graph. As seen in Figure 81 an imposed vibration at 1KHz did not have a large impact on the ultrasonic thickness measurements. Thickness measurements varied by less than 2%. The average ambient temperature during these observations was 79°F. These measurements were taken when the valve was open to 100%. The thickness measurements for the inlet and outlet did not change as observed in this experiment.

5.5.4 Ambient Noise Effect on Ultrasonic Transducer Thickness Reading

In order to determine if ambient noise common in industrial settings had an impact on the ultrasonic measurements the experimental apparatus was subjected to simulated noise ranging 67dB to 117dB and throughout the noise ranges, inlet and outlet ultrasonic thickness measurements were observed. A sound system was used as the source of noise.

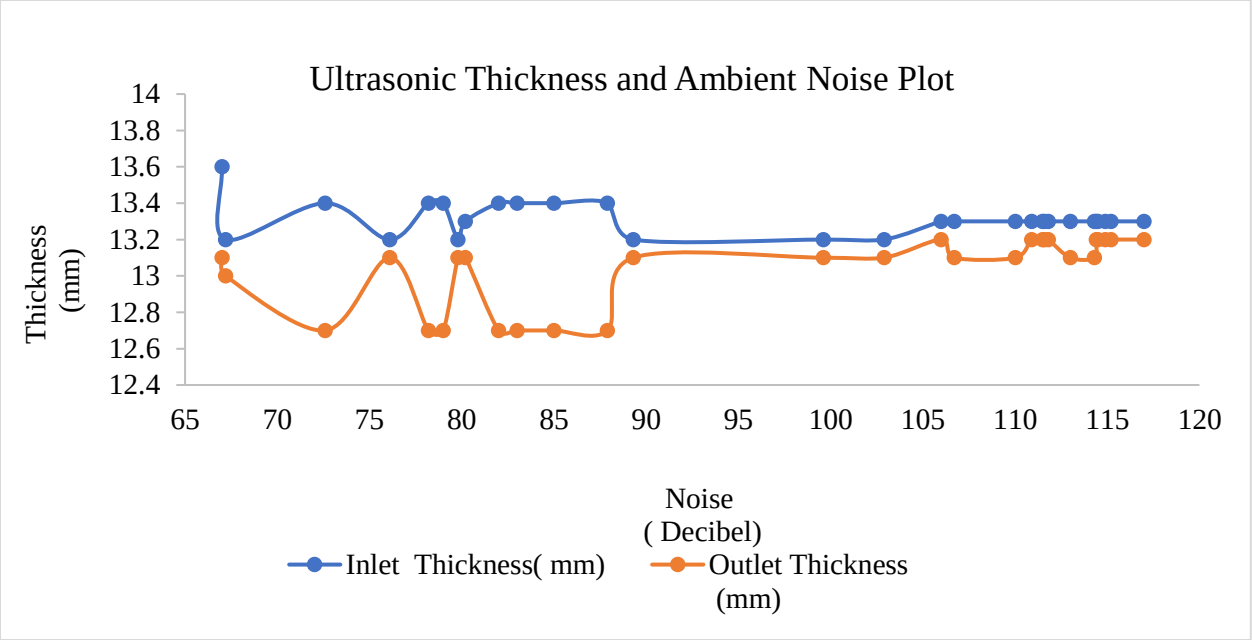

Figure 82. Ultrasonic thickness and ambient noise plot.

Figure 82 shows the ultrasonic thickness measurements as a function of ambient noise in dB. A digital decibel meter was used to measure the noise levels and during the test there were minimal changes in both the inlet and outlet ultrasonic thickness readings between noise measurement in dB and the ultrasonic thickness measurements.

It can be seen that the inlet thickness from 67 dB showed a variation of the thickness from 13.6 mm to 13.2 mm and then after 67 dB, observed until 79.8 dB. Inlet readings grew from 79.8 dB to 82 dB and then remained constant from 82 dB to 87.9 dB. The inlet thickness and the noise in dB assumed a linear relationship between 102.9 dB and 106 dB when the thickness varied from 13.2 mm to 13.3 mm, but a constant relationship was observed from 106.7 dB to 107 dB for the inlet. Although there was some variability imposed on the ultrasonic thickness measurements by the ambient noise, this was generally within 2%.

5.5.5 Ambient Air Pressure Effects on Ultrasonic Transducer Thickness Reading

Table 12 below shows how the ambient air pressure impacted the ultrasonic thickness reading. The air pressure was provided by an air compressor with the pressure varying from 0 PSIg to 125 PSIg. During this testing the ambient air temperature was noted, and the corresponding noise and the air pressure were also recorded. The ambient temperature was maintained at 79.7 °F.

Table 12 Ambient pressure effects on ultrasonic thickness readings

Ambient Pressure (PSI)	Inlet Thickness (mm)	Outlet Thickness (mm)	Mass Flow Rate (kg/min)	Process Temperature (F)	Noise (dB)
0	13.7	12.9	131.28	82.23	75.53
25	13.7	12.9	131.21	83.32	110.32
50	13.7	12.9	130.03	83.36	116.03
75	13.7	12.9	131.46	83.39	123.23
100	13.7	12.9	131.56	83.57	124.46
125	13.7	12.9	131.06	83.59	126.11

The ultrasonic thickness readings did change as the ambient pressure was varied from 0 PSIg to 125 PSIg. During this testing the fluid mass flow rate remained constant while the valve was in a fully open position. When there was no air pressure exposed to the ultrasonic transducers, the noise level was 75.53 dB and the average process temperature was 83.24$℉$.

5.5.6 Valve Positioning and Thickness Measurements Effects

The next test was designed to determine if the valve position had an impact on the ultrasonic thickness measurement. Table 13 shows the results of these tests. It is readily apparent that the valve position did not impact the ultrasonic thickness readings.

Table 13 Valve Positioning and Thickness Measurements Effect

Inlet Thickness (mm)	Outlet Thickness (mm)	Mass flow kg/min	Valve Position %
13.4	12.9	131.31	100
13.4	12.9	127.23	75
13.4	12.9	68.11	50
13.4	12.9	0	0

As the valve position changed from fully open to fully closed the ultrasonic thickness measured did not change.

5.5.7 Ambient effects and Valve Position Findings

The ambient conditions tested show that temperatures, noise, vibration and air pressure had varied impacts on the ultrasonic thickness readings. Air pressure had no impact and ambient noise and vibration had minimal impact on ultrasonic thickness readings.

When the ultrasonic transducers for the inlet and the outlet were exposed to air pressures ranging from 0 PSIg to 125 PSIg, no changes were observed for the inlet and outlet ultrasonic thickness measurements. The position of the valve was varied from 0% to 100% again with no impact on the ultrasonic thickness for the inlet and outlet measurements.

Vibration was introduced on to the valve body by with a hammer at a low frequency of $1KHz$ with vibration varied from 0 m/s^2 to 200 m/s^2. There were relatively minimal changes observed in the thickness readings for the inlet and outlet thickness measurements. When the ultrasonic transducer was exposed to ambient noise, there was minimal impact on the ultrasonic thickness readings from 67dB to 117 dB. There were changes during this noise exposures for the inlet and outlet thickness measurements observed. This indicate that ultrasonic transducers are a viable and robust method of monitoring corrosion rates in control valves.

5.6 Industrial Safety and Quality Assurance

5.6.1 Ultrasonic Thickness Monitoring Technology Exposure to Industrial Conditions

This section discussed safety, quality assurance and quality control measures for the ultrasonic thickness monitoring technology used to evaluate thickness loss of the one-inch valve body. The ultrasonic thickness meter has multiple components i.e. transducer electronics , batteries that provide supply for the meter, a pulser, receiver, synchronous generator, amplifier, a digital display and cables. This research proved that after 300 °F of ambient temperature exposure, the ultrasonic thickness meter lost signal and therefore the thickness readings were not valid after 300℉. But the existing apparatus was capable of reliably measuring the thickness up to 250℉.

The ultrasonic thickness monitoring technology used in this research was not designed for chemical process areas or hazardous conditions and if the right circumstance are present, ultrasonic can be a source of ignition [52]. There are other ignition sources such as static electricity, equalizing current, lightning, electromagnetic fields, optical radiation, open flame and hot gases [52]. The ultrasonic thickness monitoring technology may be designed, manufactured and encapsulated in an explosion proof casing to minimize some of the hazards that may be present in a chemical process plant environment. For hazardous area applications, components of the ultrasonic thickness monitoring technology shall be designed to withstand such conditions. The quality of materials used for the ultrasonic thickness monitoring technology shall be selected to ensure that the ultrasonic transducer does not become a source of ignition.

5.7 Thickness Measurement Precision and Measurement Reliability

This section discussed the quality of thickness measurements for the three experiments conducted. A digital caliper gauge was used to take thickness measurements for all three valves when there was no flow to validate the ultrasonic thickness measurements. Measurements were taken within the area where the ultrasonic transducers were mounted using a digital caliper gauge. The digital caliper has a range of zero inches to eight inches with an accuracy of 0.01inches. The ultrasonic transducer thickness meter used had a range of 0.05 inches to 9.0 inches with a resolution of 0.0001 inches and an accuracy of$\pm 0.5\% n + 0.1$.

Figure 84, 85 and 86 shows the method used to determine the inlet and out thickness using digital caliper .

Figure 83. Digital caliper measurements I

Figure 84. shows digital caliper used for thickness measurements on the valve installed for the 1152 hours of operation.

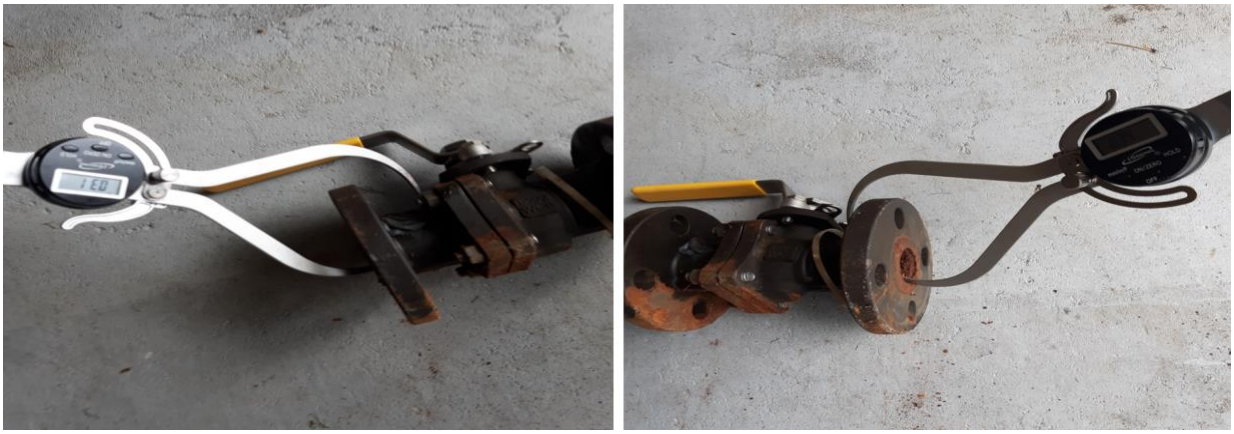

Figure 84. Digital Caliper Gauge Measurements II.

Figure 85. shows digital caliper used for thickness measurements on the valve installed for the 408 hours of operation.

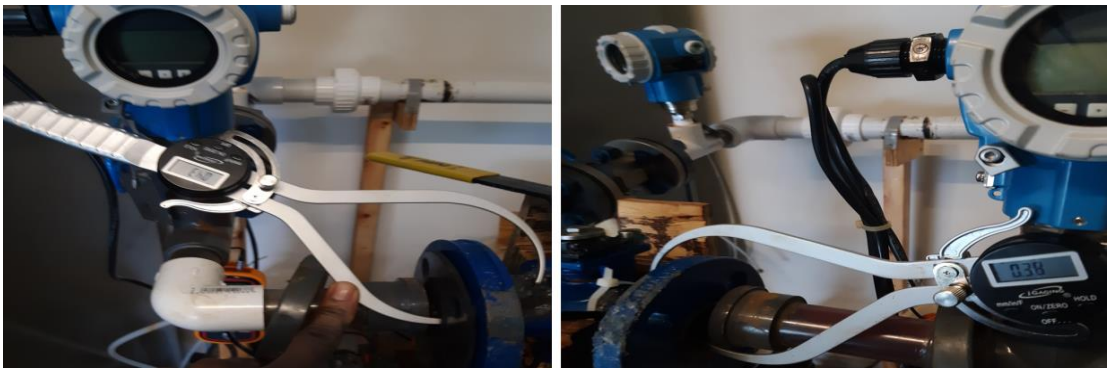

Figure 85. Digital Caliper Gauge Measurements.

Figure 86. shows digital caliper used for thickness measurements on the valve installed for the 240 hours of operation.

Figure 87 below shows the final the values of ultrasonic transducer measurements for both the inlet area and outlet area on the valves used during the experiments and readings taken using digital caliper gauge. These were values from the valve body when the system run for 1152 hours, 408 hours and 240 hours respectively. The 1152 hours of run time shows a difference of 0.24 inches and 0.15 inches for the inlet and outlet thickness measurements respectively. The

408-run time shows 0.29 inches difference for the inlet measurement and 0.07 inches difference for the outlet thickness measurements.

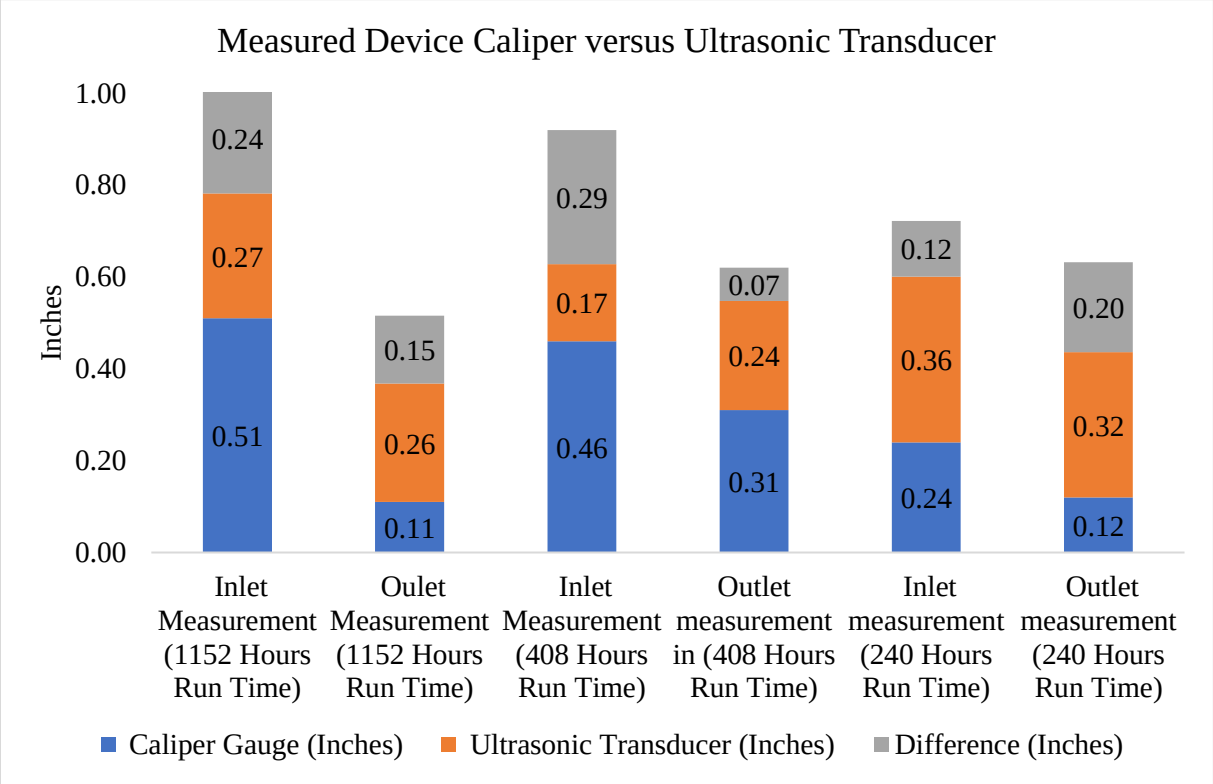

Figure 86. Find thickness measurements caliper gauge versus ultrasonic transducer.

The valve used for the 240 hours of runtime shows a difference of 0.12 inches for the inlet thickness measurements and 0.20 inches difference for the outlet measurements. These differences stated above are between the final values of ultrasonic thickness measurements for each valve used in the three experiments and the digital caliper gauge measurements taken on the three valves.

Thickness readings obtained from ultrasonic transducers are not necessarily accurate due to the limitations of the ultrasonic sound beam. Some of the ultrasonic beams may reflect as soon as a surface of the material is reached. Geometrical shapes and overlapping surfaces may introduce inaccuracies in the thickness measurements . It is possible that the ultrasonic thickness

transducer measured flaws in the internal of the valve body material rather than flaws to the back wall of the body of the valve [54]. A doubling effect occurs when the readings of an ultrasonic thickness measurements doubles the actual thickness of a material. When the ultrasonic transducer is worn out, there is the possibility of doubling effect. This is due to the inherent limitation of ultrasonic technology. Statistical evaluation is necessary when multiple ultrasonic transducer was installed or embedded on a valve body for thickness evaluation of valve body.

CHAPTER VI

CONCLUSIONS AND FUTURE WORK

The objective of this research was to determine the possibility of monitoring corrosion in real time using ultrasonic technology on a one-inch carbon steel body valve contacting a corrosive fluid. The process variables that were monitored during this work were fluid temperature, ambient temperature, pressure, volumetric flow rate, total dissolved solids and fluid pH. Significant amounts of thickness data was collected under these fluid conditions with the ultrasonic transducer mounted on the valve body. These data were modeled statistically to evaluate normality, linearity and significance of the ultrasonic thickness measurements. Ambient conditions were also varied to evaluate the impact of temperature, pressure, vibration and noise on the ultrasonic thickness measurements. This chapter outlines the conclusions drawn from the experiments carried out in this research.

6.1 NaCl Fluid Condition

An investigation of corrosion on a valve body was conducted in the presence of NaCl solution for a period of 1,152 hours. The NaCl solution was circulated via a pump through a hydraulic loop at a near constant flow rate of 35.6GPM and an ultrasonic thickness meter was used to collect thickness loss data on inlet and outlet locations. During this experiment, the differential pressure monitored across the valve observed at 2 PSI was not large enough to restrict flow in the system. Thickness measurements were collected during this period of experiment but there was little loss of material as observed by the ultrasonic thickness meter.

Visual inspection of the process fluid daily showed that corrosion was ongoing, and the material lost or degradation after the valve internals was inspected also validated the presence of corrosion. Digital microscopic images of the control valve internals, i.e. the inlet and outlet, showed significant amounts of iron oxides forming layers at the inlet of the valve. The flow rate was not high enough to erode the iron oxides formed on the surface of the valve internals. During the experiment where sodium chloride solution was used as the circulating fluid, the ultrasonic traducers were not permanently mounted on the valve body. This added significant error to the measurements. Another potential source of error came from transducer drift because it was not calibrated frequently enough. In addition, the inherent nature of ultrasonic technology introduces error.

But it is more important to know relative changes in the thickness than the actual valve thickness. Therefore, the transducers for both the inlet and outlet locations had to be calibrated multiple times to mitigate the ultrasonic transducer drift. A calibration frequency of about 240 hours is suggested. The ultrasonic transducers were mounted and removed daily on the valve body and this method also introduced error. The mounting conditions of the ultrasonic transducer changed each time it was mounted on the valve body. These errors were evident in the linear regression analysis slightly and there was significant variability evident for the ultrasonic thickness measurements. The coefficient of determination was 67.6% for the inlet location and 64.3% for the outlet location where ultrasonic transducers were mounted on the valve body. The data observed proved that close to 40% of the data in each case for the inlet and outlet did not fit the model. This type of method is used in industry and have been validated in this experiment as prone to errors.

The linear regression analysis conducted proved that for the 1,152 hours of runtime with an aqueous sodium chloride operating fluid there was a significantly positive relationship between the ultrasonic thickness readings, and the time these measurements were observed.

The experiment conducted to verify the possibility of monitoring corrosion on a 1-inch valve using ultrasonic technology has been validated. The corrosion behavior observed was consistent with other research where sample coupons were used with coupon immersed in NaCl solution.

6.2 Acetic Acid and Sodium Chloride Condition

An operating fluid of aqueous NaCl, acetic acid was used to accelerate rate of corrosion. The total runtime was 408 hours. Within a period of 408 hours, severe corrosion was visually observed and thickness losses for both the inlet and outlet location of the valve body became evident. Material loss was observed used the ultrasonic thickness meter and these observations were made for both the inlet location and the outlet location of the valve body. Corrosion of the valve body was relatively faster in the acetic acid mixtures as the pH was maintained below 4. There was more material loss at the inlet of the valve than the outlet of the valve per physical inspection conducted on the valve.

During the experiment with acetic acid and sodium chloride mixtures used as the circulating fluid, the ultrasonic traducer was permanently mounted on the valve body that was monitored for corrosion. Circulated sodium chloride and acetic acid through the hydraulic loop this way with the transducers installed permanently, eliminated the error introduced by remounting the ultrasonic transducer daily.

The transducers for both the inlet and outlet locations were only calibrated once prior to the transducers being mounted permanently on the valve body for 408 hours. The mounting conditions of the ultrasonic transducer did not change each time that thickness reading needed to be taken on the daily basis. The error reduction and variability were less and were validated in the linear regression model for the acetic acid and sodium chloride condition. The coefficient of determination was 85.4% for the inlet and 79.8% for the outlet locations where ultrasonic transducer were mounted on the valve body. The data observed proved that about 80 % of the data observed in each case for the inlet and outlet did fit the model. It is evident that this method is less prone to errors. When the system circulated acetic acid mixed with NaCl for 408 hours, there was a significantly strong relationship between the ultrasonic thickness measurements and the time these measurements were taken for both the inlet and outlet locations.

Another experiment was conducted under acetic acid and sodium chloride conditions but in this case for 240 hours of runtime with the ultrasonic transducers mounted on the valve body yielded a similar result in terms of the linear regression analysis. The coefficient of determination during the 240 hours of run under acetic acid and sodium chloride mixtures was 93% and 97% for the inlet and outlet location. The data indicated that less than approximately 10 % of the data in each case for the inlet and outlet did not fit the model. It is evident that this method was less prone to errors. In addition, for the 240 hours of runtime, with the ultrasonic transducers embedded on the valve body, the outlet readings were very close to being linear as seen in. normal probability-probability plot discussed. When the system was run using acetic acid mixed with NaCl for 240 hours, there was a significantly strong relationship between the ultrasonic thickness measurements and the time these measurements were taken for both the inlet and outlet.

Statistical models were employed to evaluate the linearity, normality and statistical significance of the three experiments conducted. The statistical models showed that thickness loss for both inlet and outlet locations were somewhat nonlinear in nature. Statistical models for all the experiments conducted proved that the p values for all three experiments were less than the significant level of 0.05. Therefore, the statistical significance of all three experiments was validated.

During the period of investigation, there was no significant pressure drop across the control valves to restrict flow within the system. The pressure dropped for the three experiments averaged 1.7 PSI. Monitoring corrosion through thickness loss of a valve body was verified. The inlet and outlet measurements of thickness of material loss was verified using ultrasonic transducers. The presence of acetic acid mixed with sodium chloride at a pH of less than 4, yielded a rapid response in terms of corrosion seen in a short amount of time, when the valve body was exposed to the mixture of the acetic acid and NaCl.

The statistical distribution of the inlet and the outlet measurements was also validated. The linear regression analysis conducted for all three experiments show that, in each case, the correlation coefficient was significant between ultrasonic thickness measurements and time the thickness measurements were observed. Therefore, the model can be used to predict ultrasonic thickness measurements for the time values that are within the range of observation.

6.3 Coupling, Ambient Conditions and Measurement Precision

These experiments revealed that when an ultrasonic transducer was embedded on to a one-inch ball valve body, glycerin was not a good coupling gel if used for more than 12 hours. Where it is desired to use a coupling gel for a longer period, SONO 600 high temperature

coupling gel was preferred. During the investigations using aqueous NaCl/acetic acids solutions and with the ultrasonic transducer embedded on the valve body, with SONO 600 high temperature coupling gel used for coupling, the desired acoustic impedance was maintained. Therefore, reliable ultrasonic thickness readings were observed. SONO 600 high temperature coupling gel can last longer than 5,000 hours when used as a coupling gel for ultrasonic thickness measurements. Valve inspection after all valves were removed from the hydraulic loop showed similar corrosion products and characteristics seen in all three experimental conditions.

Ambient conditions were evaluated for these experiments and it was observed that, hot temperatures and cold temperatures add variability to the thickness measurements. If high levels of precision are required the temperature should be incorporated into the calibration. The ultrasonic thickness readings varied up to 2.7 mm when the ambient temperature varied from 11.7°F to 300°F within the vicinity where the ultrasonic transducer was mounted on the valve body. When the transducers were exposed to vibration at 1KHz from $0 m/s^2$ to $200 m/s^2$ and noise between $67 dB$ to $117 dB$ there was negligible variation observed in the ultrasonic thickness readings. At ambient temperatures 300°F and above, the ultrasonic signal was lost and thickness readings above 300°F were not valid. Variations in ultrasonic thickness measurements observed due to changing ambient conditions require further studies to introduce correction factors for these ambient conditions. Introduction of correction factors will generate a more reliable ultrasonic thickness reading.

The ultrasonic measurement final values were validated against caliper readings taken after the valves were removed from the hydraulic loop and it was evident that the caliper measurements were different in values from the ultrasonic thickness measurements. It was particularly evident that for all the experiment conditions the caliper showed larger values for the

inlet location and lower values for the outlet location of the valves. The mean difference for the inlet locations for all three valves was 0.22 inches while the outlet locations had a mean difference of 0.12 inches for all three experiments. These measurement differences proved that corrections factors are needed between ultrasonic thickness measurements and actual physical measurement. These outcomes will form the basis for next generation of carbon steel ball valves having ultrasonic technology embedded to monitor corrosion online and in real time.

6.4 Recommendations for Future Work

This research was limited in scope due to funding and therefore the thickness data collected that inferred that corrosion inside the valve could not be transmitted or collected into a data acquisitions system or asset management system. Companies such as Metso Valve Company, Samson Controls Incorporated have smart positioners that can be explored as intermediary elements to transmit ultrasonic thickness measurements from valves to a remote human machine interface, and these data can be used for engineering analysis and decision making.

The thickness data that was collected can now be superimposed onto a control valve with a smart positioner and this data transmitted over a current loop displayed on a distributed control system. Collecting these data in a form of signals and transmitted to a data acquisition system is an important research interest to be considered in the future. Data collected by this means could be used for further analysis in terms of predicting thickness loss over time and overall reliability of a valve in a hydraulic loop. Future work will present an opportunity for these data to be analyzed and incorporated into petrochemical asset management system for predictive data analytics.

The hydraulic loop for these experiments was small in scale with a 1-inch interconnection PVC piping. Future work may consider investigating larger interconnection piping with a greater than one-inch valve, and consideration given to a globe control valve. With a large scale or industrial type flow loop, flows greater than 35 gallons per minute may also be considered in a future experiment. Future work may also consider investigating correction factors for ambient conditions i.e. temperature, noise and vibration which was proved in this research that these ambient conditions adversely impacted ultrasonic thickness measurements.

REFERENCES

[1] A. S. Nivitchanyong, “Aspects of Corrosion Cost in Thailand,” p. 27.

[2] H. Zhang, R. Yang, Y. He, G. Y. Tian, L. Xu, and R. Wu, “Identification and characterisation of steel corrosion using passive high frequency RFID sensors,” *Measurement*, vol. 92, pp. 421–427, Oct. 2016, doi: 10.1016/j.measurement.2016.06.041.

[3] W. Hwang, S. Bae, J. Kim, S. Kang, N. Kwag, and B. Lee, “Acoustic emission characteristics of stress corrosion cracks in a type 304 stainless steel tube,” *Nucl. Eng. Technol.*, vol. 47, no. 4, pp. 454–460, Jun. 2015, doi: 10.1016/j.net.2015.04.001.

[4] F. H. Estupiñán-López *et al.*, “Transient Analysis of Electrochemical Noise for 316 and Duplex 2205 Stainless Steels Under Pitting Corrosion,” *Int J Electrochem Sci*, vol. 6, p. 13, 2011.

[5] G. Du, W. Wang, S. Song, and S. Jin, “Detection of corrosion on 304 stainless steel by acoustic emission measurement,” *Anti-Corros. Methods Mater.*, vol. 57, no. 3, pp. 126–132, May 2010, doi: 10.1108/00035591011040083.

[6] L. Han and S. Song, “A measurement system based on electrochemical frequency modulation technique for monitoring the early corrosion of mild steel in seawater,” *Corros. Sci.*, vol. 50, no. 6, pp. 1551–1557, Jun. 2008, doi: 10.1016/j.corsci.2008.02.009.

[7] S. M. Elsariti and Haftirman, “Behaviour of Stress Corrosion Cracking of Austenitic Stainless Steels in Sodium Chloride Solutions,” *Procedia Eng.*, vol. 53, pp. 650–654, 2013, doi: 10.1016/j.proeng.2013.02.084.

[8] W. Kim, J. Chai, and I. Kim, “Development of a majority vote decision module for a self-diagnostic monitoring system for an air-operated valve system,” *Nucl. Eng. Technol.*, vol. 47, no. 5, pp. 624–632, Aug. 2015, doi: 10.1016/j.net.2015.03.006.

[9] A. N. Anikeev, I. V. Chumanov, and V. V. Sedukhin, “Investigation of Valves with a Weld Microstructure Layer Resistant to the Hydrogen Sulfide Corrosion,” *Procedia Eng.*, vol. 150, pp. 1063–1067, 2016, doi: 10.1016/j.proeng.2016.07.215.

[10] F. Subari, H. F. Maksom, and A. Zawawi, “Corrosion Behavior of Eutectic Molten Salt solution on Stainless Steel 316L,” *Procedia - Soc. Behav. Sci.*, vol. 195, pp. 2699–2708, Jul. 2015, doi: 10.1016/j.sbspro.2015.06.465.

[11] A. I. Sunny, G. Y. Tian, J. Zhang, and M. Pal, “Low frequency (LF) RFID sensors and selective transient feature extraction for corrosion characterisation,” *Sens. Actuators Phys.*, vol. 241, pp. 34–43, Apr. 2016, doi: 10.1016/j.sna.2016.02.010.

[12] F. G. Rivera, G. Edwards, E. Eren, and S. Soua, “Acoustic emission technique to monitor crack growth in a mooring chain,” *Appl. Acoust.*, vol. 139, pp. 156–164, Oct. 2018, doi: 10.1016/j.apacoust.2018.04.034.

[13] J. A. Pascoe, D. S. Zarouchas, R. C. Alderliesten, and R. Benedictus, “Using acoustic emission to understand fatigue crack growth within a single load cycle,” *Eng. Fract. Mech.*, vol. 194, pp. 281–300, May 2018, doi: 10.1016/j.engfracmech.2018.03.012.
[14] S. M. Ali, K. H. Hui, L. M. Hee, and M. S. Leong, “Automated valve fault detection based on acoustic emission parameters and support vector machine,” *Alex. Eng. J.*, vol. 57, no. 1, pp. 491–498, Mar. 2018, doi: 10.1016/j.aej.2016.12.010.
[15] S. S. Jamali, D. J. Mills, R. A. Cottis, and T. Y. Lan, “Analysis of electrochemical noise measurement on an organically coated metal,” *Prog. Org. Coat.*, vol. 96, pp. 52–57, Jul. 2016, doi: 10.1016/j.porgcoat.2016.01.017.
[16] Y. Hou, C. Aldrich, K. Lepkova, L. L. Machuca, and B. Kinsella, “Monitoring of carbon steel corrosion by use of electrochemical noise and recurrence quantification analysis,” *Corros. Sci.*, vol. 112, pp. 63–72, Nov. 2016, doi: 10.1016/j.corsci.2016.07.009.
[17] A. I. Aljoboury, A.-H. I. Mourad, A. Alawar, M. Abou Zour, and O. A. Abuzeid, “Stress corrosion cracking of stainless steels recommended for building brine recirculation pumps,” *Eng. Fail. Anal.*, vol. 17, no. 6, pp. 1337–1344, Sep. 2010, doi: 10.1016/j.engfailanal.2010.03.008.
[18] T. Amann, M. Waidele, and A. Kailer, “Analysis of mechanical and chemical mechanisms on cavitation erosion-corrosion of steels in salt water using electrochemical methods,” *Tribol. Int.*, vol. 124, pp. 238–246, Aug. 2018, doi: 10.1016/j.triboint.2018.04.012.
[19] A. Rauf and W. F. Bogaerts, “Employing electrochemical frequency modulation for pitting corrosion,” *Corros. Sci.*, vol. 52, no. 9, pp. 2773–2785, Sep. 2010, doi: 10.1016/j.corsci.2010.04.016.
[20] T. Kanemaru *et al.*, “A fluorescence scanning electron microscope,” vol. 12, p. 6.
[21] D. den Engelsen, P. G. Harris, T. G. Ireland, G. R. Fern, and J. Silver, “Contrast and decay of cathodoluminescence from phosphor particles in a scanning electron microscope,” *Ultramicroscopy*, vol. 157, pp. 27–34, Oct. 2015, doi: 10.1016/j.ultramic.2015.05.009.
[22] A. Saluja, J. Costain, and E. Van, “Non-Intrusive Online Corrosion Monitoring,” p. 6.
[23] R. W. Revie and H. H. Uhlig, “Corrosion and Corrosion Control : An Introduction to Corrosion Science and Engineering,” p. 513.
[24] P. R. Roberge, “Corrosion Engineering : Principles and Practice,” p. 770.
[25] “Mars Fontana-Corrosion Engineering(www.iranidata.com).pdf.” .
[26] E. McCafferty, *Introduction to Corrosion Science*. New York, NY: Springer New York, 2010.
[27] R. E. Melchers, “Extreme value statistics and long-term marine pitting corrosion of steel,” *Probabilistic Eng. Mech.*, vol. 23, no. 4, pp. 482–488, Oct. 2008, doi: 10.1016/j.probengmech.2007.09.003.
[28] A. Groysman, *Corrosion for everybody*. Dordrecht ; New York: Springer, 2010.
[29] “Fundamentals of Fluid Mechanics, 6th Edition.pdf.” .
[30] H. M. Shalaby, A. Al-Hashem, M. Lowther, and J. Al-Besharah, “INDUSTRIAL CORROSION AND CORROSION CONTROL TECHNOLOGY,” p. 662.
[31] O. Singh, *Applied thermodynamics*. New Delhi: New Age International (P) Ltd., Publishers, 2009.
[32] I. Ihara, “Ultrasonic Sensing: Fundamentals and Its Applications to Nondestructive Evaluation (a draft),” p. 20.
[33] J. D. N. Cheeke, *Fundamentals and applications of ultrasonic waves*. Boca Raton: CRC Press, 2002.

[34] M. Kutz, Ed., “Frontmatter,” in *Mechanical Engineers’ Handbook*, Hoboken, NJ, USA: John Wiley & Sons, Inc., 2006, pp. i–xv.
[35] J. Krautkrämer and H. Krautkrämer, *Ultrasonic Testing of Materials*. Berlin, Heidelberg: Springer Berlin Heidelberg, 1990.
[36] K. Kim, D. Choi, and S. Im, “The application of ultrasonic waves and envelope energies in a closed chamber based on an air/methane mixture,” *Ultrasonics*, vol. 91, pp. 92–102, Jan. 2019, doi: 10.1016/j.ultras.2018.07.009.
[37] S. Rahemi Ardekani, A. Sabour Rouh Aghdam, M. Nazari, A. Bayat, E. Yazdani, and E. Saievar-Iranizad, “A comprehensive review on ultrasonic spray pyrolysis technique: Mechanism, main parameters and applications in condensed matter,” *J. Anal. Appl. Pyrolysis*, vol. 141, p. 104631, Aug. 2019, doi: 10.1016/j.jaap.2019.104631.
[38] S. Arefi-Oskoui, A. Khataee, M. Safarpour, Y. Orooji, and V. Vatanpour, “A review on the applications of ultrasonic technology in membrane bioreactors,” *Ultrason. Sonochem.*, vol. 58, p. 104633, Nov. 2019, doi: 10.1016/j.ultsonch.2019.104633.
[39] S. Kumar, C. S. Wu, G. K. Padhy, and W. Ding, “Application of ultrasonic vibrations in welding and metal processing: A status review,” *J. Manuf. Process.*, vol. 26, pp. 295–322, Apr. 2017, doi: 10.1016/j.jmapro.2017.02.027.
[40] T. Gudra, D. Banasiak, K. Herman, and K. Opieliński, “Comparative analysis of the results of snowfall level measurements performed using ultrasonic aerolocation method in real conditions in different climatic areas,” *Appl. Acoust.*, vol. 125, pp. 71–79, Oct. 2017, doi: 10.1016/j.apacoust.2017.04.011.
[41] S. M. Enamorado *et al.*, “Development of a recording water flow meter using ultrasonic measurement of water levels in a slotted U-pipe,” *Agric. Water Manag.*, vol. 88, no. 1–3, pp. 263–268, Mar. 2007, doi: 10.1016/j.agwat.2006.10.003.
[42] A. Cavuto, M. Martarelli, G. Pandarese, G. M. Revel, and E. P. Tomasini, “Train wheel diagnostics by laser ultrasonics,” *Measurement*, vol. 80, pp. 99–107, Feb. 2016, doi: 10.1016/j.measurement.2015.11.014.
[43] K. Dugmore, D. Jonson, and M. Walker, “A comparison of signal consistency of common ultrasonic couplants used in the inspection of composite structures,” *Compos. Struct.*, vol. 58, no. 4, pp. 601–603, Dec. 2002, doi: 10.1016/S0263-8223(02)00131-9.
[44] J. E. Bringas, Ed., *Handbook of comparative world steel standards*, 2nd ed. W. Conshohocken, PA: ASTM, 2002.
[45] Y.-M. Cheong, K.-M. Kim, and D.-J. Kim, “High-temperature ultrasonic thickness monitoring for pipe thinning in a flow-accelerated corrosion proof test facility,” *Nucl. Eng. Technol.*, vol. 49, no. 7, pp. 1463–1471, Oct. 2017, doi: 10.1016/j.net.2017.05.002.
[46] P. R. Roberge, *Handbook of corrosion engineering*. New York: McGraw-Hill, 2000.
[47] “Fundamentals of Thermodynamics 8th ed.pdf.” .
[48] M. X. Wei, S. Q. Wang, and X. H. Cui, “Comparative research on wear characteristics of spheroidal graphite cast iron and carbon steel,” *Wear*, vol. 274–275, pp. 84–93, Jan. 2012, doi: 10.1016/j.wear.2011.08.015.
[49] “A student’s guide to Data and Error Analysis.pdf.” .

[50] M. Dekking, Ed., *A modern introduction to probability and statistics: understanding why and how*. London: Springer, 2005.
[51] D. C. Montgomery, E. A. Peck, and G. G. Vining, “Introduction to Linear Regression Analysis,” p. 679.
[52] A. Bahadori, *Hazardous Area Classification in Petroleum and Chemical Plants: A Guide to Mitigating Risk*, 0 ed. CRC Press, 2013.
[53] A. Mitra, *Fundamentals of quality control and improvement*, 3rd ed. Hoboken, N.J: Wiley, 2008.
[54] “GE Inspection Technologies DM5E Ultrasonic Thickness Gauge Manual.pdf.” .
[55] "Discover Valve," [Online]. Available: https://www.discovervalve.com/mm5/merchant.mvc?&Store_Code=D&Screen=PROD&Product_Code=102674.
[56] "JB Weld," [Online]. Available: https://www.jbweld.com/collections/epoxy-putty-sticks/products/steelstik-epoxy-putty-stick.
[57] "Magnaflux," [Online]. Available: https://www.magnaflux.com/Magnaflux/Products/Ultrasonic-Couplants/Sono-600.htm.
[58] "Omni Instruments," [Online]. Available: https://www.omniinstruments.co.uk/omni-tm-8812-ultrasonic-thickness-gauge.html.
[59] "National Institute of Standards and Technology," [Online]. Available: https://www.itl.nist.gov/div898/handbook/eda/eda_d.htm.